Calculational Methods for Nuclear Heating

M.A. Abdou

July 1973

UWFDM-66

FUSION TECHNOLOGY INSTITUTE

UNIVERSITY OF WISCONSIN

MADISON WISCONSIN

Calculational Methods for Nuclear Heating

M.A. Abdou

Fusion Technology Institute
University of Wisconsin
1500 Engineering Drive
Madison, WI 53706

http://fti.neep.wisc.edu

July 1973

UWFDM-66

Calculational Methods for Nuclear Heating

by

M. A. Abdou
and
C. W. Maynard

July 1973

FDM 66

Nuclear Engineering Department
University of Wisconsin
Madison, Wisconsin

Table of Contents

Preface to FDM-66 and FDM-67

The contents of the FDM-66 and FDM-67 reports are parts of a Ph.D. thesis entitled, "Calculational Method for Nuclear Heating and Neutronics and Photonics Design for CTR Blankets and Shields" by M. A. Abdou under the supervision of Professor C. W. Maynard.

To facilitate the distribution of the FDM reports, the contents of the thesis is divided into two parts. FDM-66 contains Chapters 1, 2, and 3. These chapters deal with the calculational methods for nuclear heating and are self-contained. Chapters 4, 5, and 6 are the contents of FDM-67. Chapter 4 is an investigation of discrete-ordinates calculational models for fusion neutronics and photonics. Chapter 5 deals with the nuclear design of blanket and shield. The thesis conclusions and recommendations are given in Chapter 6.

Although each of the two FDM reports are self-contained, cross reference by chapter is frequently made. Therefore, the pages are numbered consecutively throughout the two reports. The list of references and table of contents are given, however, in each report.

ABSTRACT

CALCULATIONAL METHODS FOR NUCLEAR HEATING

AND

NEUTRONICS AND PHOTONICS DESIGN FOR CTR BLANKETS AND SHIELDS

MOHAMED ABD EL-AZIZ ABDOU

Under The Supervision Of

Professor Charles W. Maynard

The general concern of this thesis research is to solve some of the theoretical and calculational problems involved in the neutronics and photonics analysis of fusion reactor blankets, magnet shields, and magnets. In this analysis, the basic problem is the calculation of "response" rates of interest. The general form for a response rate is

$$R = \int_{\vec{P}} F_R(\vec{P})\ \psi(\vec{P})\ d\vec{P}$$ where $F_R(\vec{P})$ is the response function, $\psi(\vec{P})$ is the angular flux, and $\vec{P}$ represents a point in the phase space $(\vec{r},\vec{V})$. The investigation in this thesis is divided into three parts: 1 - the development of models for calculating the response functions for nuclear heating, called fluence-to-kerma factors (sometimes referred to as energy deposition parameters) and other responses of interest, 2 - the accurate determination of ψ, and 3 - a study of the neutronics and photonics performance of CTR blankets and shields using the results from

parts 1 and 2.

Theoretical models derived in this work for calculation of fluence-to-kerma factors are based on an accurate solution of the nuclear kinematics. A computer program, called MACK, which uses this solution for calculation of the energy deposition parameters from nuclear data in ENDF/B format is described. The program is general, self-consistent, reliable, and has many options that allow deriving results appropriate for use in any desired application with a minimum of effort. The fluence-to-kerma factors are then calculated for materials of interest for fusion reactor applications and the results are presented and analyzed. A scheme for investigating the validity of the fluence-to-kerma factor values is also developed and applied to the results of the present work. The relationship between these parameters and photon production and the consistency of nuclear data and processing codes are examined. A sensitivity study of the energy release factors to the input parameters is carried out. Calculation of other response functions such as for helium and hydrogen production is automated for multigroup representation by integrating the required processing with the computational capability developed for kerma factors.

The order of approximations required to obtain the flux to a desired accuracy using the discrete ordinates S_n method varies from one nuclear system to another. The effects of the order of angular quadrature, scattering anisotropy, spatial mesh spacing, and geometrical model on the solution of the neutron and photon transport equations are investigated in this work for the unique characteristics of fusion reactor blankets and shields. With these developments in hand, all response rates of

interest in the blanket, shield, and magnet can be calculated for any design and the neutronics and photonics analysis of the system becomes feasible. The last part of this thesis is an application of these developments. Previous work in this area concentrated on the question of tritium breeding but since this has been shown not to be a problem, more important aspects of the nuclear design such as nuclear heating, charged particle production, and energy multiplication are investigated. A quantitative study of the shield is also carried out with the composition and thickness of the shield optimized to meet the various requirements at low cost.

ACKNOWLEDGMENTS

I consider myself fortunate to have had the opportunity of working under the supervision of Professor C. W. Maynard. His guidance, invaluable help, fruitful suggestions, and constant encouragement at all times are gratefully acknowledged.

For encouragement and guidance during my first year of graduate study, and for continued aid and encouragement throughout the duration of this research, sincere thanks are due Professor Wm. F. Vogelsang.

I am also indebted to Dr. D. Klein of Westinghouse Electric Corporation and to Professor R.W. Conn for providing important comments and constructive advice. Special thanks are extended to Professor M. Ebel of the physics department for helpful discussions.

I am deeply appreciative of students, staff and faculty members of the Nuclear Engineering Department and Fusion Design Team at the University of Wisconsin for assistance and encouragement throughout the course of this educational experience. In particular I would like to thank Professors R. Boom, M. W. Carbon, J. Donhowe, M. M. El-Wakil, G. A. Emmert, W. K. Foell, and H. K. Forsen. Among others of my colleagues to whom thanks are due are A. Mense and J. Welch.

Many thanks are extended all members of the Radiation Shielding Information Center at Oak Ridge National Laboratory for their patience and cooperation in supplying many of the nuclear data and computer programs needed for this work. Sincere thanks are also due Dr. W. E. Ford III

of ORNL for invaluable and professional assistance in preparing the gamma production data.

In the past few months, my wife, Zizi, has endured too much to mention. Her encouragement and assistance were essential elements in the successful completion of this work.

The diligent work of Miss Diana Paddock, Mr. George Bussey and Mr. Chi-Kin Lin in typing and preparation of this thesis made the final efforts go smoothly.

CHAPTER 1

INTRODUCTION

With the advances in plasma physics, a number of approaches are being pursued towards the goal of utilizing fusion energy. While there are several alternative schemes for plasma confinement and power production, many of the major technological problems are similar in all cases.

In principle, the fusion reactor can be operated on several fuel cycles, D-T, D-D, and D-He^3. The governing reactions in these cycles are

$$D + T \rightarrow He^4\ (3.5) + n(14.1),$$
$$D + D \rightarrow He^3\ (0.8) + n(2.6)$$
$$D + D \rightarrow T\ (1.0) + p(3.0)$$
$$D + T \rightarrow He^4\ (3.5) + n(14.1),$$
$$D + He^3 \rightarrow He^4\ (3.7) + p(14.7)$$

where the numbers in parantheses are the average kinetic energies in MeV associated with the particles emitted. In D-T cycles, 80% of the energy released is in the form of the kinetic energy of the neutrons. Hence, these neutrons possess the major source of recoverable energy in a fusion reactor operated on this cycle. It has been shown [113] that equal numbers of 2.6 and 14.1 MeV neutrons are emitted in steady state D-D reactors and for the same power, the number of 14.1 MeV neutrons is roughly the same in the two cycles. Therefore, except for tritium regeneration requirements in D-T reactors, the problems associated with handling the 14.1 MeV neutrons are very similar for both D-D and D-T systems. While most of the problems investigated in this work are independent of the reactor type and neutron energy, any reference in this study to a fusion reactor is to be interpreted as being one operated on

a D-T cycle and utilizing the magnetic confinement. Reference to a fusion neutron will refer to a 14.1 MeV neutron, unless otherwise indicated.

It was only a few years ago, that people began to realize that in addition to plasma physics, many technological problems had to be solved in order to design and construct a practical fusion reactor system. Figure 1 shows a simplified schematic of a conceptual fusion reactor. The alpha particles produced in D-T reactions are trapped in the magnetic field but the 14.1 MeV neutrons escape freely. Since these neutrons carry the main source of recoverable energy in the system they must be slowed down in a region, called the blanket, surrounding the plasma. Converting their kinetic energy into heat, which can then be transported into the "conventional" part of the plant for the production of electricity, is one of the major functions of the blanket. In addition, since tritium is not available in nature, at least a tritium atom per fusion reaction must be produced through nuclear reactions in the blanket. This implies that lithium has to be employed in one form or another for breeding purposes. The blanket extracts (and possibly multiplies) roughly 95 to 99% of the kinetic energy of the neutrons. If these neutrons were to stream directly to the superconducting coils, the total power output of the plant would not be sufficient to supply the refrigeration requirements to keep the magnets at $4^{o}K$. Hence, an efficient shield must be designed for placement between the blanket and magnet.

Several formidable problems are encountered in the design of such a system. The most critical of these is associated with the first wall

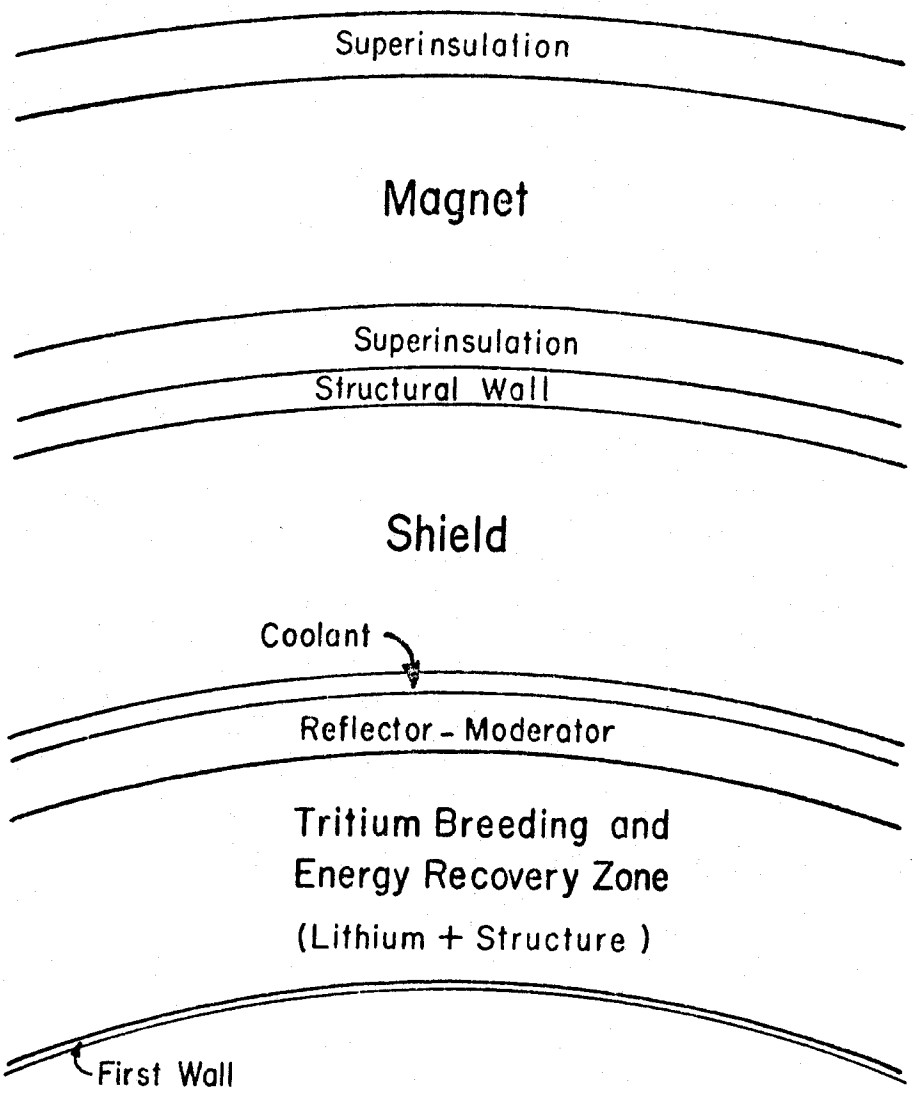

SCHEMATIC OF BLANKET AND SHIELD REGIONS

Figure 1.1

as it is exposed to high currents of high energy neutrons, charged particles and electromagnetic radiation. As a result of the neutron interactions in the wall, the heat generation rate is very large and thus the design of an efficient heat transfer system, such as one using a liquid metal coolant flowing in a strong magnetic field, represents no small effort in itself. The helium and hydrogen production, atomic displacements, and transmutation rates in the first wall are so high that radiation damage to it currently represents another feasibility problem. Similar difficulties are encountered in designing the blanket structure, although they are less severe than in the first wall.

Since the ultimate goal of fusion reactors is power production, it is essential in designing an economically sound reactor to calculate the rate of heat generation in the system. Accurate determination of the spatial distribution of nuclear heating is fundamental in designing a heat transfer system with low pumping losses, and high thermodynamic efficiency.

Magnet shield design involves more than the selection of appropriate materials and determining the thickness required to attenuate the neutrons and photons to a tolerable level. Neutron and photon interactions are inevitably associated with heat generation. The temperature distribution must be known in order to insure the physical integrity of the shield. Thus, accurate calculation of energy deposition is an essential aspect of shield design. In addition, it is necessary to calculate a wide variety of reaction rates to assess the radiation damage, tritium contamination (e.g. in boron), transmutation effects, radioactivity, and afterheat.

The operation of the magnet depends basically on cooling the superconducting coils to low temperatures. The heat removal from $4^{o}K$ to room temperature is accomplished with efficiencies less than 0.1%. In addition, because of the tremendous amount of energy stored in the magnetic field, the stability and physical integrity of the magnet cannot be compromised. Furthermore, not only the nuclear radiation must be shielded against, but the cryogenic system also requires an efficient protection against thermal radiation. To compound the difficulties one notes that superinsulators are known to fail under relatively low doses. Thus, a study of heat generation is fundamental to the design of the magnet, cryogenic system, and superinsulation.

Scope Of This Work

It is clear from the above discussion that the neutronics and photonics analysis is a fundamental prerequisite for the most important areas of the nuclear design of fusion reactor systems. The general concern of this thesis research is to solve some of the theoretical and calculational problems involved in this analysis.

In the neutronics and photonics analysis of fusion reactor blankets and shields, the basic problem is the calculation of "response rates". A response rate takes, in general, the form

$$R = \int_{\vec{p}} F_R(\vec{p})\ \psi(\vec{p})\, d\vec{p} \qquad (1.1)$$

where $F_R(\vec{p})$ is the response function, $\psi(\vec{p})$ is the angular flux, and $\vec{p}$ represents a point in the phase space $(\vec{r},\vec{v})$. The investigation in this work is divided into three parts: 1- the development of models for

calculating all response functions of interest, 2 - the accurate determination of ψ, and 3- a study of the neutronics and photonics behavior of fusion reactor blankets, magnet shields, and magnets, using the developments from parts 1 and 2.

Of the most important response rates that needs to be accurately determined is the nuclear heating. In fission reactors, this is straightforward to a good approximation since the energy released in the fission reaction ($\sim$200 MeV) is the major contribution to heat generation. In fusion reactors, however, the high energy neutrons can undergo a variety of reactions which are all important contributors to the heating. The energy released by each reaction has to be determined from an accurate solution of the nuclear kinematics. The response function, F_R, for nuclear heating is called the fluence-to-kerma factor. In chapter 2, theoretical and computational models for calculation of energy deposition from basic nuclear data for all neutron reaction types in any energy range are developed. Based on the developments discussed in chapter 2, the fluence-to-kerma factors are calculated for materials of interest for fusion reactor applications and the results are presented and analyzed in chapter 3. A scheme for investigating the validity of the fluence-to-kerma factor values is also developed in chapter 3 and applied to the results of the present work. The relationship between these parameters and photon production is also examined. Chapter 3 concludes with a sensitivity study of the energy release factors to the input parameters. Calculation of other response functions such as for helium and hydrogen production is automated for multigroup representation by integrating the required processing with the computational capability developed for kerma factors.

Determination of the flux is a problem with which we have considerable experience from fission reactors. We also know that exact analytic solutions to general transport theory problems are not possible and numerical solutions with the concomittant necessity of introducing some approximations are the only means to predict neutron and photon transport. The order of approximations required to obtain the solution within a desired accuracy varies from one nuclear system to another. This is investigated for the unique characteristics of fusion reactor blankets and shields in chapter 4.

With the developments in chapters 2,3, and 4, all response rates of interest in the blanket, shield, and magnet can be calculated for any design and the neutronics and photonics analysis of the system becomes feasible. Chapter 5 is an application of these developments. Previous work in this area concentrated on the question of tritium breeding but since this has been shown not to be a problem, more important aspects of the nuclear design such as nuclear heating, charged particle production, and energy multiplication were investigated. A quantitative study of the shield is also carried out with the composition and thickness of the shield optimized to meet the various requirements at low cost.

CHAPTER 2

DEVELOPMENTS OF THEORETICAL AND COMPUTATIONAL TECHNIQUES FOR CALCULATION OF FLUENCE-TO-KERMA FACTORS

I. INTRODUCTION

Calculation of the heat-generation rate and dose due to interaction of nuclear radiation with matter is of prime importance in practically any nuclear system.

In fission reactors, the energy released in the fission reaction is the major contribution to the heat generation. The energy released in the fission reaction is known and most of it is deposited locally and therefore the calculation of heat generation rate in the fission reactor core can be easily calculated once the fission reaction rate is known. Contribution to energy deposition from other types of neutron reactions, secondary gammas, etc., is usually about 10% of the total and can be calculated using some simplifying assumptions.

In fusion systems, on the other hand, the high energy neutrons can undergo a variety of reactions and the energy release by each reaction type must be calculated accurately in order to determine the heat generation rate in the first wall, blanket, shield and magnet. In this chapter, theoretical and computational models for calculation of energy deposition from basic nuclear data for all neutron reaction types in any energy range are developed.

For the purposes of calculation, the heating rate due to neutron reactions with nuclei of the target material is divided into two types of contribution; the first type is heat generated by neutron reactions, and the second is heat generated by secondary gamma-radiation produced by these neutron reactions. As an example, consider the (n,p) reaction. The energy deposited of the first type is the kinetic energy of the

recoil nucleus, the proton emitted and of any charged particle (e.g. β-) which may be emitted from the activated residual nucleus. The energy deposition by the gamma-photons emitted is treated separately.

Heating by neutrons at any spatial point can be expressed as

$$H(r) = \int \phi(\vec{r},E) \sum_{ji}\sum N_j(\vec{r})\sigma_{ij}(E)E_{ij}(E)dE(eV/cm^3sec). \qquad (1.1)$$

where

$\phi(r,E)$ = neutron flux at spatial point r and energy E,

$N_j(\vec{r})$ = number density of element j at point r, (atoms/cm^3)

$\sigma_{ij}(E)$ = microscopic cross section of element j for reaction i at neuron energy E (cm^2/atom)

$E_{ij}(E)$ = energy deposited per reaction i in element j (eV).

The units have been chosen as those normally employed in nuclear calculations.

The terms k_{ij} and K_j defined as

$$k_{ij}(E) = \sigma_{ij}(E)E_{ij}(E) \qquad (1.2)$$

$$k_j(E) = \sum_i k_{ij}(E) \qquad (1.3)$$

are flux and density independent. Hence, the heating rates can be calculated from particle transport results for any system if the factors k_j are predetermined for all materials in the system.

k_{ij} is called the microscopic kerma factor for reaction i in element j. The term "kerma" is an acronym standing for the Kinetic Energy Released in Materials. The phrase "fluence-to-kerma factors" was introduced by the International Commission on Radiological Units and

Measurements [1]. The term "kerma" will be used throughout this report as defined by equation 1.2 and 1.3 on the previous page, with E_{ij} as defined next.

$E_{ij}(E)$ is the energy released in element j per reaction i induced by a neutron of energy E. The energy release considered here is the energy which can be assumed to be deposited locally, i.e., within a negligible distance from the site of the reaction. This implies that E_{ij} is the sum of the kinetic energies of the recoil nuclei, charged particles emitted, and charged particles produced by radioactive decay of the residual nucleus and such other processes as internal conversion. The addition of the contribution from radioactive decay to energy deposition depends on the type of calculation performed, time dependent or steady state. This comment will be elaborated on later.

The gamma-ray kerma factors are defined in a similar manner and can be determined from

$$k_\gamma^j = \sigma_{pe}^j E + \sigma_{pp}^j (E - 1.02) + \sigma_{ca}^j E \qquad (1.4)$$

where

$k_\gamma^j(E)$ = gamma kerma factor for element j (MeV . cm^2/atom)

E = photon energy (MeV)

σ_{pe}^i = photoelectric microscopic cross section for element j (cm^2/atom)

σ_{ca}^j = Compton microscopic absorption cross section for element j (cm^2/atom)

σ_{pp}^j = pair production microscopic cross section for element j (cm^2/atom)

In pair production, 1.02 MeV (two electron masses) of the photon energy is not available for local heat disposition. The two .51 MeV photons produced by the pair are accounted for in the transfer cross sections of gamma energy multi-group cross section sets, hence the energy balance is maintained. Implicit in the use of Eq. (1.4) is the assumption that photoelectric, pair production, and Compton scattering are the only processes that contribute to energy deposition, thus all other possible processes are assumed negligible.

The evaluation of gamma kerma factors (Eq.(1.4)) is straightforward and is usually performed by the codes which generate multigroup photon cross sections such as MUG [8] and GAMMA [9]. Therefore, gamma kerma factor calculations present no problem at present.

Calculation of neutron kerma factors, on the other hand, is complicated by the variety of reactions which a neutron can undergo, and the emission of more than one particle in many of these reactions. However, the kinematics and theory are still simple and the limitation on the accuracy of a neutron kerma calculation is set by the availability and accuracy of the nuclear data.

Prior to the work reported here there were several efforts at calculating kerma factors. Some of these are reported in references [2-7]. However, these efforts were directed mostly toward calculating kerma for elements which are major constitutents in the human body. Furthermore, they involved several simplifying assumptions such as neglecting inelastic scattering entirely, anisotropy of elastic scattering, and several others. The work of Ritts et al. [6] included a larger number of reactions and was certainly an improvement over all preceeding work.

They calculated kerma factors for 11 elemental constitutents of the human body. This work was extended [7] to calculate kerma for seven elements of interest in fusion reactor blankets. However, Ritts et. al. in their work did not have a general format or algorithm for calculating kerma and the same effort had to be duplicated for each material or for a new evaluation of the basic data for the same material. In addition, it involved some approximations in calculation of the secondary neutron energy distribution and the excitation of residual nuclei in non-elastic reactions.

The Evaluated Nuclear Data File (ENDF)[10] provides a unified format that is used to store and retrieve evaluated sets of neutron and photon cross sections. The ENDF formats are versatile and flexible enough that almost any type of neutron interaction mechanism can be accurately described. Further, the nuclear data in the ENDF/B library is continuously revised, re-evaluated, and updated. Thus, it provides the most suitable up-to-date nuclear data library.

A computer program was written to calculate neutron fluence-to-kerma factors from nuclear data in ENDF/B format based on the theoretical model described in the following section. The name of the code is MACK (MACK: Mohamed Abdou Computes Kerma).

The basic purpose of the MACK program is to calculate neutron-induced kerma factors as a function of neutron energy. The calculation is carried out for a discrete energy mesh flexibly specified by input options for any desired energy range. In addition, several calculational routines were included in the program to generate energy group kerma factors and energy group cross sections (group constants, not transfer

matrices) for any reaction type desired. These options provide a rapid and economical way of obtaining cross sections in multigroup form for calculation of reaction rates of interest; e.g., helium, hydrogen and tritium production. The MACK code also has a built-in resonance treatment and the resonance cross sections can be computed, Doppler-broadened at an arbitrary temperature, from resonance parameters (ENDF/B file 2). This provides the code with independence from other programs in processing ENDF/B data for resonance nuclides.

In the following section, the kinematics equations for the nuclear reactions are solved. A brief description of the algorithm for the MACK program and the models for processing nuclear data in ENDF/B format are discussed in section III.

II. THEORY FOR KERMA FACTOR CALCULATIONS

The macroscopic kerma factor for an element j was defined in the introduction to be

$$k_j = \sum_i k_{ij} \qquad (2.1)$$

$$k_{ij}(E) = \sigma_{ij}(E)\, E_{ij}(E) \qquad (2.2)$$

where

E = incident neutron energy (eV)

$\sigma_{ij}(E)$ = microscopic cross section of element j for reaction i at incident neutron energy E (cm^2/atom)

$E_{ij}(E)$ = energy released per reaction i in element j (eV)

From the above equations, it is clear that the basic quantity to be calculated for generating kerma factors is the energy released by each type of reaction, E_{ij}, and this is the subject of this section.

Since we need to consider only kerma for an element, the subscript j will be dropped from here on. Furthermore, since one reaction will be considered at a time in the following discussion, the subscript i will also be dropped unless a distinction is needed. Throughout this section, several quantities will be used as defined below (for each reaction)

E_r = kinetic energy of the recoil nucleus

E_R = sum of kinetic energies of recoil nucleus and charged particles emitted.

E_H = total energy release from the reaction considered ($E_H = E_{ij}$)

A = AWR = ratio of the nuclear mass of the element to that of the neutron.

Reaction Types

For kerma calculation, the nuclear reactions are conveniently classified

into the seven types given in Table 1. In Table 1, MT is the ENDF/B reaction number and LR is a flag used in ENDF/B3 to allow inclusion of information about the (n,n') part of a combined inelastic reaction (other than γ-ray emission) by presenting these reactions with MT = 50-91 (inelastic scattering to levels and continuum) and using the appropriate MT number in the LR flag field.

The methods used to calculate the energy released by each type of reaction are summarized below. The kinematics are derived from energy and momentum conservations; however, the details are not given here.

Since ENDF data generally extends only to 15 MeV at present, which is the energy range required for most applications, contributions to the kerma factors from (n,3n) reactions and from secondary nuclear reactions caused by charged particle products of the primary reaction are neglected.

Elastic Scattering

The only contribution to kerma elastic scattering is the deposition of the kinetic energy of the recoil nucleus, E_r; i.e.

$$E_H = \bar{E}_r \qquad (2.3)$$

E_r is a function of the scattering angle of the neutron. The average recoil energy is obtained by weighting $E_r(\theta)$ by the differential scattering cross section.

$$\bar{E}_r = \frac{2AE}{(A+1)^2} \quad (1 - \overline{\cos \theta_{cm}}) \qquad (2.4)$$

Table 1

REACTION TYPES

For the Purpose of Kerma Calculation, The Nuclear Reactions are Classified Into the Following Types

	REACTION TYPE	MT
1- (n,n)	Elastic	2
2- (n,n')γ	Inelastic Level	51-90
3- (n,n')γ	Inelastic Continuum	91
4- (n,mn')a_{c_1},a_{c_2} ...	(n,mn') Charged Particles	22,23,24,28 and
	m = 1 or 2	51-91 with Flag LR
5- (n,a_{c_1} ,a_{c_2} ,a_{c_3} ...)	(n, Charged Particles)	103-109 700-799
6- (n,γ)	Radiative Capture	102
7- (n,2n)		16

where

$\overline{\cos(\theta_{cm})}$ = average of the cosine of the center-of-mass scattering angle.

$$\overline{\cos(\theta)} = \frac{\int_{-1}^{+1} \mu\sigma(\mu,E)d\mu}{\int_{-1}^{+1} \sigma(\mu,E)d\mu} = F_1 \qquad (2.5)$$

where

$\mu = \cos\theta$

F_1 = first coefficient of the Legendre polynomial expansion of the differential scattering cross section.

Inelastic Level Scattering

The average energy of the recoil nucleus is given by

$$\bar{E}_r = E - \bar{E}_{n',1} - E_\lambda \qquad (2.6)$$

where

E = incident neutron energy

E_λ = energy of the excited level

$\bar{E}_{n',1}$ = average kinetic energy in the laboratory system of the emitted neutron

$\bar{E}_{n',1}$ is given by

$$\bar{E}_{n',1} = \frac{2AE}{(A+1)^2}\left[\frac{A^2+1}{2A} - \frac{(A+1)E_\lambda}{2E} + \sqrt{1 - \frac{A+1}{A}\frac{E_\lambda}{E}}\,\overline{\cos\theta}_{cm}\right] \qquad (2.7)$$

where

$\overline{\cos\theta}$ = average of the cosine of the scattering angle in the center-of-mass,

A = atomic weight of the particular isotope (if the material considered is a mixture of isotopes) in which the level considered is excited.

The energy deposition per inelastic level reaction can be written as:

$$E_H = \bar{E}_r + f_c E_\lambda \qquad (2.8)$$

f_c is the fraction of E_λ converted to heat. For example, if internal conversion competes with γ-emission, then f_c is given by

$$f_c = C_F/(1+C_F) \qquad (2.9)$$

where

C_F = internal conversion factor

(n,n')γ to the continuum

Here the average recoil energy is given by

$$\bar{E}_r = E - \bar{E}_{n',1} - \bar{\varepsilon} \qquad (2.10)$$

where

$\bar{\varepsilon}$ = average excitation of the residual nucleas

$$\bar{\varepsilon} = \frac{A^2+1}{A(A+1)} E - \frac{A+1}{A} \bar{E}_{n',1} \qquad (2.11)$$

and $\bar{E}_{n',1}$ = average kinetic energy of the secondary neutron emitted in the laboratory system.

The energy distribution of the secondary neutron, $P(E\to E')$, can be broken down into partial energy distribution $f_k(E\to E')$, where each of the partial distributions can be described by different analytic representations

$$P(E\to E') = \sum_{k=1}^{NK} P_k(E) f_k(E\to E')$$

and at a particular incident neutron energy E,

$$\sum_{k=1}^{NK} P_k(E) = 1$$

The ENDF format allows several analytic formulations for the partial energy distributions, $f_k(E\to E')$.

An expression for $\bar{E}_{n',1}$ is evaluated as follows

$$\bar{E}_{n',1}(E) = \frac{\int_{E'min}^{E'max} E' \, P(E \to E') dE'}{\int_{E'min}^{E'max} P(E \to E') dE'}$$

$$= \sum_{k=1}^{NK} P_k(E) \int_{E'min}^{E'max} E' \, f_k(E \to E') dE'$$

$$= \sum_{k=1}^{NK} P_k(E) \, \bar{E}_{n',1,k} \qquad (2.12)$$

The analytic form of $\bar{E}_{n',1,k}$, depends on the analytic formulation of $f_k(E \to E')$.

For the evaporation spectrum,

$$f(E \to E') = \frac{E' e^{-E'/\theta(E)}}{I}$$

where I is normalization constant which depends on E'_{min} and E'_{max}. ENDF assumes that $E'_{min} = 0$. Using this assumption, we obtain

$$\bar{E}_{n',1,k} = \theta \frac{2e^{x_1} - \{1 + (1+x_1)^2\}}{e^{x_1} - (1+x_1)} \qquad (2.13)$$

where

$$x_1 = \frac{E'_{max}}{\theta}$$

For a simple fission spectrum (Maxwellian)

$$f(E \to E') = \frac{\sqrt{E'}}{I} e^{-E'/\theta(E)} \qquad (2.14)$$

and invoking the assumption that $E'_{min} = 0$, there results

$$\bar{E}_{n',1,k} = \theta \left[\frac{3}{2} - \frac{x_1^{3/2}}{\{\frac{\sqrt{\pi}}{2} e^{x_1} \operatorname{erf}(\sqrt{x_1}) - \sqrt{x_1}\}} \right] \qquad (2.15)$$

The other allowable representations for $f_k(E \rightarrow E')$ in ENDFB are discussed in a later section.

(n,n') Charged Particles

In this type of reaction, in addition to the secondary neutrons, the emission of one or two charged particles occurs. The reaction is generally of the form

$$_{Z_1}X^{A_1}(n,n')a_{c_1}, a_{c_2}, \ldots\ldots a_{c_n}, {}_{Z_2}Y^{A_2}$$

Define

$$E_R = E_r + E_{a_{1_c}} + E_{a_{2_c}} + \ldots + E_{a_{n_c}} \qquad (2.16)$$

where

E_r = kinetic energy of recoil nucleas Y

$E_{a_{i_c}}$ = kinetic energy of the i^{th} charged particle

In kerma calculation, we are not concerned with the partition of energy between charged particles and the recoil nucleus since all charged particles (and the "recoil nucleus") will deposit their kinetic energy at or near the site of collision. This allows the evaluation of E_R applying only the energy conservation principle

$$\bar{E}_R = E - \bar{E}_{n',1} - |Q_o| - \epsilon_Y \qquad (2.17)$$

where

$\bar{E}_{n',1}$ = average energy of the neutron emitted in the laboratory system

Q_o = Q-value for the combined reaction when the residual nucleus is left in the ground state,

ϵ_Y = average excitation of the residual nucleus

Assuming that in an $(n,n')a_{c_k},a_{c_2}\ldots a_{c_n}$ type reaction the neutron is emitted first, $\bar{E}_{n',1}$ can be evaluated as discussed before for inelastic to discrete or continuum level scattering depending on the state of the intermediate nucleas left after the emission of the neutron.

If the residual nucleus, after emitting the neutron and charged particles, is left in the isolated level region, E_R and the corresponding kerma factor must be evaluated for each possible level. If the residual nucleus is left in the continuum range (infrequent for reactions induced by neutrons of energy less than 14 MeV), the evaluation of the average energy of the residual nucleas requires information about the energy spectra of the charged particles emitted. Currently, ENDFB does not provide such information.

In reactions of the type $(n,2n)a_{c_1},a_{c_2}\ldots a_{c_n}$; E_R can be evaluated from the last equation with $\bar{E}_{n',1}$ as the sum of the average energies of the two neutrons.

The total energy release per reaction, E_H, is the sum of E_R and E_{decay} where E_{decay} is the contribution to heat deposition by particle emission (usually β^- or β^+) from the decay of the activated residual nucleus. Methods for calculating E_{decay} will be given after discussing the kinematics of the other types of reactions.

Charged Particle Reactions

The reaction discussed here is of the type

$$Z_1X^{A_1}(n;a_{c_1},a_{c_2}\ldots a_{c_n})Z_2Y^{A_2}$$

where $a_{c_1},a_{c_2}\ldots$ are charged particles; e.g. (n,α), (n,p), $(n,\alpha T)$. The partition of the kinetic energy of the emitted charged particles and the residual nucleus is not needed.

$$E_H = E_R + E_{decay}$$

where

$$E_R = E_{a_{c_1}} + E_{a_{c_2}} + E_{a_{c_n}} + E_r$$

The residual nucleus is frequently left in one of the excited states and the kerma factor for this type of reaction is the sum of the kerma factors to each level, i.e.

$$k = k_0 + k_1 + k_2 + ... + k_N + k_{con} \qquad (2.18)$$

where N is the number of levels and the subscript con denotes continuum.

Denoting E_R, and E_H for the i^{th} level by E_{Ri} and E_{Hi} respectively, we can write

$$E_{Ri} = E + Q_o - \varepsilon_{Yi} \qquad (2.19)$$

where

Q_o = reaction mass Q-value (Q-value to the ground state)

ε_i = energy of level i excited in the residual nucleus.

The quantities E_{Hi} and k_i are

$$E_{Hi} = E_{Ri} + E_{di} \qquad (2.20)$$

and

$$k_i = \sigma_i E_{Hi} \qquad (2.21)$$

where σ_i = reaction cross section for the i^{th} excited state,

and E_{d_i} = contribution to energy deposition by radioactive decay of the i^{th} level (except γ emission)

The expression for k can be easily expressed as

$$k = \sigma[\ (E + Q_o) - E_\gamma + E_{decay}] \qquad (2.22)$$

where

$$E_\gamma = P_1\varepsilon_1 + P_2\ \varepsilon_2 + \ldots + P_N\varepsilon_N \qquad (2.23)$$

$$E_{decay} = P_0 E_{d0} + P_1 E_{d1} + \ldots + P_N E_{dN} \qquad (2.24)$$

and

ε_i = energy of the i^{th} level

P_i = probability that the i^{th} level will be excited given that a reaction has occurred. $= \sigma_i/\sigma$

If other processes compete with γ emission, the ε_i's in the above expression should be adjusted. For example, if internal conversion competes with γ emission from the i^{th} level, then ε_i should be adjusted to

$$\varepsilon_{im} = \varepsilon_i (1-f_c) \qquad (2.25)$$

with

$$f_c = C_F/(1+C_F) \qquad (2.26)$$

where C_F = internal conversion factor.

Radiative Capture

The kinetic energy of the recoil nucleus in an (n,γ) reaction is obtained by momentum and energy balance which yield

$$E_r = E + Q + M_r c^2 - M_r c^2 \sqrt{1 + \frac{2(Q+\frac{AE}{A+1})}{M_r c^2}} \qquad (2.27)$$

where

Q = the reaction Q-value

A = ratio of the nuclear mass of the target nucleas to that of the neutron

$M_r c^2$ = mass of the residual nucleas in energy units $= (A+1)m_n c^2 - Q$

$m_n c^2$ = energy equivalent of the neutron mass (939.512 MeV).

If radioactive decay occurs after an (n,γ) reaction E_H is the sum of E_r and E_{decay}.

(n,2n) Reaction

(n,2n) reactions followed by charged particle emission were treated previously. We are concerned here with (n,2n) reactions followed by γ emission (or internal conversion). The recoil energy of the nucleus is given by

$$\bar{E}_r = E - (\bar{E}_{n_1,1} + \bar{E}_{n_2,1}) - B - \bar{\varepsilon}_{A-1} \qquad (2.28)$$

where

$\bar{E}_{n_1,1}$ = average kinetic energy of first neutron emitted in the laboratory system

$\bar{E}_{n_2,1}$ = average kinetic energy of second neutron emitted in the laboratory system

B = binding energy of the last neutron in the target nucleus.

$\bar{\varepsilon}_{A-1}$ = average excitation of the residual nucleas

Assuming that the (n,2n) reaction is a two-step process, i.e. one neutron followed by another, $\bar{\varepsilon}_{A-1}$ can be shown to be

$$\bar{\varepsilon}_{A-1} = \frac{A^2+2}{A(A+1)} \quad E - B - \frac{1}{A-1} \left[\frac{A^2-2}{A} \bar{E}_{n_1,1} + A \bar{E}_{n_2,1} \right] \qquad (2.29)$$

The average energy of each neutron can be calculated from the energy distribution of that neutron as was done previously. Evaluation of $\bar{\varepsilon}_{A-1}$ requires knowledge of the energy distribution for each of the two neutrons. If only the combined energy spectrum of the two neutrons is known, the calculation of $\bar{E}_r$ without approximation is possible only when the residual nucleas is left in the ground state.

The contribution to the energy deposition from internal conversion and radioactive decay - if any - should be added to $\bar{E}_r$ to get E_H.

Kerma Factors for a Mixture of Isotopes

The kerma factors for a mixture of isotopes can be obtained by summing the macroscopic kerma factors for all isotopes present in the mixture. For example, consider an element or a mixture which consists of several isotopes. The kerma factor for the mixture is

$$K_m = \sum_j K_j \qquad (2.30)$$

and

$$K_j = N_j k_j \qquad (2.31)$$

where

k_j = microscopic kerma factor for the j^{th} isotope in the mixture.

N_j = number density of the j^{th} isotope in the mixture

K_m = macroscopic kerma factor for the mixture

It may be desirable for some natural elements (e.g. Mo, Fe, etc.) which consist of several isotopes to directly evaluate the kerma factors for the element without calculation of the K_j's. This requires appropriate definitions of the various physical quantities involved in kerma calculations. The guiding rule is that the definitions of the physical quantities and the equations for K_m must reproduce equation 2.30. A definition of the Q-value for a mixture of isotopes is discussed below.

Consider a reaction which occurs in one or more of these isotopes, then by definition

$$\text{Q-value for the } j_{th} \text{ isotope} = Q_j = E_{R_j} - E \qquad (2.32)$$

where E_{R_j} is the kinetic energy of the product particles and E is the kinetic energy of the colliding particles. Since the

kinetic energy released in the mixture must equal the sum of the kinetic energies released in the various isotopes in the mixture, we can write

$$N_m \sigma_m E_{R_m} = \sum_j N_j \sigma_j E_{R_j} \qquad (2.33)$$

where E_{R_m} is the kinetic energy of the product particles per reaction in the mixture. Making use of the definitions of Q_j and σ_m which is

$$\sigma_m = \sum_j \frac{N_j \sigma_j}{N_m}$$

we can rewrite Eq. 2.33 as

$$E_{R_m} - E = \sum_j Q_j \frac{\sigma_j N_j}{\sigma_m N_m} \qquad (2.34)$$

Since the left hand side of equation 2.34 is the kinetic energy released by or required for a reaction in the mixture, the right hand side is recognized as the Q-value for the mixture, i.e.,

$$Q_m = \sum_j Q_j \frac{\sigma_j N_j}{\sigma_m N_m} \qquad (2.35)$$

Since definition (2.35) is derived by using only a conservation principle Eq. (2.33) and the basic definition of the Q-value for an isotope, it is a unique definition compatible with the definition of the Q-value for an isotope and it should be acceptable for all physics calculations that use the Q-value in its normal definition.

Similar definitions for the various physical quantities for a mixture of isotopes can be easily developed by applying similar arguments. For example, the average energy of a secondary neutron from a reaction in the mixture and the decay energy can be written as

$$\bar{E}_{n',l,m} = \sum_j \frac{N_j \sigma_j}{N_m \sigma_m} \bar{E}_{n',l,j} \qquad (2.36)$$

and

$$E_{decay,m} = \sum_j \frac{N_j \sigma_j}{N_m \sigma_m} E_{decay,j} \qquad (2.37)$$

Writing an equation for the kerma factor for any reaction in a mixture in the same form as for a single isotope with the physical quantities involved as defined above, it is easy to see that it satisfies Equation 2.30. This is no surprise since kerma itself is a physical quantity and Equation 2.30 is merely an expression for a physical conservation law. In other words, any definition of the physical quantities for a mixture of isotopes that satisfies the physical laws (e.g. energy and momentum conservation) would necessarily be compatible with Eq. 2.30.

A special case implicitly included in Eq. 2.35-2.37 is a reaction which occurs only in one isotope. In this case, Eq. 2.36 reduces to

$$\bar{E}_{n',l,m} = \bar{E}_{n',l,J}$$

where J is the isotope in which this reaction occurs. An example is inelastic level scattering where each level belongs to a particular isotope. Therefore, in applying Eq. (2.7) for a mixture of isotopes, A should be taken as the atomic weight ratio for the particular isotope in which the level considered is excited.

From the above discussion, it can be seen that for single isotopes energy independent parameters such as the Q-value, decay energies, etc. are energy dependent for a mixture of isotopes because σ_j/σ_m is generally energy dependent for any reaction except

the special case of a reaction that occurs only in one isotope.

Another observation worth making is that kerma calculations cannot be accurately made if nuclear data is available only for the mixture and not for the constituent isotopes. For example, the use of only an abundance-weighted Q-value for a reaction such as (n,p) would result in a negative kerma factor for that reaction in an energy range whose width depends on the thresholds of the reaction in and the abundance of the constituent isotopes.

Energy Deposition Due to Radioactive Decay

Particle emission from the decay of the activated residual nuclei must be considered in the calculation of neutron kerma factors as it is another mechanism for local energy deposition. Since radioactive decay is time dependent, the kerma factors for nuclear reactions followed by radioactive decay is time dependent.

However, the most important contribution to energy deposition from radioactive decay is generally from short-lived residual nuclei since the mean-life time for decay decreases rapidly as the disintegration energy increases. The contribution from activated residual nuclei with a mean life time greater than a few days is usually neglibly small. Thus, kerma factors in which radioactive decay is considered only for half-lives less than an arbitrary cut-off (e.g. 10 days)are suitable for steady state heating rate calculations. If the heating rate is to be calculated for a short period of operation of the nuclear system (e.g. start-up), then the contribution from radioactive decay should be calculated separately from the contribution to energy deposition by charged particle recoil from nuclear reactions. Clearly, the latter is always time-independent (energy release not heating rate).

The most frequent type of decay is by emission of β particles. β^+ decay may occur after (n,2n) reactions and β^- after (n,γ) and (n, charged particles) reactions. Since β particles are emitted with an energy spectrum, the average kinetic energy of β particles, $\bar{E}_\beta$ must be calculated. Previous works[6,7] assumed the average kinetic energy of a β particle to be 30% of the end-point for all

isotopes and end-point energies. This assumption severely underestimates $\bar{E}_\beta$.

The basic problem in calculating $\bar{E}_\beta$ is the calculation of the energy distribution of the β-particles. Fermi's theory [12,13] of β decay predicts the probability of emitting a β-particle with kinetic energy E for endpoint energy E_0 to be

$$P(W) = GF(Z,W)(W^2-1)^{1/2}(W_0-W)^2W \qquad (2.38)$$

where,

$$W = \frac{E(MeV)}{0.51} + 1, \qquad (2.39)$$

$$W_0 = \frac{E_0(MeV)}{0.51} + 1$$

Z is the atomic number, and G is a quantity independent of W and its actual magnitude is not important in the following discussion. F(Z,W) is a complicated function which accounts for the effect of the nuclear coulomb potential on the emitted β-particle. The form of the F factor is discussed in Reference 12 and 13 and more detailed references are listed there. A relativistic expression for F is given as

$$F(Z,W) = \left\{\frac{4(1+s/2)}{[\Gamma(3+2s)]^2}\left(\frac{2r}{\hbar/m_oc}\right)^{2s}\right\}\left\{(W^2-1)^s e^{\pi y}\ |\Gamma(1+s+iy)|^2\right\} \qquad (2.40)$$

where

$$S = \left[1-\left(\frac{Z}{137}\right)^2\right]^{1/2} - 1 \qquad (2.41)$$

r = nuclear radius

$\hbar/m_oc = 3.86 \times 10^{-11}$ cm

Γ = complex gamma function

$$y = \frac{aZW}{137\sqrt{W^2-1}} \qquad \begin{cases} a = +1 \text{ for } \beta^- \text{ decay} \\ a = -1 \text{ for } \beta^+ \text{ decay} \end{cases} \qquad (2.42)$$

For $|s|<<1$, F(Z,W), to a good approximation, is given by

$$F(Z,W) \simeq \frac{2\pi y}{1-e^{-2\pi y}} \qquad (2.43)$$

with y as given in Eq. (2.42)

The average energy of a β particle, $\bar{E}_\beta$, can be written as

$$\bar{E}_\beta(\text{MeV}) = 0.51 \frac{\int_1^{Wo} (W-1)P(W)dW}{\int_1^{Wo} P(W)dW} \qquad (2.44)$$

with P(W) given by Eq. (2.38) and F(Z,W) by Eq. (2.40). The nonrelativistic appriximation, Eq. 2.43, has less than 2 per cent error in evaluating $\bar{E}_\beta$ for Z<40. For Z = 0, F(Z,W) is unity.

Eq. (2.44) was evaluated numerically using Eq. (2.43) for F(Z,W) and the results are tabulated in Appendix C for a wide range of Z and E_0 for both β^- and β^+. The ratio, R, of $\bar{E}_\beta$ to the endpoint energy is also tabulated. Several conclusions can be drawn from investigation of R.

The results show that R is generally an increasing function of E_0 and is always greater than 30% for E_0 greater than about 0.5 MeV. It increases rapidly with E_0 and Z up to an E_0 of about 3 MeV after which it varies more slowly. In Figure 1, R is plotted as a function of E_0 for Z = 30 for β^- and β^+ compared with R for Z = 0 for which the coulomb correction is not included. Figure 1 and the tabulated results in Appendix C show that for each endpoint energy R decreases for β^- and increases for β^+ when the nuclear coulomb effect is taken into consideration. The change in R for both β^- and

β^+ is more pronounced at smaller E_0. These observations can be explained as follows. The nuclear coulomb potential represents a potential well for the electrons and a barrier for the positrons. Therefore, in β^- decay a surplus of low-energy electrons is produced resulting in a lower R. For β^+ decay, F(Z,W) of Eq. 2.43 is $\simeq 2\pi|y|e^{-2\pi|y|}$ for low-energy positrons. This is a typical barrier transmission factor. Since $|y|$ increases as Z increases and E decreases (Eq. 2.42) the nuclear coulomb effect is most noticable at high Z and low E. The barrier transmission factor nearly eliminates the emission of low-energy positrons resulting in a higher R. At very low E_0 the β^+ spectrum is almost non-zero only in the neighborhood of E_0 and therefore, R approaches unity as E_0 tends to zero.

$\bar{E}_\beta$ for a given E_0 and Z can be obtained by linear interpolation of R in tables of Appendix C. For isotopes with two or more β spectra with different endpoint energies, $\bar{E}_\beta$ must be calculated separately for each spectrum and summed weighted by the intensities.

As an example of calculating the contribution to the kerma factor from radioactive decay consider radiative capture in Li^7.

$$Li^7(n,\gamma)Li^8 \xrightarrow[T_{1/2} = .84S]{\beta^-} Be^8 \Longrightarrow 2\alpha$$

Li^8 decays by a 100% intensity β spectrum to the 2.90 MeV level of βe^8 which disintegrate immediately to two α particles. Q_{β^-} and Q_α are calculated as 16.002 and 0.095 MeV respectively. Hence, the endpoint β kinetic energy is 13.102 and each α particle has kinetic energy equal to 1.497 MeV. From results in Appendix C for Z = 3, we get $\bar{E}_\beta$ = 6.315 MeV. Hence, the contribution from radioactive decay per (n,γ) reaction in Li^7 is 9.31 MeV. Incidentally, the Q-value for the (n,γ) reaction in Li^7 is 2.032 MeV, and thus

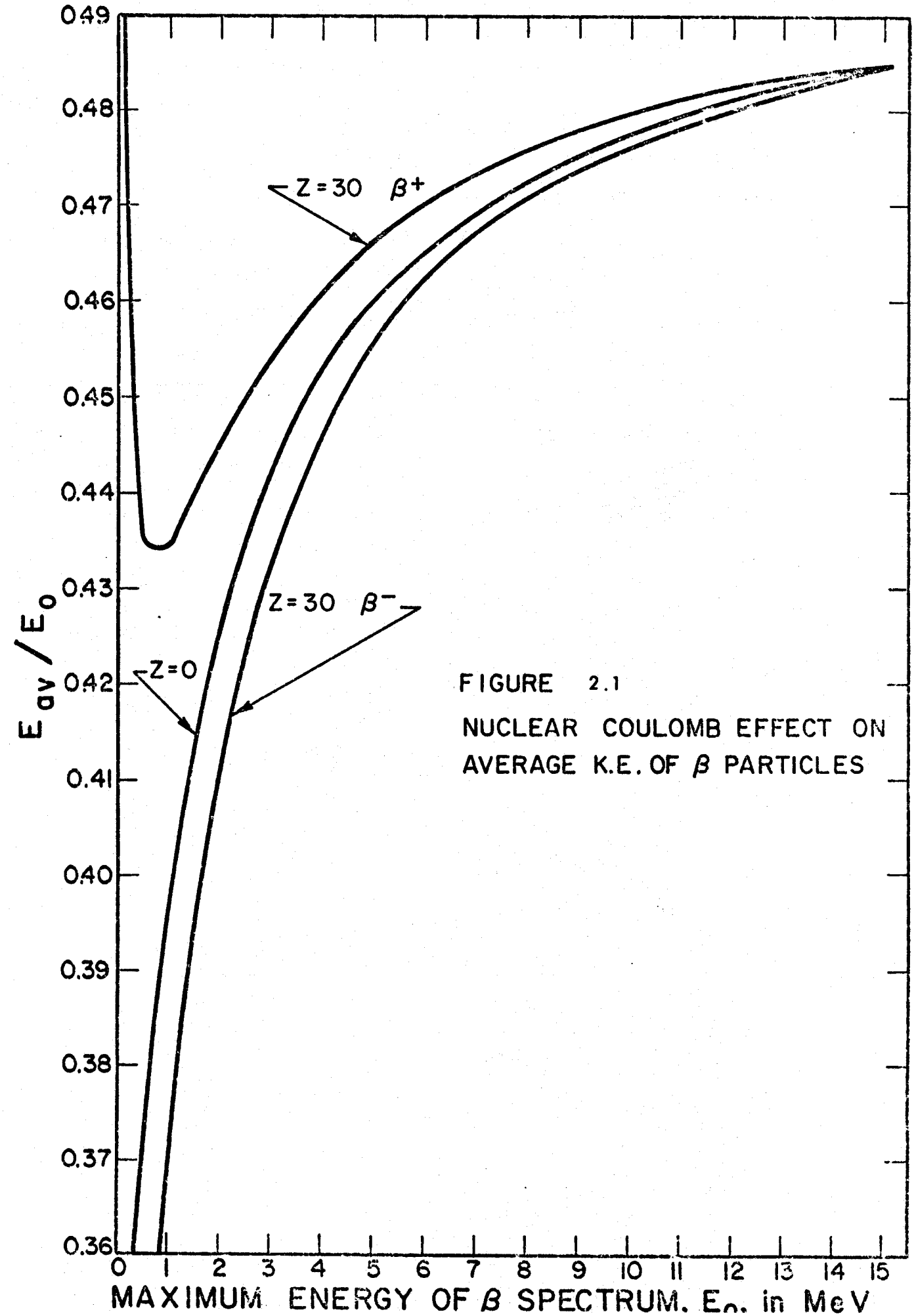

FIGURE 2.1

NUCLEAR COULOMB EFFECT ON AVERAGE K.E. OF β PARTICLES

the kerma factor for that reaction is dominated by the contribution from the decay of the activated residual nucleas.

The average energy of β decay is not usually given in the table of isotopes [14] nor in other compilations of radioisotopes. The β endpoint energy, relative intensities, fraction of electron capture, α-particle energies, half-lives and other required information are usually given in such compilations. This suggests generating a library for the average energy release from radioactive decay for all reactions and isotopes of importance. Such a library will not be only useful for adding the contribution of radioactive decay to kerma factors but also will provide necessary information for calculation of decay heat in nuclear devices. It is also suggested that the average energy release fron radioactive decay following a nuclear reaction be specified in ENDF/B file 1 section 453.

The MACK code provides several options for adding the energy release contribution of radioactive decay that follows a nuclear reaction to the energy release calculated from recoil of charged particles. These options are fully described in the input description section given in the Appendix.

A final point worth mentioning is about the contribution to energy release by gamma emission from radioactive decay. Since the gammas are frequently of high energy, they are transported through the medium away from the site of the neutron reaction and they do not contribute to the local energy deposition. The energy deposition by these gammas can be properly accounted for

by adding them to the secondary gamma production source.

III. ENDF DATA PROCESSING

Nuclear data in ENDF/B format is processed by MACK according to the ENDF "file" order. MACK processes ENDF neutron interaction data files. These files are titled:

File 1 - General Information

File 2 - Resonance parameter data

File 3 - Neutron cross sections

File 4 - Angular distribution of secondary neutrons

File 5 - Energy distribution of secondary neutrons

File 6 - Energy-angular distributions of secondary neutrons

File 7 - Thermal neutron scattering law data

File 1 Data

The descriptive information (MT = 451) is read and printed as it provides a brief description and documentation of the evaluated data. AWR (atomic weight ratio) and LRP (a flag that indicates that resonance parameters are given in file 2) are read and stored.

File 2 Data

File 2 contains data for both resolved and unresolved resonance parameters. For materials that have resonance parameters in file 2, the cross sections calculated from the resolved and for unresolved resonance parameters must be added to the appropriate data in file 3 to get the correct cross sections for radiative capture, fission, elastic scattering and total.

Calculation of cross sections in the resonance region is generally an expensive process. An alternative, for codes such as

MACK that process ENDF data but whose basic purpose is not generating pointwise cross sections, is to read point cross sections for resonance nuclides from an input tape generated by codes such as SUPERTOG[16] or ETOX[21]. This procedure, however, has the obvious disadvantage of depending on another code of the same size or larger. Therefore, a resonance treatment was built into MACK. This resonance treatment was adapted from the well-developed techniques used in some ENDF processing codes (ref. 16-21). MACK also has an option that allows for by-passing the resonance calculations and reading point cross sections for the appropriate reactions in resonance nuclides from an input tape.

The calculation of pointwise cross sections in the resonance region in MACK is discussed in APPENDIX B. These calculations need to be carried out only if the resonance energy range is within the energy range (specified by input) for kerma and group cross section calculations.

The resolved resononance parameters given in single-level Breit-Wigner or multi-level Breit-Wigner representations are processed in MACK. An option is available to get Doppler broadened cross sections at an arbitrary input temperature. In the region of unresolved resonances, the program permits all the three formats of ENDF/B for specifying the average resonance parameters. The details of the resonance region treatment in MACK are given in APPENDIX B.

After all resonance cross sections are computed in both the resolved and the unresolved resonance region, point average cross

sections are calculated in subroutine RXSECT at the appropriate kerma energy mesh points and stored on a scratch device. These cross sections are read in and added to file 3 data later in subroutine SIGPR to obtain the final energy point cross sections.

File 3 Data

The smooth cross sections are read from file 3 and a new cross section set is formed at the energy mesh used for kerma calculation using ENDF/B interpolation schemes. For each reaction, the LR flag is read and stored together with the reaction MT number in order to properly identify the reaction type when the kerma calculation is performed. The reactions Q-values are also stored since they are of basic importance for kerma calculations.

The partial cross sections for charged particle reactions (700's series) are also processed and for each reaction (e.g. (n,p)) the following quantities are calculated

$$E_\gamma(E) = \frac{1}{\sigma}\left[\sigma_1 E_1 + \sigma_2 E_2 + \text{---} + \sigma_N E_N\right]$$

where σ_i = partial cross section for exciting i^{th} level

E_i = energy of the i^{th} level

σ = total reaction (e.g. (n,p)) cross section

An array of E_γ is calculated for each charged particle reaction ((n,p) , (n,d), etc.) since it is needed for kerma calculations for these reactions (see equation 2.22).

If energy group-averaged cross sections are desired by input option, they are calculated from file 3 data smooth cross sections and interpolation schemes using a straight forward average according to the prescription

$$\overline{\sigma}_{g,x} = \frac{\int_g W(E)\sigma_x(E)dE}{\int_g W(E)dE}$$

where x denotes the process; e.g., (n,γ), (n,α), etc.; g denotes the energy group, and W(E) is the weighting function.

The point cross sections are processed and generated in subroutine XSECN. The resonance contribution is added in subroutine SIGPR. Group cross sections are calculated in subroutine CROSG.

File 4 Data

File 4 contains representations of angular distributions of secondary neutrons, and in particular, the distributions for elastically scattered neutrons and for the neutrons resulting from discrete level excitation due to inelastic scattering. Angular distribution data is given in either:

1. Legendre coefficients in the CM (center of mass coordinate system),
2. Tabulated normalized probability distribution in the CM,
3. Legendre coefficients in the LAB (laboratory coordinate system),
4. Tabulated normalized probability distribution in the LAB system.

For elastic scattering, a transformation matrix may be given to be used to transform the data from one frame of reference to the other.

From the theoretical formulation given before, the average of the cosine of the scattering angle in the center-of-mass system for elastic and inelastic level scattering is needed in order to calculate the average kinetic energy of the recoil nucleas in each of these reactions. This is equal to the first coefficient of the Legendre polynomial expansion (in CM system) of the scattered neutrons. If data is given in the first form mentioned above, the

quantity needed is obtained directly by interpolation at the required energy points. For the second type of data, we use

$$\cos\ (\theta_{cm})_E = \int_{-1}^{+1} \mu P(\mu,E)d\mu$$

where $\mu = \cos(\theta_{cm})$

$P(\mu,E)$ = normalized probability distribution of the scattering direction cosine.

The third type is also processed. If the transformation matrix is given it is used, otherwise the code uses the approximation in the papers by Zweifel and Hurwitz[22] and Amster[23] to transform the data from LAB to CM system. The approximations work well only in the case

$$\gamma = \frac{1}{A}\sqrt{\frac{E}{E+Q(\frac{A+1}{A})}} < 1$$

For elastic scattering ($\gamma = \frac{1}{A}$) this condition is always met. However, for some cases of inelastic scattering (and usually for energies close to the threshold energy), this condition is not satisfied. The anistropy in nonelastic reactions is neglected at energies for which the condition is not met.

If data is given as tabulated probability distributions in LAB, Legendre coefficients in the LAB are generated and the treatment mentioned above is used to transform these coefficients into the CM system.

File 5 Data

File 5 contains data for energy distribution of secondary neutrons. The energy distributions are expressed as normalized probability distributions and can be broken down into partial energy distributions.

The partial energy distributions are represented by several forms, as designated by the "LF-number." The energy distribution laws currently allowed in ENDF/B are the following types:

A. LF = 1 Arbitrary tabulated function.

B. LF = 5 General evaporation spectrum.

C. LF = 7 Simple fission spectrum.

D. LF = 9 Evaporation spectrum.

E. LF = 10 Watt spectrum

MACK processes the average energy of the secondary nuetron for nonelastic reactions from file 5 as discussed below.

$$\overline{E}_{n',1}(E) = \frac{\int_{E'min}^{E'max} E'P(E\rightarrow E')\,dE'}{\int_{E'min}^{E'max} P(E\rightarrow E')dE'}$$

This can be written in the form

$$\overline{E}_{n',1}(E) = \sum_{k=1}^{NK} P_k(E) \int_{E'min}^{E'max} E' f_k(E\rightarrow E')dE'$$

$$= \sum_{k=1}^{NK} P_k(E)\overline{E}_{n',1,k}$$

where NK is the number of partial energy distributions and

$$\overline{E}_{n',1,k}(E) = \int_{E'min}^{E'max} E' f_k(E\rightarrow E')dE'$$

The analytic formula for $\overline{E}_{n',1,k}$ depends on the analytic formulation (LF) number of $f_k(E\rightarrow E')$. Expressions for $\overline{E}_{n',1,k}$ for LF = 7 and LF = 9 were given earlier in Equations 2.13 and 2.15. $\overline{E}_{n',1,k}$ for LF = 1

is obtained by numerical integration of $E'f_k(E\rightarrow E')$. For partial distribution given as a general evaporation spectrum $f(E\rightarrow E')=g(E'/\theta(E))$, a new partial distribution $f(E\rightarrow E')=G(E\rightarrow E')$ is obtained and numerical integration is performed. The Watt spectrum (LF = 10) is not programmed into the code since its basic use is for fissionable materials and from a physics point of view it cannot be used in its present format to represent the energy distributions of secondary neutrons in nonelastic processes other than fission.

E'_{min} is specified by ENDF/B to be zero and for LF = 7 and LF = 9, E'_{max} = E-U where U is independent of energy. Those limits were used in the code. However, their usage results in an error in the calculation of the average energy of the secondary neutron and the average excitation of the residual nucleus. The laboratory energy of a secondary neutron can never be zero and the maximum is frequently not representable in the form E-U (with U independent of energy).

Finally, a calculational flow chart for the MACK program is given in figure 2.2.

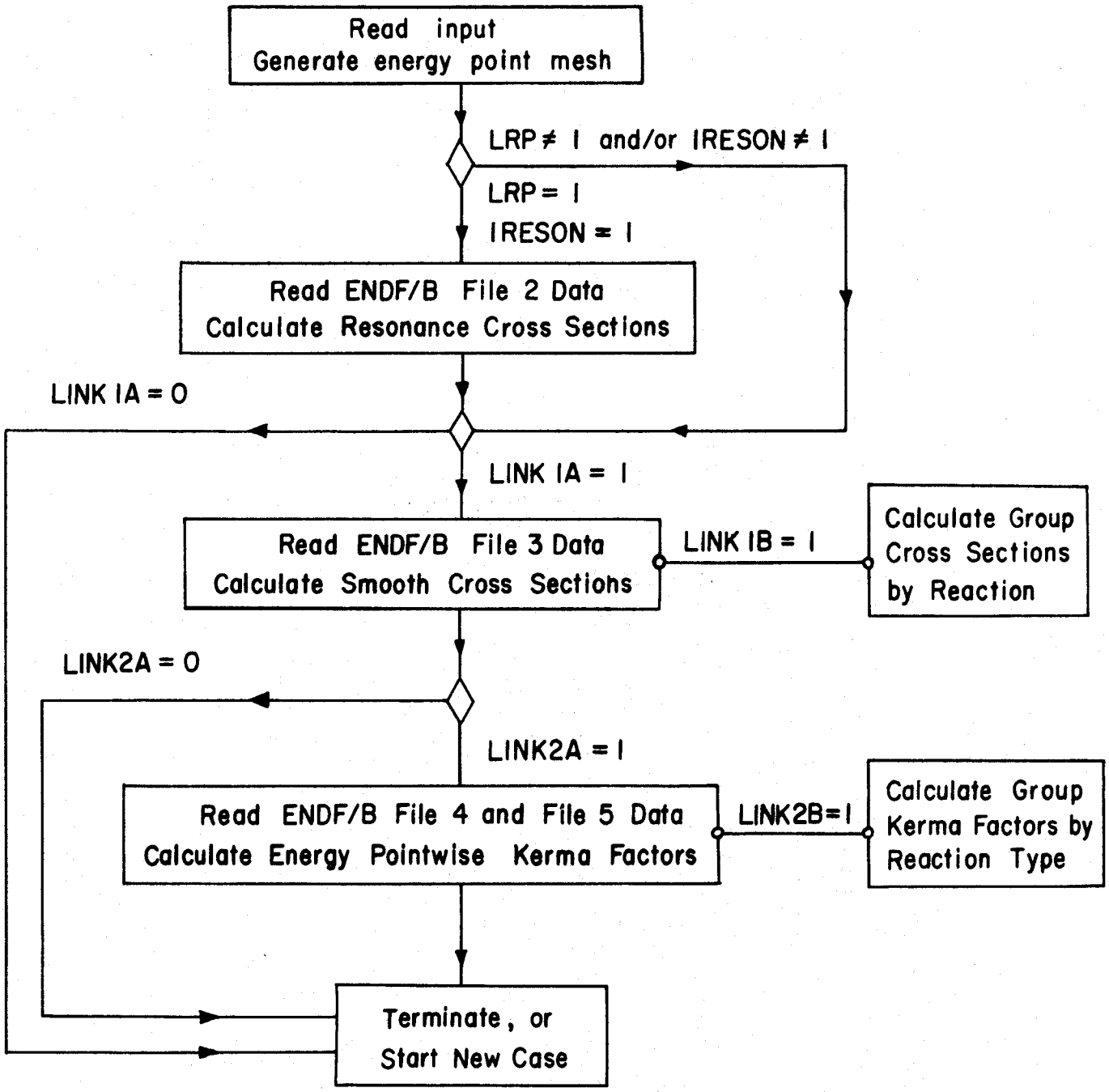

FIGURE 2.2

Calculational Flow Chart for MACK

CHAPTER 3

FLUENCE-TO-KERMA FACTORS

Results, Analysis, and Sensitivity to Nuclear Data

3.1 INTRODUCTION

A theoretical model and computational algorithm for calculation of neutron fluence-to-kerma factors were developed in the preceeding chapter. The computer program, MACK,which was written based on this algorithm to calculate kerma factors from nuclear data in ENDF format, was also described. Since the neutron kerma factors have a wide range of application in other fields in addition to CTR, MACK was written as a general purpose program. It allows great flexibility in generating kerma factors. The energy mesh, group structure, weighting spectra, decay energies, and several other parameters are arbitrarily defined by input values as appropriate for the use to which the data will be applied.

In order to carry out the neutronics and photonics analysis given in a later chapter of this thesis, the neutron and gamma kerma factors and the neutron cross sections by reaction were generated for materials of interest in CTR. A list of these materials is given in table 3.1. In addition to being of prime importance to the nuclear design of the blanket and magnet shield, the data generated is important to other future studies in the CTR area as well as in other nuclear fields. Therefore, the calculated parameters were organized as nuclear data libraries in a general format with efficient retrieval routines.

The energy mesh, group structure, and weighting spectra used in generating these libraries are described in section 2. In section 3, comparison and analysis of neutron kerma factors for the most important CTR materials is given. The validity of the neutron kerma factors calculated in the present work is investigated in section 4. The relation-

ship between neutron energy release parameters and secondary photon production and the consistency of nuclear data and processing codes are also discussed in section 4. For the sake of completeness, this section is concluded with a comparison of the neutron kerma factors obtained from present and previous work. The sensitivity of the energy release parameters to input parameters is explored in section 5.

3.2 Generation of Pointwise and Group Kerma Factors and Partial Cross Sections

Pointwise and group libraries of kerma factors and partial cross sections were generated for CTR materials. A list of these materials is given in Table 3.1 with the corresponding ENDF/B MAT numbers which are also used as the identification numbers in the libraries. The most recent ENDF/B III evaluations were used except for materials with MAT numbers 3023, 3111, and 3000. Flourine was generated from the UK library data. MAT 3023 refers to vanadium data calculated from a recent ORNL evaluation [27] which included (n,n'α) and (n,n'p) reactions. The present ENDF/B evaluation for molybdenum (MAT 1111) does not provide any information about the (n,charged particles) reactions. Since the energy deposition by these reactions at high energy can be as large as 50% of the total neutron heating, it is necessary to include these reactions in kerma calculations. The molybdenum (n,p) cross sections in the UK library and the (n,α) cross sections given in reference [28] were used as zero-order approximations and added to the evaluation and the complete data set for molybdenum was given the identification number 3111.

Reactions considered in kerma factor calculations for each material are listed in Table 3.2. Several evaluations of the present ENDF/B do not provide information about some of the important nuclear data such as the (n,n'α) and (n,n'p) reactions. In all but a few evaluations, the individual level excitation cross sections are not

provided for the (n,α) and (n,p) reactions. The total cross sections for these reactions are often given with an "effective" Q-value. The effect of such lack of information on the validity of the results is investigated in several places in this chapter.

As explained in the previous chapter, charged particle emission from the radioactive decay of residual nuclei should be included in calculating neutron kerma factors. The radioactive decay contribution is included with an arbitrary cut-off half-life of 50 days. The radioactive decay data such as half-lives, decay schemes, β endpoint kinetic energy, etc. given in the latest table of isotopes [14] were used. The average β- particle kinetic energy was determined from the tables given in appendix C. The calculated decay energies are given in Table 3.3 for the appropriate reactions in each material.

The energy mesh used for generating the pointwise kerma factors is described next followed by a description of the group structure and weighting spectra used for calculating group parameters. Generation of gamma kerma factors is also discussed.

3.2.1 Pointwise Neutron Kerma Factors

The pointwise library was generated at 1000 energy points equally spaced in lethargy in three energy ranges. The first energy range extends from thermal energy to 1 eV with lethargy interval, ΔU, of 0.206; the second covers the 1 eV to 1 MeV energy range with ΔU of 0.024, and the third range employs a lethargy interval of 0.00677 from 1 to 15 MeV. The energy mesh emphasizes the 1 to 15 MeV energy range because of its importance in blanket and shield calculations.

Since the neutron cross sections, and hence the kerma factors, show strong variation with energy in many nuclides in the 1 ev to 1 MeV range the energy mesh in this range was chosen such that there are at least five energy points within the boundaries of each group of the GAM-II energy group structure described shortly. The ten energy points in the thermal range was found adequate to accurately describe a Maxwellian or any other appropriate weighting spectrum in this range.

The pointwise library was saved for future use such as 1-generating neutron energy release parameters and partial cross sections at any desired group structure; and 2-inclusion of pointwise kerma factors in nuclear data libraries such as the UK and ENDF/B evaluations.

3.2.2 Energy Group Neutron Kerma Factors and Partial Cross Sections

The multigroup neutron kerma factors and cross sections by reaction were generated from the pointwise data discussed above for the GAM-II one hundred group structure shown in Table 3.4. The group average, f_g, of an energy dependent parameter, f(E), is obtained from

$$f_g = \frac{\int_{E_1}^{E_2} W(E)\, f(E)dE}{\int_{E_1}^{E_2} W(E)dE}$$

where E_1 and E_2 are the group energy limits and W(E) is a weighting function. A discussion of the weighting spectra appropriate for fusion systems follows.

Weighting Spectrum

In choosing a weighting spectrum, W(E), appropriate for fusion systems, it is desirable to use a single weighting function which is adequate for all materials at all spatial points. For practical systems, this necessarily involves some approximations. In the following, an attempt is made to develop a weighting scheme that introduces a minimal error in fusion systems nuetronics calculations.

In typical CTR systems, nearly monoenergetic neutrons impinge on the first wall; the blanket and shield are source free. As known from slowing down theory [25], in the absence of absorption and inelastic scattering, the flux assumes a 1/E behavior below an asymptotic energy, E_{as}, which is roughly equal to $\alpha^3 E$, where E_s is the source energy and the parameter α is equal to $(A - 1/A + 1)^2$. For niobium and lithium, the parameter α is equal to .9579 and .5596 and for a 14 MeV source energy the asymptotic energy is equal to 12.4 and 2.5 MeV, respectively. The behavior of the flux changes significantly in the presence of nonelastic reactions. The presence of absorption has the effect of depressing the flux. Although the effect of inelastic scattering can not be treated analytically in most cases, its effect in qualitative terms is to change the 1/E energy dependence of $\phi(E)$ to E^{-n} with n roughly a constant within the energy limits of an energy group for a fine group structure.

Figure 3.1 shows the flux, $\phi(E)$, versus energy at several spatial points in a typical blanket of a D-T fusion system. The blanket consists of a 1 cm niobium first wall, 42 cm region of 95% Li plus 5% Nb, a 20 cm stainless steel and a 7 cm Li region. The first wall

inner radius (cylinderical geometry) is three meters and the blanket is followed by a one meter mixture of 70% stainless steel plus 30% B_4C. The neutron group fluxes were obtained from a 100 group transport calculation. $\phi(E)$ was obtained at the midpoint energy of each group by dividing the group flux by the energy width for the group. This method of calculating $\phi(E)$ does not provide accurate information about the exact variation of the flux within the groups but it suffices for our purpose here to assume a linear variation of the logarithm of the flux with the logarithm of energy within each group.

The first curve in Figure 3.1a which covers the energy range above 1 KeV shows $\phi(E)$ versus E in the middle of the first wall. Since the mean free path for a 14 MeV neutron in niobium is about 4.5 cm (typical for other proposed first wall materials) a large portion of the source neutrons pass through the 1 cm thick first wall without collision. Hence, the flux in the first wall is high at 14 MeV and decreases very rapidly (faster than E^{-15}) as the energy decreases down to about 12 MeV. At lower energies, $\phi(E)$ varies with E as E^{-n} with n of approximately 2.3 from 5 to 3 MeV, 1.8 from 3 to 1.5 MeV and 0.4 at lower energies. The second curve corresponds to the flux at a point 25 cm from the first wall, i.e. close to the middle of the lithium region. The qualitative behavior of this curve is the same as that of the first wall. The transition energy below which the flux assumes the E^{-n} behavior is, however, considerably lower and is approximately 6 MeV. Above the transition energy, the flux

increases with E as E^5 which is more slowly than in the first wall and the absolute magnitude of $\phi(E)$ is an order of magnitude lower at 14 MeV. Below the transition region, $\phi(E)$ varies also with E as E^{-n} with an n of about 1.8 from 5 to 1.5 MeV and 0.5 at lower energies. The third plot in Figure 3.1 is for $\phi(E)$ 50 cm from the first wall which is deep in the stainless steel region of about two mean free paths (for a 14 MeV neutron). The transition energy is about 6 MeV and the flux varies qualitatively with energy as in the lithium region but faster below the transition energy and slower above.

Figure 3.1b shows $\phi(E)$ versus E for E less than 1 KeV for the three blanket positions of Figure 3.1a. The general behavior of $\phi(E)$ at such low energies varies considerably with the position in the blanket and shield. The strong absorption of lithium-6 affects the spectrum markedly at such low energies in the lithium and neighboring regions. At these low energies, the fraction of neutrons scattered into this energy range by inelastic scattering in structural material (5% by volume in the example considered here) and lithium decreases rapidly and most of the neutrons slowed down to this low energy range come from elastic scattering. In addition, because of the 1/v behavior of the (n,α) reaction in Li-6 the absorption increases so rapidly that the 1/E general behavior of $\phi(E)$ is no longer maintained. In the lithium region flux shown in Figure 3.1b, $\phi(E)$ decreases as the energy decreases roughly as $E^{1/2}$ from about 100 down to 30 eV than linearly at lower energies. Because almost all neutrons in the first wall at this low energy come from the lithium region $\phi(E)$ in the first

wall behaves roughly as that in the lithium. The third curve in Figure 3.1b is for $\phi(E)$ 50 cm from the first wall which is several mean free paths for neutrons of intermediate energies. Because most of the neutrons below 1 KeV at such a point come from slowing down in iron rather than transport from the lithium region the 1/E behavior is maintained down to about 10 eV. Below about 2 eV, the flux in the ion region drops as the energy decreases because of absorption in iron and the decrease in the albedo at the lithium-iron interface. The behavior of $\phi(E)$ with E in the shield region below about 1 KeV is roughly the same as in the lithium region because of the strong 1/v absorption in B-10 (the shield in the reference system discussed here employs 30% by volume B_4C).

In the energy range zero to 0.4 eV no information about the energy dependence can be obtained from the above calculations because the GAM-II group structure employed in these calculations has only one energy group covering this range. Predictions of the flux spectrum at such low energies is complicated by the presence of upscattering in addition to downscattering and strong absorption such as in Li-6 and B-10.

Upscattering is generally important only below a characteristic energy, E_m, of about 0.2 eV. In large systems with no sources from fast neutrons above E_m and no absorption the thermal flux is Maxwellian. In the presence of weak absorption, the neutron flux below E_m is conveniently fitted to a Maxwellian distribution with an empirical neutron temperature, T_n, which is related to the system thermodynamic

temperature, T, by the relation [25]

$$T_n = T(1 + C \frac{\sigma_{ao}}{\xi\sigma_{so}})$$

where C is a constant of approximately 1.6, ξ is the average logarithmic energy decrement per collision, and $\sigma_{ao}(E)$ and $\sigma_{so}(E)$ are the absorption and scattering cross sections at E = KT. The ratio $\sigma_{ao}/\xi\sigma_{so}$ must be less than about 0.2 for the concept of the neutron temperature to be meaningful, otherwise the energy spectrum of thermal neutrons departs too much from Maxwellian. For natural lithium, the ratio $\sigma_a/\xi\sigma_s$ is 260.4 at 20°C. Therefore, in natural or enriched lithium the energy spectrum of thermal neutrons is far from Maxwellian and will vary roughly linearly with energy as a result of the strong absorption of thermal neutrons in Li-6. The same conclusion is true for any system with a large concentration of B-10 or any other strong absorber. In any event, the energy range from zero to a few hundred electron volts is relatively unimportant in the blankets and shields of a D-T fusion reactor as will be seen later in this chapter.

In summary, the energy dependence of the CTR neutron spectra can be divided into four energy ranges, thermal, epithermal up to about 1 KeV, slowing down or moderating region from about 1 KeV to a transition energy (approximately 12 MeV in the first wall and roughly 6 MeV in the rest of the blanket), and above the transition energy to 15 MeV. At thermal energies, the spectrum is not well known at present and $\phi(E)$ is likely to increase linearly with energy. From thermal to about 1 KeV, the energy spectrum of the neutrons varies with spatial position and $\phi(E)$ increases with energy in the first wall, the lithium, and high boron concentration

regions and assumes 1/E behavior at other regions. From about 1 KeV to the transition energy, the flux decreases with energy with a piecewise constant power of roughly 0.4 to 0.7 up to 1.5 MeV and 1.7 to 3 at higher energies. Above the transition energy, the flux increases (with a few exceptions) with energy as E^n with n between 3 and 30. Although the neutron energy spectra may be different for other blankets of different composition and configuration the energy dependence is generally within these bounds.

Since the region above the transition energy is of great importance in calculating the various blanket parameters, a more detailed spectrum needs to be considered in this energy range. Because of ion motion the D-T neutron source has a Gaussian-like distribution of energy centered around 14.06 MeV. Therefore, the spectrum decreases with energy above 14.06 MeV. Again, this effect does not appear in the spectrum of Figure 3.1 because the GAM-II group structure has only one energy group in the energy range 13.5 to 15.0 MeV.

A weighting spectrum that accounts for the energy distribution of the D-T neutrons was developed at LASL [29]. This spectrum is shown in Figure 3.2 and has the form:

$$W(E) = \frac{A}{E} + B \int dT\, f(T) \exp\left\{-\frac{5}{4}\frac{(E - E_o)^2}{E_o\, KT}\right\}$$

where f(T) is the fraction of the D-T neutrons which are generated when the plasma temperature is between T and T + dT. The broadening of the D-T neutron spectrum is taken into account in the expoential term. The average energy, E_o, of a D-T neutron is 14.06 and the parameters A and

B were chosen so as to put 25% of the flux into the 14 MeV peak [29]. Although the 14 MeV spectrum broadening was derived for Scyllac-type reactors (pulsed) it is fairly typical of all other reactor types.

The sensitivity of the energy group constants to variations in the weighting spectrum determines, to a large extent, the degree of elaboration required in spectrum weighting. Hence, it is necessary here to investigate the sensitivity of neutron group kerma factors and partial cross sections to changes in the weighting spectrum. Since the blanket and shield spectrum varies with energy to a power that varies in several energy ranges, the difference between the group constants obtained from flat and a 1/E weighting will be examined. In the thermal region, the results for these two weighting functions will be compared to the Maxwellian weighted constants. The effect of the D-T neutron energy distribution on high energy group constants will also be discussed.

Li-6, Li-7 and vanadium are chosen here for investigating the sensitivity of the group constants to variations in weighting spectra. Li-6 and Li-7 are chosen because the neutron spectrum in the blanket is affected most by these two materials. Furthermore, about 80% of the neutron heating is generated in the lithium region. Although the first wall is the most critical section from a heat removal point of view, most of the energy deposition in the wall is generated by the secondary photons since the wall material is usually of a high atomic number. The sensitivity of group kerma factors to the weighting spectrum will be examined for vanadium because it has the highest neutron to gamma

energy deposition ratio and also because the thermal group is unusually important in this material.

Tables 3.6, 3.7 and 3.8 show the kerma factor by group for flat, 1/E and LASL weighting spectra for Li-7, V, and Li-6, respectively. The results are presented for the groups that

a. have the largest contributions to heat generation,

b. have fine cross section structure for these materials,

and c. show the largest change in group constants for these weighting spectra.

As seen from Tables 3.6 to 3.8, changing the weighting spectrum, W(E), from constant to 1/E changes the group kerma factors by less than 0.2% for groups of energies above 1 MeV. In this energy range, the kerma factors generally increase with energy and hence the 1/E weighting results in lower group average than the flat-weighted. In the KeV energy range, the difference between the group constants obtained from constant and 1/E weighting is higher than in the MeV range because the GAM-II group structure employs a wider lethargy range per group in the KeV region. However, the difference is also small and about 0.5%.

The LASL weighting spectrum, W_L, is 1/E below 12.5 MeV and therefore, it reproduces the same 1/E group averaged constants in all but the first two groups. The 14 MeV peak in W_L increases with E up to 14.06 MeV then decreases. Since the 14.06 is lower than the midpoint energy for the first group, the W_L-group averaged kerma factors for this group are smaller than those produced by 1/E weighting. The 14 MeV peak in W_L covers about two thirds of the energy width of the second group and is

rapidly increasing with energy in this range. The largest difference between the W_L and 1/E weighted group kerma factors occur in this group and is about 1.4% for Li-7 and 5% for vanadium.

In contrast to all other energy groups, the thermal group in all three materials shows a large change of about 43% in group constants when the weighting spectrum is changed from constant to 1/E. This effect is due to the 1/v behavior of the kerma factors at thermal energies for the three materials. This in turn is due to the 1/v behavior of the Li^7 and V(n,γ) and Li^6 (n,α) cross sections. Questions relating to thermal group weighting are examined below.

In general, the kerma factors at thermal energies are much smaller than at higher energies. In the thermal energy range, elastic scattering and radiative capture are the only two mechanisms for energy deposition in most materials. The recoil energy from elastic scattering is very small because of the low incident energy. Although the binding energy for an additional neutron is relatively large in all materials the nuclide recoil energy from an (n,γ) reaction is small because of momentum conservation. Therefore, energy deposition by thermal neutron interactions is small in most materials. The three materials investigated in this section are among the exceptions. The thermal kerma factor is large for Li-7 and V because of β- decay following radiative capture and is large for Li-6 because its (n,α) reaction is exothermic and has a large 1/v cross section at low energy. In these three materials, the energy release per reaction is constant at thermal energies (the energy dependence is extremely small). Therefore, the pointwise kerma factor varies

inversely with $\sqrt{E}$. Thus, the change in the thermal group kerma factor due to changing W(E) from constant to 1/E can be easily shown to be

$$C_1 = \frac{\bar{k}_a - \bar{k}_b}{\bar{k}_b} = \frac{E_2 - E_1}{\sqrt{E_1 E_2}\ \ln \frac{E_2}{E_1}}$$

where the subscripts a and b denote 1/E and flat-weighted quantities, respectively and E_1 and E_2 are the lower and upper energy limits of the group. With E_1 equal to .022 and E_2 equal to .414, C_1 is 43%. The change in the thermal group factor when the weighting function is changed from W(E) = E to W(E) = 1/E can also be obtained for 1/v kerma factors as

$$C_2 = \frac{\bar{k}_a - \bar{k}_c}{\bar{k}_c} = -1 + \frac{2}{3}\ \frac{\sqrt{E_1 E_2}\left(E_1 + \sqrt{E_1 E_2} + E_2\right)\ln E_2/E_1}{E_2^2 - E_1^2}$$

where the subscripts a and c denote 1/E and E-weighted quantities, respectively. C_2 is equal to 72% for E_1 equal to .022 and E_2 equal to .414 eV.

For 1/v pointwise kerma factors, the average over a Maxwellian distribution is simply

$$\bar{k}_m = \frac{\sqrt{\pi}}{2}\left(\frac{T_{no}}{T_n}\right)^{1/2} k_o$$

where T_n is the absolute temperature of the neutrons, T_{no} is the neutron temperature at reference energy E_o in the energy range where 1/v behavior prevails, and k(Eo) is the pointwise kerma factor at Eo. The thermal group in the GAM-II group structure extends from .414 down to an arbitrary

cut-off of .022 or lower. In the energy range 0.2 to 0.414 the upscattering can usually be ignored and the spectrum closely resembles that at higher energies. The effect of using a Maxwellian weighting on the thermal group kerma factor is shown in Table 3.9 for Li-6 at several neutron temperatures. From the results in this table, the following observations can be made. The flat weighting severely underpredicts the group average for a Maxwellian-like flux. The 1/E weighting is also unacceptable if the energy spectrum of thermal neutrons is Maxwellian with neutron temperature of about 300°K. It is also apparent from Table 3.9 that changing the weighting spectrum from 1/E to Maxwellian in the energy range .2 to .414 eV has little effect on the group average. The group kerma factor averaged over a Maxwellian distribution decreases with the neutron temperature as $T_n^{-1/2}$ and at about 700°K it is roughly equal to that obtained from 1/E weighting. For kerma factors and cross sections that exhibit $1/\sqrt{E}$ behavior, the average over 1/E weighting from E_1 to E_2 is equal to the average over a Maxwellian weighting from zero to E_2 if E_1 satisfies the equation

$$\sqrt{T}\ (\sqrt{E_2} - \sqrt{E_1}\ ) = .443\ \sqrt{E_1 E_2}\ \ln E_2/E_1$$

where T is the Maxwellian neutron temperature in energy units with the assumption that very little error is made in extending the upper limit of integration over the Maxwellian from E_2 to infinity. The above discussion about the thermal group averaging should not overemphasize the importance of this group. For the fusion blanket given earlier in

this section, the thermal group is of very little importance in calculating the neutron heating. However, for a nuclear system with a 1/E flux distribution and thermal neutrons following a Maxwellian distribution for 700°K representing only 1% of the integrated flux from thermal to 15 MeV, the neutron heating by thermal neutrons represents more than 20% of the total neutron heating in Li-6 and B-10. The effect of the weighting spectrum on the total neutron heating rate in Li-6, Li-7 and V is shown in Tables 3.6 through 3.8. In these tables, η_s is the neutron heating per unit fluence for uniform (GAM-II) group flux and η_w is the neutron heating per unit fluence for the first wall flux of the CTR blanket discussed earlier in this section. From these tables it can be seen that η_w changes only by about .1% when the weighting spectrum is changed from uniform to 1/E. η_s changes by .06% for Li-7, 3.7% for vanadium and 7.4% for Li-6. The large change in η_s for vanadium and Li-6 is essentially because of the change in the kerma factor for the thermal group. In the uniform GAM-II group flux, the thermal group has 1% of the total population of neutrons. In a lithium blanket, however, the thermal neutron flux is only 10^{-10} of the total flux in a large portion of the lithium region with a maximum of roughly 10^{-5} at the lithium-iron interface in the reference design for Figure 3.1. Therefore, the thermal group contribution to neutron heating is negligible in fusion blankets. The same conclusion is valid for magnet shields with high boron concentration.

From the above results it is concluded that the group kerma factors and partial cross sections are relatively insensitive to weighting spectra which lie between W(E) = constant and W(E) = 1/E for groups above thermal.

This result is for the GAM-II one-hundred group structure and is different for other group structures. A measure of the adequacy of the group structure is the sensitivity of the group constants to the weighting spectrum. In this context, it can be concluded that the GAM-II group structure is adequate for fusion systems in the energy range from 1 eV to about 12 MeV. Although Li-6, Li-7 and V were considered above, similar observations have been noted on other materials and it is believed that the result apply, in general, for all other materials investigated in this work.

From the study presented above, it is concluded that an appropriate weighting spectrum, W(E), for D-T fusion systems is as follows. Above 1 KeV, the use of LASL weighting function is justified because it does reproduce the gross behavior of fusion spectra on one hand and the average group constants are relatively insensitive to detailed variations in the weighting spectrum on the other hand. This result applies only to fine group structures such as GAM-II one hundred group structure. Below 1 KeV, W(E) = E is reasonable because 1 - the most important blanket and shield regions have neutron energy spectra that increase roughly linearly with energy, 2 - the group constants are relatively insensitive to more detailed variations in the weighting spectrum for fine group structures, and 3 - the energy range below 1 KeV is of little importance for neutron heating and reaction rates of interest in the regions where the neutron spectrum departs too much from $\phi(E) = cE$. The thermal group has a negligible effect on the neutronics results for the fusion systems considered in this work and it sufficies to use W(E) = E for thermal neutrons.

3.2.3 Gamma Kerma Factors

Gamma multigroup cross sections were generated with the MUG code for the 43 group structure shown in Table 3.5. This group structure was constructed using an equal energy width of .75 MeV for groups above 8 MeV and .25 MeV in the 1 to 8 MeV range. The gamma cross section variation with energy for the most important CTR materials was taken into account in constructing this group structure.

The gamma kerma factors were generated at the same group structure with 1/E weighting.

3.3 Comparison and Analysis of Neutron Kerma Factors for CTR Materials

Samples of the neutron fluence-to-kerma factors calculated in the present work are shown in figures 3.3 to 3.16. The materials chosen for presentation in this section are those of prime interest for use in CTR blankets, shields and magnets. The kerma factors are plotted in figures 3.3 to 3.14 for the energy range 1 eV to 15 MeV at 100 points generated by taking every tenth point from the 1000-point energy mesh described in the previous section. This choice reproduces clearly the gross behavior of the neutron kerma factors for all materials but does not exhibit all the fine details and in particular some of the very narrow resonances.

Before discussing the results it is useful to summarize the technique for calculating the total nuclear heating. In the preceeding chapter, the nuclear heating was divided into two contributions. The first type is the energy deposition by charged particles and recoil nuclei from the neutron reactions and the second type is the heat generated by the secondary gammas. This classification is rather artificial and is made only to facilitate the calculations. In any nuclear system both types occur. The relationship between the two types of heating is summarized in the following equations;

$$H(\vec{r}) = H_n(\vec{r}) + H_\gamma(\vec{r})$$

$$H_n(\vec{r}) = \sum_j N_j(\vec{r}) \int \phi_n(\vec{r},E_n)\, k_{nj}(E_n)\, dE_n$$

$$H_\gamma(\vec{r}) = \sum_j N_j(\vec{r}) \int \phi_\gamma(\vec{r},E_\gamma)\, k_{\gamma j}(E_\gamma)\, dE_\gamma$$

where $\vec{r}$ = denotes spatial variables

H = total nuclear heating

H_n = neutron heating

H_γ = gamma heating

$k_{nj}(E_n)$ = neutron kerma factor in element j for an incident energy E_n,

$k_{\gamma j}(E_\gamma)$ = gamma kerma factor in element j for a photon of energy E_γ

ϕ_n = neutron flux,

The gamma flux, ϕ_γ, is obtained by solving the transport equation with the secondary photon production source

$$S_\gamma(\vec{r},E_\gamma) = \sum N_j(\vec{r}) \int \phi_n(\vec{r},E_n)\ \sigma_p^j\ (E_n,E_\gamma)\ dE_n$$

$$\sigma_p^j(E_n,E_\gamma) = \sum_i \sigma_i^j\ (E_n)\ f_i^j(E_n,E_\gamma)$$

where

σ_p^j = photon production cross section in element j

$\sigma_i^j(E_n)$ = microscopic neutron cross section in element j for gamma producing reaction i at neutron energy E_n

$f_i^j(E_n,E_\gamma)$ = number of photons produced with energy E_γ per reaction i in element j induced with neutrons of energy E_n.

Thus the nuclear heating is a function of the nuclide densities, neutron and gamma flux spectrum in addition to the neutron and gamma kerma factors. The ratio of H_γ to H_n varies considerably from material to material.

Materials which attenuate neutrons mostly through inelastic scattering reactions have, generally, small neutron kerma factors and large photon production cross sections. Furthermore, these materials are in most cases of high atomic number and they attenuate the photons effectively resulting in a high H_γ to H_n ratio. Therefore, in comparing the neutron kerma factors for various materials it is not true in many cases that the material with the smallest k_n has the lowest nuclear heating. This is generally true, however, for materials of the same (or nearly so) atomic number.

Comparing the neutron kerma factors for several materials for the purpose of comparing "energy multiplication" also does not yield useful results in many cases since the energies of the secondary neutrons and photons are not included in local energy deposition factors. Furthermore, k_n combines the energy release per reaction with the neutron reaction cross sections. Hence, a lower neutron kerma factor does not necessarily imply energy "gain" or "loss". For example, an endothermic (n,α) reaction usually yields a higher k_n, than the exothermic (n,γ) reaction.

The purpose of the above comments was to show that it is difficult in some instances to draw conclusions about "energy breeding", relative magnitude of total heating rate, etc. in various materials by comparing the neutron kerma factors alone. It is also sometimes difficult to get information about energy breeding from the reaction Q-values alone. The ratios of exothermic and endothermic reaction rates to the total reaction rate should be examined. In addition, a material can have a net "energy gain" in one system and "energy loss" in another system depending on the spectra and the energy ranges of importance for exothermic and

endothermic reactions. Some materials are exceptions, however, and many conclusions can be reached by inspecting the neutron kerma factors alone as long as care is exercised. In all cases, the required information can be obtained, of course, from calculating the various response rates in the nuclear system of interest.

Since the neutron heating depends strongly on the spectrum it is helpful here to introduce two reference spectra. The first is the blanket first wall flux given in the preceeding section and will be referred to as the FWS (fusion wall spectrum). The second is a constant flux in all groups of the GAM-II one hundred group structure shown in table 3.4. The GAM-II one hundred group structure employs 0.1 lethargy unit intervals from 15 MeV to 111 KeV and 0.25 lethargy unit intervals at lower energies. Therefore a uniform GAM-II goup flux represents a C_1/E spectrum above 111 KeV and a C_2/E spectrum below with $C_2 = .25\ C_1$. The integrated flux below 111 KeV is approximately equal to that above i.e. 50% of the total. Hence, the uniform GAM-II spectrum emphasizes the low energy range while the FWS emphasizes the high energy range. These two spectra represent the opposite ends of the shield and blanket spectra. Two integral quantities for comparing neutron kerma factors based on these spectra are defined as follows:

η_s = heat generated per unit fluence per atom for uniform GAM-II group flux (qualitative shield spectrum)

η_w = heat generated per unit fluence per atom in the reference CTR first wall system

Table 3.10 tabulates the values of η_s and η_w for CTR materials calculated from the kerma factor results of this work. Very useful information can be deduced from comparing η_s and η_w for the same material and comparing

each of them for different materials. η_s and η_w will be used for various purposes in the rest of this work.

Figures 3.3 to 3.16 show that the energy dependence of the neutron kerma factor, k_n, for a material does not resemble that of the total cross section for the material in the high energy region. In general, the total cross section decreases with energy in the MeV region while k_n increases because the energy release per reaction increases linearly or faster while the total cross section decreases slowly with energy. On the otherhand, in the resonance region, the energy dependence of k_n follows closely that of the total cross section. In the electron volt region, k_n decreases with energy for all but a few materials. In this energy range, k_n is dominated by $\frac{1}{\sqrt{E}}$ (or nearly so) reactions such as (n,γ) in most materials or (n,α) in Li-6 and B-10. The energy release per reaction is rather constant in these cases and k_n follows roughly the energy dependence of the cross sections.

The kerma factor plots are arranged in groups of two or three materials on the same graph for comparison purposes. Figure 3.7 shows the kerma factor for the three basic elements in the human body. More than 95% of the dose in a Standard Man results from energy depositon in hydrogen, carbon and oxygen for incident neutron energies greater than 1 KeV. Below 10 eV the dose comes mostly from neutron interactions in nitrogen. Although k_n for carbon is higher than k_n for oxygen over most of the range the oxygen dose in Standard Man is higher because of elemental percentages. Kerma factors for hydrogen, carbon and oxygen will prove extremely useful in chapter 5 in calculating the dose in the coil insulators.

Figure 3.3 shows that k_n for Li-6 is higher than for Li-7 over the entire energy range from 0 to 15 MeV (This contradicts previous results by Ritts et al. [7]; see section 3.4). Since both materials have the same atomic number the total nuclear heating in Li-6 is always higher than in Li-7 for equal nuclide number density for any spectrum. Table 3.10 shows that η_s for Li-6 is about 800 times η_s for Li-7 but η_w is higher by only a factor of six. Therefore, in the first few mean free paths (for 14 MeV neutrons) of natural lithium (7.42% Li-6 and 92.58% Li-7) the nuclear heating in Li-7 is higher than in Li-6. In the rest of the blanket the reverse is true. Above 5 MeV, the energy deposition in Li-7 is mainly due to the (n, n'α) reaction and elastic scattering. The elastic scattering contribution dominates in Li-7 at lower energies down to about 0.1 MeV where the (n,γ) reaction comes into play. k_n for Li-7 at thermal energies is essentially that of radiative capture which is followed by the 0.85 second β- decay of Li-8. In Li-6, more than 50% of the energy release comes from the (n, n')d reaction for incident energies above 6 MeV with elastic, (n,α) and (n,2n)α reactions contributing the other 50%. The (n,α) reaction has an exothermic Q-value in Li-6 of 4.786 MeV and a large $\frac{1}{v}$ cross section at low energy. For incident energies less than 200 KeV, almost all the heat generated in Li-6 comes from this reaction. In an optically thick Li-6 region with a 14 MeV neutron source, the (n,α) reaction rate is more than 90% of the total nonelastice reaction rate. Hence, more than 4 MeV is converted from mass to kinetic energy and Li-6 is an excellent clean "energy breeder". Except for the radiative capture reaction, all nonelastic reactions in

Li-7 are endothermic and hence there is an "energy loss" in Li-7 through conversion of kinetic energy to mass. The situation is different in Li-7 for incident energies of about 1 KeV or lower. In this low energy range, the (n,γ) reaction dominates and there is a gain in energy of 11.3 MeV per reaction (2 MeV neutron binding energy and 9.3 MeV from the $\beta-$ decay of Li-8 to Be-8 which disintegrates into two alpha particles). The energy multiplication in natural lithium at low energies is governed, however, by the Li-6 (n,α) reaction which has a much larger cross section than the (n,γ) in Li-7.

Figure 3.5 shows the neutron kerma factor, k_n, for the two isotopes of natural boron which is the basic neutron absorber in most shields. k_n is much higher for B-10 than for B-11 in the entire energy range from zero to 15 MeV. This is primarily because of the large energy release from the (n,α) and (n,t) reactions in B-10 above 3 MeV and mostly the (n,α) alone at lower energies. Both reactions are exothermic with Q-value of 2.79 MeV for (n,α) and 0.23 MeV for (n,t) in addition to 0.95 MeV average decay energy per (n,t) reaction. Except for radiative capture, all nonelastic cross sections in B-11 are endothermic. η_s for B-10 is three orders of magnitude higher than η_s for B-11. Therefore, the heating rate in natural boron (19.6% B-10 and 80.2 % B-11) is essentially that of B-10 for a typical shield spectrum. For high energy-shifted spectra such as the first wall spectrum, the neutron heating in B-10 is also more than 70 times the neutron heating in B-11.

Neutron kerma factors for Li-6 and B-10 are larger over most of the energy range than the neutron kerma factors for the other materials

discussed in this section. Although k_n for B-10 is higher than that of Li-6 at energies below 7 MeV Li-6 is a better energy multiplier. The B-10 (n,α) cross section is larger than the Li-6 (n,α) cross section but the (exothermic) Q-value for the latter is about 1.7 times the Q-value for the former.

Figures 3.6 through 3.16 show the neutron kerma factors for other materials of great importance for use in CTR. Vanadium and niobium are proposed for use as the first wall material. Iron, chromium and nickel are the basic constituents of stainless steel which may be used as the first wall material in the first generation of fusion reactors. In addition, stainless steel will very likely be employed for high energy neutron attenuation in the shield and as structural material for the magnet. Copper is used as the stabilizer for the superconducting magnet. Graphite and water are frequently utilized for neutron moderation and reflection purposes in the conceptual designs of the blanket and shield.

Figure 3.16 compares the neutron kerma factors for the important elements in stainless steel, Fe, Cr, and Ni. It can be seen from this graph that k_n for nickel is roughly twice that of iron from 3 to 15 MeV. Hence, k_n for stainless steel can not be approximated by that of iron as is frequently assumed [30]. Stainless steel has usually 10 to 15% nickel. For a typical CTR blanket, approximating the neutron kerma factor for a stainless steel first wall by that of iron underestimates the neutron heating by more than 10%. For the C/E flux in the range 0 to 15 MeV the neutron heating per Ni atom is about three times the neutron heating per Fe atom and approximating the stainless steel kerma

factor by iron underestimates the neutron heating in the shield and magnet by more than 20%.

The neutron kerma factors for natural copper and iron are compared in figure 3.12. Below 10 MeV, copper has a higher kerma factor. η_s for copper is about 50% higher than η_s for iron and about 45% lower than for nickel. The copper gamma kerma factor is also (slightly) higher than for iron and nickel. Therefore, for a typical CTR shield spectrum at the magnet edge the total heating rate per unit volume in copper is roughly 25% higher than in stainless steel (the number of nuclei per unit volume is approximately the same for the two materials).

Figure 3.9 compares k_n for the two of the strongest candidates for use as the CTR first wall material, niobium and vanadium. The neutron kerma factor is also compared for iron, niobium, and vanadium in figure 3.15 for the energy range 1 to 15 MeV which is the range of importance for energy deposition in the first wall. Above 5 MeV, k_n is highest for iron followed by vanadium and lowest for niobium. The main reason for that is the relative magnitude of the (n,α) and (n,p) cross sections for the three materials in this energy range. From table 3.10, η_w for iron is about 2.7 times that of niobium and 2.1 times that of vanadium. η_w for vanadium is 1.26 times η_w for niobium. The difference in the first wall neutron spectra for the three materials does not affect significantly the relative magnitude of η_w. However, the gamma heating in the first wall is considerably higher than the neutron heating (a factor of about 10 for niobium). The relative magnitude of the gamma production source and the gamma kerma factors are not in the same order as for the

neutron heating. A detailed analysis of the nuclear heating in these three and other materials is given in chapter 5.

3.4 Validity of Neutron Kerma Factor Results and the Consistency of Nuclear Data and Processing Codes

3.4.1 INTRODUCTION

Theoretical and computational models for calculation of neutron fluence-to-kerma factors were developed in chapter 2. In the previous two sections of this chapter, the data libraries generated with these models were described and samples of the kerma factor results were presented. The question of the validity of these results is inevitable, however. The answer to this question can be divided into two parts. The first is about the adequacy of the basic nuclear data from which neutron kerma factors were generated. The second is about the validity of the theoretical model and the correctness of the computations. The first part is very difficult to answer and detailed investigation of the accuracy that can be placed on presently available nuclear data is certainly beyond the scope of this work except in the sensitivity sense. However, the most recent, and presumably the best, nuclear data has been used in this work. In addition, a partial answer is given in a later section and the questionable validity of available nuclear data for some materials is brought up.

The best verification of the validity of neutron kerma factors is comparison with integral experiments. Such experiments are not available at present for most of the materials considered in this work. In addition such measurements involve a major effort and therefore such an approach is out of question here. The next approach is direct (desk

calculator-type) calculations of the neutron kerma factors at several key energy points. This method provides a check on the correctness of the computations only since the same kinematics equations given in chapter 2 are used. This approach was used extensively and showed that the computation procedure of the MACK program is carried out correctly.

On the following pages, two other general approaches that provide an overall check on both the validity of the solutions of the kinematic equations and the correctness of computations are developed.

3.4.2 Verification of the Kerma Factor Results by Comparison with Energy Deposition Obtained from an Overall Energy Balance for a Finite Volume

The main purpose of the kerma factors is the calculation of nuclear heating in any system. A basic requirement of such calculations is conservation of energy. Therefore, consider a segment of any nuclear system as shown in figure 3.18. The neutron multigroup cross sections, neutron transport calculations, neutron and gamma energy deposition must all satisfy the basic law of energy conservation. The total energy transported into the system is the sum of the total neutron energy, E_{ni}, and gamma energy, $E_{\gamma i}$. The total energy transported out of the system is the sum of E_{no} and $E_{\gamma o}$. E_n and E_γ can be written as

$$E_n(\vec{r}_s) = \int_{A_s} \int_0^\infty J_n(\vec{r}_s, E)\ E\ dE\ dA_s \qquad (3.4.1)$$

$$E_\gamma(\vec{r}_s) = \int_{A_s} \int_0^\infty J_\gamma(\vec{r}_s, E)\ E\ dE\ dA_s \qquad (3.4.2)$$

Inside the segment, a gain or loss of kinetic energy occurs because of the exothermic and endothermic reactions in which conversion of kinetic energy into mass or vice versa take place. External neutron and gamma sources might be present in the segment as well. Therefore, an energy balance for the segment can be written as

$$\text{"energy absorbed"} = H_n + H_\gamma$$

$$= (E_{ni} + E_{\gamma i}) - (E_{no} + E_{\gamma o}) + E_{sn} + E_{s\gamma}$$

$$+ \sum_j \sum_i R_{ij} Q_{ij} + \sum_j \sum_{i'} R_{i'j} E_{Di'j} \qquad (3.4.3)$$

where H_n = neutron heating rate

H_γ = gamma heating rate

R_{ij} = reaction rate (integrated over the segment volume) for reaction i in element j where reaction i is a reaction in which conversion of kinetic energy to mass or vice versa occur (e.g. inelastic scattering is not included but (n,γ) is)

$$R_{ij} = \int_{\text{volume}} \int_0^\infty N_j(\vec{r})\ \phi_n(\vec{r},E)\ \sigma_{ij}(E)dE\ d\vec{r}$$

Q_{ij} = Q-value for reaction i in element j

$E_{Di'j}$ = decay energy per reaction i' in element j

The decay energy term must correspond exactly to that used in calculation of H_n and H_γ. The neutron and gamma heating rates integrated over the

segment volume are given by

$$H_n = \sum_j \int_{volume} \int_0^\infty \phi_n(\vec{r},E)\ k_{nj}\ (E)\ N_j(\vec{r})dE\ d\vec{r} \qquad (3.4.5)$$

$$H_\gamma = \sum_j \int_{volume} \int_0^\infty \phi_\gamma(\vec{r},E)\ k_{\gamma j}\ (E)\ N_j(\vec{r})dE\ d\vec{r} \qquad (3.4.6)$$

The gamma flux is related to k_n and neutron reactions as discussed in the last section.

From the definition of the various terms in equation 3.4.3, it can immediately be seen that this equation can be satisfied only if 1-neutron total and transfer cross sections, 2-neutron kerma factors, 3-neutron transport calculations, 4-gamma production cross sections, 5-gamma total and transfer cross sections, and 6-gamma transport calculations are all consistent and do preserve the energy. The neutron and gamma multigroup cross sections preserve the energy if the basic nuclear data and the processing codes are consistent. The consistency of the neutron kerma factors in equation 3.4.3 depends also on the basic nuclear data and processing code.

Since the gamma calculations are coupled to the neutron calculations only through the secondary photon production source, equation 3.4.3 can be broken down into the following two equations

$$H_n = E_{ni} - E_{no} + \sum_j \sum_i R_{ij}Q_{ij} - S_{E\gamma} + A' \qquad (3.4.8)$$

where,

$$A' = \sum_j \sum_{i'} R_{i'j} E_{Di'j} + E_{sn} \qquad (3.4.8)$$

$$H_\gamma = E_{\gamma i} - E_{\gamma o} + S_{E\gamma} + E_{s\gamma} \qquad (3.4.9)$$

Assuming that the transport calculations are carried out correctly, equation 3.4.8 is a test of the consistency of the neutron multigroup cross sections, gamma production cross sections and the neutron kerma factors.

For practical purposes, the energy multigroup representation is considered for carrying out the test of satisfying the energy balance equations. This adds another uncertainty since an effective neutron or gamma energy must be known for each neutron and gamma energy group. The effective energy for an energy group is a function of the energy limits of the group and the energy dependence of the flux within the group. Furthermore, an effective particle or photon energy for the group is implicitly assumed in generating multigroup cross sections and kerma factors through averaging over weighting spectra. However, unless the weighting spectrum used in generating the multigroup cross sections and kerma factors is adequate for the system under consideration or the results are insensitive to such weighting the nuclear heating, flux, reaction rates are inevitably in error. For our purpose here, we will assume that the multigroup cross sections and kerma factors available are adequate for use in the energy balance equation with negligible error for the nuclear systems that will be examined shortly and we

concentrate now on obtaining an adequate effective group energy for use in calculating the energy leakage terms in equations 3.4.3, 3.4.7, and 3.4.8.

The value of the effective neutron energy for an energy group can be obtained from investigating the conservation relation for steady state systems which has the form

$$\vec{\nabla}\cdot\vec{J}\ (\vec{r},E)dV + \Sigma_t(\vec{r},E)\phi(\vec{r},E)dV$$

$$= \int \Sigma_t\ (\vec{r};\ E'\rightarrow E)\phi(\vec{r},E')dE' + S(\vec{r},E)dV \qquad (3.4.10)$$

where J, ϕ, and Σ_t are the particle current, flux, and total collision cross section, respectively. S is the independent source, dV is an element of volume, and $\Sigma_t(r;\ E'\rightarrow E)$ is the transfer cross sections from E' to E. Multiplying the above equation by E and integrating over the energy range of an energy group g yields a conservation relation for the energy of the whole population of neutrons in the group g in dV.

$$\int_g E\ \nabla\cdot J(\vec{r},E)dE\ dV + \int_g E\ \Sigma_t(\vec{r},E)\phi(\vec{r},E)\ dE\ dV$$

$$= \int_g E\ dE \sum_{g'} \int_{g'} \Sigma_t\ (\vec{r},E'\rightarrow E)\phi(\vec{r},E')dE'$$

$$+ \int_g E\ S(\vec{r},E)dE\ dV \qquad (3.4.11)$$

Now, define

$$E_{eJ} = \frac{\int_g E\ \nabla\cdot J(\vec{r},E)dE}{\int_g \nabla\cdot J(\vec{r},E)dE} \tag{3.4.12}$$

$$E_{eR} = \frac{\int_g E\ \Sigma_t(\vec{r},E)\phi(\vec{r},E)dE}{\int_g \Sigma_t(\vec{r},E)\phi(\vec{r},E)dE} \tag{3.4.13}$$

$$E_{eT} = \frac{\int_g E\ dE \int_{g'} \Sigma_t(\vec{r},E'\to E)\phi(\vec{r},E')dE'}{\int_g dE \int_{g'} \Sigma_t(\vec{r},E'\to E)\phi(\vec{r},E')dE'} \tag{3.4.14}$$

$$E_{eS} = \frac{\int_g ES(\vec{r},E)dE}{\int_g S(\vec{r},E)dE} \tag{3.4.15}$$

Equation 3.4.11 can be rewritten as

$$E_{eJ} \int_g \nabla\cdot J(\vec{r},E)dE\ dV + E_{eR} \int_g \Sigma_t(\vec{r},E)\phi(\vec{r},E)dE\ dV$$

$$= \sum_{g'} E_{eT} \int_g dE \int_{g'} \Sigma_t(\vec{r},E'\to E)\phi(\vec{r},E')dE'$$

$$+ E_{es} \int_g S(\vec{r},E)dE\ dV \tag{3.4.16}$$

From equations 3.4.12 through 3.4.15, the quantities E_{eJ}, E_{eR}, E_{eT} and E_{eS} are space dependent and a function of the energy limits for group g. E_{eT} is also a function of the energy limits for group g´. Each of these parameters represents a physical quantity. E_{eJ} is the effective (or average) energy per neutron in group g streaming out of dV. E_{eR} is the effective energy per neutron undergoing collision in group g. E_{eT} is the average energy per neutron scattered out of group g´ into group g. E_{eS} is the average energy per independent source neutron emmitted in group g. Clearly, the four quantities are not equal for practical systems. Hence, strictly speaking, there is no single "effective neutron energy" for each group that can be used to calculate all terms of energy balance in an energy group. If all four quantities are assumed to be equal equation 3.4.16 reduces to the transport equation in multigroup form.

The quantities E_{eR} and E_{eJ} needed for use in equation 3.4.3 are not equal unless the energy dependence of $\nabla \cdot J$ is the same as the energy dependence of $\Sigma_t \phi$. This can not be generally true since J is the integral over the angular variable of the angular flux times the direction vector while ϕ is the integral of the angular flux only. However, since it is difficult to obtain the exact variation of the flux and current with energy within an energy group it is important to find out the error in using the midpoint energy, E_{mid}, of the energy range E_1 to E_2 in calculating

$$\bar{E} = \frac{\int_{E_1}^{E_2} E\, f(E)\,dE}{\int_{E_1}^{E_2} f(E)\,dE} \qquad (3.4.17)$$

For f(E) = constant, $\bar{E} = E_{mid}$. For f(E) = E and f (E) = $\frac{1}{E}$, it can be seen that in both cases

$$\left| \frac{\bar{E} - E_{mid}}{E_{mid}} \right| < \frac{(\Delta U)^2}{12} \qquad (3.4.18)$$

where ΔU is the lethargy width of the energy range E_1 to E_2. Therefore, for an energy group of lethargy width of 0.1, the average energy for an energy distribution, f(E), can be approximated with the midpoint energy to an accuracy of better than 0.1% if f(E) has the form E^n where n ranges from -1 to 1.

The within group flux in a fusion blanket varies with energy as E^n with n from -.3 to -1 below 12 MeV and greater than 3 above. The fraction of the neutrons, hence the energy, above 1 MeV is large. Since ΔU for the GAM-II group structure is 0.1 for groups in this energy range the error in calculating quantities such as the energy spatial leakage for such groups using the midpoint energy as the effective energy for the group is less than 0.1%. Furthermore, the error for the first two or three groups (largest energy and a considerable fraction of the total number of neutrons for several mean free paths away from the source) is

negative, and for most of the lower groups is positive, resulting in a cancelation of most of the error. In the shield region, however, the within group flux is roughly 1/E and is shifted towards low energies. At low energies, the GAM-II group structure has a lethargy width per group of .25 and the 46 group structure shown in table 3.19 has 0.75 lethargy width. For these groups, the uncertainty in calculating the effective neutron energy per group is about 0.5% for the hundred group structure and 4% for the 46 group structure. In any case, the calculation of the neutron energy leakage term in equations 3.4.3 and 3.4.8 is accurate to better than 3% for fusion blanket and shield spectra when the effective energy for the neutrons within an energy group is approximated by the midpoint energy of the group.

Consider now the nuclear system shown in figure 3.19. This system represents a proposed design for a fusion blanket and shield. For our purpose here, it is merely a nuclear device with a 14 MeV neutron source impinging on the first wall. A 46 neutron energy group transport calculation was obtained for this cylindrical geometry-system using the ANISN code. The multigroup cross sections were obtained from the DLC-2D library [31] which was generated from ENDF/BIII with the SUPERTOG code [16] using a 1/E weighting spectrum. The 100 group data of DLC-2D were properly collapsed into the 46 group form using a typical fusion spectrum. The secondary gamma source was calculated as described in the last section with the gamma production cross sections obtained from a variety of sources. The Li-6, Li-7, Nb and C-12 photon production cross sections were obtained from reference 7. Iron and lead gamma production

cross sections were processed with LAPHFØR from ENDF/B3 gamma production data as described in chapter 5. B-10 and B-11 photon production data were approximated in the shield region by C-12 data. This approximation does not introduce any significant error in the energy balance since the total gamma energy produced by boron carbide in the shield is much less than that produced by the lead and iron.

The energy balance was investigated for several zones of the system described above. Table 3.18 shows the results by zone for each term of equation 3.4.8. The reaction rate term is also shown for each zone broken down into contributions by material and reaction because of the importance of individual reaction rates to other areas of investigation and for purposes of complete documentation for this energy balance. Other details about this system are also given in chapter 5. All energies in table 3.18 are in units of MeV. The reaction rates for each zone are integrated over the zone volume and are given per centimeter along the axis per second. The volumetric neutron source in the plasma region was normalized to one neutron per second.

Table 3.18-a shows the individual terms of the energy balance for the one centimeter niobium wall. The table shows that the sum of the neutron heating rate and the total energy of the gamma source has a large error of about 16%. Since the neutron heating in this zone is only about 5% of the gamma energy source it does not contribute significantly to this error. Furthermore, it can be easily seen from table 3.18-a that the gamma energy source (derived from reference 7) alone is higher than the sum of both the gamma energy source and neutron heating required to satisfy the energy balance. A rather definite conclusion

Table of Nuclide Densities

used for the design of Figure 3.19

Material/Nuclide	Nuclide Density ($atoms/cm^3 \times 10^{-24}$)
Niobium	0.0556
95% Li + 5% Nb	
Li^6	0.00327
Li^7	0.04408
Nb	0.00278
Iron	0.0849
35% Fe + 35% Pb + 30% B_4C	
Fe	0.02971
Pb	0.01172
B^{10}	0.00652
B^{11}	0.02642
C	0.008255

can be reached from table 3.18-a that the nuclear data for niobium from which the gamma production cross sections of reference 7 are derived is not consitent with the nuclear data of the ENDF/B3 evaluation for niobium. Since niobium is one of the strongest candidates for use as a structural material in CTR and the first wall is the most critical component from a heat transfer point of view, 16% uncertainty in nuclear heating in this component is undesirable. The ENDF/B3 evaluation for niobium does not provide gamma production data and no information other than that of reference 7 was available to the author at the time this work was carried out.

Table 3.18-b shows the energy balance for zone 4 which is 20 centimeters of 95% natural lithium plus 5% niobium. The table shows that the sum of the neutron heating and gamma energy source are correct to within 3%. The gamma energy source is dominated by the contribution from niobium which was seen from the above discussion to have an error of about 16%. In addition, the Li-7 gamma source derived also from reference 7 will be shown on the following pages to have a similar error. Since the gamma energy source is only about 30% of the neutron heating in zone 4, the error in the sum of the gamma energy source and the neutron heating is only 3% in this zone which shows that the neutron kerma factors for Li-6, Li-7 and niobium calculated in the present work are correct indeed (at least in an integral sense). To put it more quantitatively, if the error in the gamma energy source is corrected by subtracting the error shown above the neutron heating rate is found to satisfy the energy balance exactly.

Table 3.18-c shows the energy balance for zone 7 which is 25 centimeters of iron. The energy balance shows that the nuclear data, neutron kerma factors and gamma production source are consistent within 3%. The magnitude of the error is not large and shows that no gross error exists in neutron kerma factors nor in the gamma production. Furthermore a fraction of this error can be attributed to the use of the midpoint energy as the effective energy of the neutrons in a group. However, since all the data in this zone, namely multigroup cross sections, neutron kerma factors and gamma production cross sections for iron were all generated from the same evaluation (ENDF/B3), a better consistency would have been expected and a few words about a possible source of this inconsistency is in order.

Currently, the nuclear data evaluations in ENDF/B and other widely used libraries are divided into neutron files and gamma files. There is no one to one correspondence between the neutron files and gamma files in most cases. For example, the neutron cross sections may be given for inelastic scattering for each individual level and for each individual reaction such as (n,p), (n,n´p), etc. while the multiplicities of gamma rays for all or some of these reactions are combined together into a continuum distribution. The attempt to combine the discrete multiplicities into a continuum can result in an increase or decrease of the total gamma energy. Another example is that the gamma files inevitably rely heavily on references and measurements different from those used for the neutron files. In many instances, the neutron cross sections for reactions such as (n,n´α) and (n,n´p) are not provided in the neutron

files while the photon production from these reactions is included in the gamma files. The cross sections for reactions to discrete levels such as (n,α) and (n,p) are not given while again the gamma contribution from these reactions is combined with other gamma production data. The point is pursued in the next subsection with a suggested "partial remedy" on the part of processing codes.

It should be pointed out clearly, however, that it was found, in the course of the present work, that the error in the energy balance when multigroup cross sections, neutron kerma factors, and gamma production cross sections are all derived from the same ENDF evaluation is usually much smaller than the error which results when the nuclear parameters are derived from different data sources. This is illustrated at the end of table 3.18-c by showing the energy balance when the gamma production data are derived from DNA evaluation 4180 Mod.1 [32] while the neutron multigroup cross sections and kerma factors are derived from ENDF/B evaluation 1180. The gamma energy source calculated from the DNA evaluation is 23% higher than the gamma source calculated from the ENDF evaluation. This example points out clearly the need to exercise a great deal of care in calculating multigroup cross sections, neutron kerma factors and secondary gamma production cross sections to ensure the consistency of the variety of nuclear data from which these parameters are derived. In calculating nuclear heating, it is the total heating which is usually of greatest concern rather than the exact partitioning into neutron and gamma heating. A slight increase or decrease in the neutron heating with a corresponding adjustment in the gamma production

data to preserve the energy results in a slight change only in the spatial dependence of nuclear heating but the integral over a finite volume will have a much better accuracy. The perfection of both neutron interaction and secondary gamma production data cannot be achieved today nor is it likely to be possible in the near future. Therefore, a compromise solution can be sought in light of the above discussion by processing the photon-production matrix simultaneously with the neutron kerma factors. This allows the development of a scheme to preserve the energy and provide more consistent nuclear parameters.

Table 3.18-d shows the energy balance for zone 10 which is 10 centimeters of 35% Fe, 35% Pb and 30% B_4C. The neutron heating in this region is more than 7 times the gamma source and therefore the energy balance represents a very good test of the correctness of neutron heating calculated with the neutron kerma factors obtained in the present work. Table 3.18-d shows that the error is only 0.7% which is well within the uncertainty expected in carrying out this energy balance as discussed earlier in this section.

From the results of this section and several similar studies for other materials, the validity of the neutron kerma factors calculated in this work is verified in an integral sense. This verification is only for the overall correctness of the theoretical model and computations of the kerma factors for a given set of nuclear data. This method of verification, however, does not guarantee the absence of compensation of error in the various energy ranges and does not answer the question about the adequacy of the basic nuclear data from which the kerma factors

are calculated. A method for a direct check of the neutron kerma factor at any energy point is developed next followed by pointwise verification of the kerma factor results obtained in the present work and comparison with previous work. The question of the basic nuclear data is discussed in the sensitivity study given later in this chapter.

3.4.3 An Alternative Algorithm for Calculating Neutron Kerma Factors

Consider a unit current beam of monoenergetic neutrons impinging on an atom. A "pointwise"energy balance can be written as follows:

Total Energy going into collision = A + B + C + D

where

A = Kinetic energy of recoil nuclei and charged particles emitted in all reactions.

B = Kinetic energy of the neutrons emerging from the neutron reactions.

C = total energy of photons produced.

D = Kinetic energy converted to mass minus mass converted to kinetic energy.

Rearranging the above equation and making use of the neutron kerma factor definition (see chapter 2), the following equation can be written

$$k_n(E) = E\,\sigma_t + \sum_i \sigma_i\, Q_i + \sum_{i'} \sigma_{i'} E_{Di'}$$

$$- \sum_j \sigma_j\, \bar{E}_{n,j} - \sum_g \sigma_g E_{\gamma,g} \qquad (3.4.20)$$

where

$k_n(E)$ = neutron kerma factor at energy E

E = kinetic energy of the incident neutron

σ_i and Q_i are cross sections and Q-value for reaction i in which conversion of kinetic energy to mass or vice versa occurs. $\sigma_{i'}$, $E_{Di'}$, are cross section and average decay energy per reaction i'.

σ_j = cross section for a secondary neutron producing reaction j

$\overline{E}_{n,j}$ = average kinetic energy of the secondary neutron produced in reaction j (a sum over the kinetic energies of all emerging neutrons if more than one neutron is produced in reaction j).

σ_g = cross section for photon producing reaction g

$E_{\gamma,g}$ = total energy of all photons produced in reaction g

The last term in equation 3.4.20 can be written as

$$E_\gamma(E) = \sum_g \sigma_g E_{\gamma,g} = \int \sigma_p(E,E_\gamma) E_\gamma \, dE_\gamma \qquad (3.4.21)$$

where $\sigma_p(E,E_\gamma)$ is the gamma production cross section for a neutron of energy E for producing a photon of energy E_γ as defined in section 3.3. Note the difference in the definitions of E_γ and $E_{\gamma,g}$. The energy dependence of the various parameters in equation 3.4.20 should be clear.

It can be easily verified that the sum over all reactions of the neutron kerma factor for each reaction as given in chapter 2 does indeed reproduce equation 3.4.20. Although equation 3.4.20 looks simpler

than the several reaction type equations given earlier it does not provide a better computational algorithm if only the neutron nuclear data are to be used. Calculation of the first three terms in the above equation is essentially equivalent to the calculations required by the kinematics equations of chapter 2 except for calculating the excitation energies of the residual nuclei from the various reactions. If only nuclear data for neutron interactions (i.e. neutron cross sections, Q-values, secondary neutron energy and angular distribution) is available, the calculation of the last term in the above equation requires the use of the solution to the kinematics equations of chapter 2 and equation 3.4.20 provides nothing new in this case.

Equation 3.4.20, however, has the merit of combining gamma energy production from all reactions into one term, E_γ. Therefore, if only the total gamma energy produced per unit flux at neutron energy E is known (measured, tabulated, etc.), the above equation provides the basis for a very efficient algorithm for calculating the neutron total kerma factor. Since E_γ is an integral quantity and can be derived from information about the gamma energy spectra from a <u>total collision</u> only, it can be measured presumably with a much better accuracy than the several nuclear parameters required for calculating the excitation energy for each individual gamma producing reaction. Furthermore, if E_γ is well known, it can also be used for normalizing the photon production energy spectra in calculating the gamma production cross sections. Hence, a knowledge of E_γ for the neutron energy range of interest is a key for calculating self-consistent and energy preserving nuclear data sets of

neutron kerma factors and gamma production cross sections.

Unfortunately, the data about gamma production suffers from large uncertainties at present. For example, Li-6, Li-7, C-12, niobium, molybdenum, boron, copper, and several other materials are of prime interest for use in the CTR. However, there exists no information about gamma production for these materials in the widely used nuclear data libraries such as ENDF/B. In addition, the unevaluated gamma production data for these materials available in literature suffer from large uncertainties as will be shown shortly.

Because the nuclear data for neutron interaction is presently much more reliable and complete than the photon production data the philosophy of this work was to develop a computational algorithm for calculating neutron kerma factors from neutron interaction data only. The excitation energies of the residual nuclei are calculated by applying the momentum and energy conservation relations as described earlier. E_γ is calculated in MACK concurrently with neutron kerma factors computations and can serve to fix the normalization of the gamma production data for purposes of preserving the energy .

Equation 3.4.20 can be rewritten as

$$T_{n\gamma}(E) = k_n(E) + E_\gamma(E) = E\,\sigma_t + \sum_i \sigma_i Q_i + \sum_{i'} \sigma_{i'} E_{Di'} - \sum_j \sigma_j \bar{E}_{n,j} \qquad (3.4.22)$$

$T_{n\gamma}$ can serve in some special cases for estimating the total nuclear

heating if it is assumed that each photon is absorbed at the place of birth. Although the total energy deposition in a sufficiently large volume calculated in this manner will be correct the spatial distribution of the nuclear heating is in error in most cases for which E_γ is not much smaller than k_n. For example, in the reference design of figure 3.19 the gamma energy deposition in the first wall is only 60% of the gamma energy produced in the region. For the lithium region (zone 4), however, this ratio is 94%.

Equation 3.4.22 is useful in desk calculator-type caculations of neutron kerma factors at any desired incident energy. In addition, since both k_n and E_γ are always positive, k_n must be smaller than $T_{n\gamma}$. This trivial observation will serve a non-trivial purpose in the following comparison of the present work results with previous work.

3.4.4 Comparison with Previous Work

As mentioned earlier there were several efforts at calculating neutron kerma factors [reference 2 through 7] prior to the present work. A comparison of the neutron kerma factors calculated in the present work with previous work is in order.

Most of the previous work was directed toward calculating kerma factors for elements which are major constituents in the human body. Several simplifying assumptions were usually employed in the previous work. The most notable of these are the neglect of the total contribution of some important reactions, ignoring the anisotropy of elastic scattering, failing to include the resonance contribution to appropriate reaction cross sections in several cases, and inadequate treatment of the partitioning of the energy deposition and secondary neutron and photon emission. In addition, none of the previous works had a general format or computational algorithm for calculating neutron fluence-to-kerma factors and the same effort had to be duplicated for each material or for a new revision of the basic nuclear data for the same material.

The present work has the following merits over the previous work:
1 - development of a complete theoretical model for calculating the neutron kerma factors for all significant reactions based on accurate solution of the kinematics equations of nuclear reactions without incorporating any significant simplifying assumption,
2 - based on this theoretical model an efficient computational algorithm was developed for calculating neutron kerma factors directly from nuclear data in the widely used format ENDF/B. The computer program MACK which incorporates this algorithm processes all reactions signif-

icant to energy deposition and recognizes all of the multiplicity of data formats currently allowed by ENDF/B. Given also the fact that most of the other widely recognized data libraries such as the United Kingdom (UK) library can be converted to ENDF/B format by already existing codes [43] the neutron kerma factors can be processed with MACK using the most widely used, and in a sense the best, nuclear data currently available.
3 - an efficient treatment of the resonance region was built into the MACK program to calculate the contribution to cross sections from the resolved and unresolved resonance parameters including the Doppler effect,
4 - these theoretical and computational models are independent of the actual values of nuclear parameters, and as nuclear data is updated or new information becomes available the only requirement for calculating a new set of kerma factors is a few minutes of machine time,
5 - the contribution to energy deposition from radioactive decay of the residual nucleus of a nuclear reaction is calculated accurately. The Fermi theory (see chapter 2) of β-decay is used to calculate the average kinetic energy of a β^- or β^+ particle for a given endpoint energy, E_0, of the β-spectrum, and atomic number, Z, of the residual nucleus.
6 - the accuracy of the kerma factors calculated with the theoretical and computational algorithms of the present work is set only by the accuracy of the basic nuclear data used.

The most recent ENDF/B3 data and in some cases the UK data were used for calculating the neutron kerma factors presented in this work. The evaluations of these libraries are far from perfect as will be noted in various places, but due to the extensive efforts spent on preparing and revising these evaluations and their wide usage they represent the

most recent and presumeably the best data available at present. Thus it is fair to say that the neutron kerma factors presented in this work are calculated to the best of our present knowledge of nuclear data. The evaluations for materials of interest for CTR were investigated with particular care and revised to ensure that the kerma factors are adequately determined.

The most recent and extensive among the previous works is that of Ritts et al reported in references 6 and 7. They made a real attempt to include a large number of significant reactions for several materials. However, their work had the following drawbacks which greatly affected the accuracy of their kerma factor results.

a - They assumed [6,7] the evaporation model to be valid in all cases for describing the secondary neutron energy distribution from inelastic scattering to continuum and (n,2n) reactions. This assumption is known to be invalid in several cases; e.g. in the Be^9 (n,2n) reactions. (The present work allows for a general format for describing the secondary neutron energy spectra.)

b - They also assumed [6] that the nuclear temperature for this evaporation model can be calculated from the Fermi gas model [44, 45] which predicts the nuclear temperature θ as $\theta(E) = \sqrt{10E/A}$ where E and θ are in MeV. This relation is very approximate, particularly for magic or near magic and light nuclei.

c - The Ritts et al treatment of the inelastic scattering to the continuum yields particularly poor results for the following reasons. They always incorporated the evaporation model for representing the secondary neutron energy spectra which, if adequate, is valid only for <u>true</u> inelastic scattering to continuum, i.e. when the <u>residual nucleus</u> is left

in the continuum energy range. However, the nuclear data they used combines all models of inelastic scattering (level and continuum) for incident energies above certain energy (in rather arbitrary fashion in most cases) and the combined cross sections are identified as the cross sections for inelastic scattering to the continuum regardless of the state of the residual nucleus. Consequently, the secondary neutron energy distribution in such cases includes the discrete spectrum from level scattering and the use of an evaporation model for this secondary neutron spectrum yields poor results for the average energy of the secondary neutron. Furthermore, the solution of Ritts et al [6 & 7] of the kinematics equations for inelastic scattering to the continuum relies on using the quantity Q_{min} which is the Q-value for the minimum excitation energy for the continuum range in the residual nucleus. Since the data they used had a different definition of inelastic scattering to the continuum, Q_{min} was given as zero in most of their nuclear data. Given the fact that Q_{min} is typically a few MeV it is clear that the neutron kerma factors calculated in Ritts et al were not correct in such cases. (The present work has intentionally avoided incorporating any Q-value in the calculations for inelastic scattering to the continuum for this reason. Rather, an accurate calculation of the known secondary neutron energy spectra was employed.)

d - In several cases, the anisotropy of the elastic scattering was entirely [4, 46] ignored in the work of Ritts et al. This resulted in very poor kerma factors, particularly in the high energy range, as will be shown shortly. (Here, the anisotropy of both elastic and inelastic scattering are treated as accurately as the data permits.

e - Some evaluations of nuclear data used by Ritts et al (05R and

ENDF/B1 & 2) provided the resonance parameters for the resonance region and the smooth cross sections given in this range were the background cross sections only. Due to the lack of a resonance treatment in Ritts technique, the contribution of the resonance cross sections was ignored [46] in such cases. This affected their kerma factor results for elastic scattering and radiative capture in the resonance region. (The MACK program developed in the present work has a "built-in" capability for calculating the contribution from both the resolved and unresolved regions including the effect of Doppler broadening.)

f - No attempt was made in the work of Ritts et al to calculate the excitation energy of the residual nucleus from the (n,2n) reaction and the gamma energy emission from this reaction was ignored, i.e. it was implicitly assumed to be deposited locally. This can be clearly seen from equation 17 in reference 6 and equation 12 in reference 7. (The excitation energy of the residual nucleus is calculated from equation 2.29 of chapter 2 in the present work).

From the above discussion it is clear that large differences between the neutron kerma factor results obtained in the present work and those calculated by Ritts can be expected even if the nuclear data used in both works were the same because of the assumptions in the calculational and processing models. In addition, due to the frequent changes in basic nuclear data from one evaluation to another the nuclear data used by Ritts (05R and ENDF/B1 & 2 libraries) several years ago is different in many instances from the most recent nuclear data used in the present work (ENDF/B3).

Tables 3.11 through 3.17 compare the neutron kerma factors obtained

in the present work with those from Ritts et al for Li^{6}, Li^{7}, C^{12}, Na^{23}, Nb, Fe and Be^{9}. The neutron kerma factors in these tables are in units of erg·barn/atom. The pointwise neutron kerma factors of Ritts et al were obtained from the Radiation Shielding Information Center at ORNL. The comparison in tables 3.11 through 3.17 shows that the difference between their results and ours is generally large, particularly in the 10 to 15 MeV energy range. The neutron kerma factors by reaction in their calculations are not available which makes it difficult to isolate the differences due to the calculational model from the differences arising from using different basic nuclear data. However, the sensitivity study of neutron kerma factors to variations in input nuclear parameters as discussed in the next section shows that, in general, "reasonable" or "realistic" changes in nuclear parameters do not produce changes in neutron kerma factors as large as the difference between the results compared here. By "reasonable" or "realistic" changes in nuclear data, we mean changes that are within the "spread" of values reported in literature for a particular nuclear parameter. The sensitivity study shows, on the other hand, that a combination of assumptions such as ignoring the contribution of some important reactions, neglecting the resonance contribution, not including the anisotropy of elastic scattering, and inadequate treatment of the secondary neutron energy spectra do indeed produce large changes in neutron kerma factors similar to the differences between the results of this work and those of Ritts. While some of the differences can be shown to be due to differences in the basic nuclear data used in the two studies, differences exceeding 20% can generally be attributed to the different calculational model and processing techniques used. In the following, some of the large dif-

ferences in tables 3.11 through 3.17 are discussed.

Table 3.14 shows that the neutron kerma factor for sodium obtained by Ritts et al is about 70% smaller than that obtained in this work in the energy range 10 to 15 MeV. This is one of a few examples for which the reason for the difference is obvious. In calculating the sodium kerma factors, they included only elastic and inelastic scattering and radiative capture. The present work included, in addition to these reactions, the (n,p), (n,α) and (n,2n) reactions. Inspection of table 3.21 reveals that the contribution of (n,p), (n,α) and (n,2n) reactions to the neutron kerma factor of sodium is more than 75% of the total from 10 to 15 MeV. Subtracting the contribution of these reactions from the k_n obtained with MACK shows that the Ritts result overestimates the kerma factor for the reactions which were included.

It is noted that their results are generally higher than ours in the energy range 10 to 15 MeV where the largest difference between the two works occur if the reactions included are the same in both cases. Further, it was noted that the difference is very large for materials in which energy deposition by elastic scattering represents a significant fraction of the total energy deposition. For example, the elastic scattering contribution to k_n at 15 MeV is about 16% in Li^6 and 29% in Li^7. Ritts et al estimate k_n at 15 MeV about 13% higher for Li^6 and 51% higher for Li^7 than the current work. However, it is observed that if the center-of-mass anisotropy of the elastic scattering is ignored for Li^7 in the 10 to 15 MeV energy range (see tables 3.12 and 3.36 and note that the units for the kerma factor employed in the two tables are different) the result is only slightly higher than their result. Therefore, it is

strongly suspected that they may have ignored the anisotropy of the elastic scattering.

Table 3.15 shows the comparison between the kerma factor obtained here and that calculated by Ritts et al for niobium. The agreement between the two works is "unusually" good at high energy. That "compensation of error" has played an important role in this agreement can be seen by noting that the nuclear data used in the two works is different in this high energy range. In addition, the difference is large in the energy range 10 eV to a few KeV which is the resonance region for niobium. For practical reasons, we selected only a few energy points at which to show the comparison in tables 3.11 through 3.17. Table 3.20 shows a detailed comparison between the niobium kerma factors of the two works at a finer energy mesh in the neighborhood of 1 KeV. These results were obtained directly from the two works without any interpolation. The basic nuclear data for niobium used in the present and in Ritts work is the same in the resonance energy region. These results show clearly that Ritts et al have ignored the resonance contribution entirely with the result that their neutron kerma factors are less than 5% of the actual values. At 1 KeV, their k_n is only about 0.04%of our value. Since the contribution to the neutron kerma factor at 1 KeV comes from elastic scattering and radiative capture; and since elastic scattering is isotropic in this energy range, the results obtained in the present work can easily be checked by hand calculations as shown at the end of table 3.20.

In subsection 3.4.2, a method was developed for investigating the consistency of the neutron kerma factor results by comparing the neutron

heating rate obtained from these kerma factors with that obtained from an energy balance over a finite volume of space for which the neutron flux and surface current are known. The method was then used to verify the results of the present work. When similar calculations are carried out with the neutron kerma factors obtained by Ritts et al it is found that the energy balance is destroyed. For example, for zone 4 (see table 3.18b) the Li^7 heating rate is 35% higher and the total neutron heating plus gamma energy source are overestimated by approximately 20% when their results are used.

In the following, we find it instructive to present a sample of the type of calculations carried out frequently in the course of this work for direct verification of the "pointwise" neutron fluence-to-kerma factor results. Equation 3.4.22 is helpful in this desk calculator-type calculation and it also allows rapid determination of an upper limit for the neutron kerma factor at an arbitrary energy point. We show here the details of such calculations for Li^7 and Be^9 at 15 MeV. The reason for this choice is that the nuclear parameters at 15 MeV can usually be obtained directly from the ENDF files without interpolation. In addition, the difference between the results of the present work and Ritts et al is typically large at this energy and particularly for the important isotopes Li^7 and Be^9.

Table 3.37 lists the nuclear parameters for Li^7 at 15 MeV and the details of the calculations for the various terms of equation 3.4.22. The average kinetic energies of secondary neutrons are calculated from the listed nuclear temperatures for evaporation spectra using the appropriate equations from chapter 2. The direct calculations show that

$k_n + E_\gamma$ is equal to 3.5702 MeV·barn/atom. k_n obtained from Ritts et al results is 5.2482 while k_n from MACK is 3.4713. Hence, without going into any details of the calculation of the gamma energy term, E_γ, it is obvious that the results of Ritts et al overestimates the neutron kerma factor for Li^7 at 15 MeV by <u>at least</u> 47%.

It is also of interest here to compare E_γ for Li^7 at 15 MeV reported in reference 7 with E_γ calculated from the ENDF/B3 data listed in table 3.37. E_γ for Li^7 is the sum of gamma energy production from inelastic, (n,2n) and (n,γ) reactions. Using the data in table 3.37 and equation 2.29 for the excitation energy of the residual nucleus from an (n,2n) reaction, we obtain

$$E_\gamma = 0.0989 \quad \text{MeV·barn/atom.}$$

The gamma production cross section data reported in reference 7 yields E_γ of 0.58 MeV·barn/atom. Hence, the reference 7 result for $k_n + E_\gamma$ overestimates the result derived from ENDF/B3 by 63% for Li^7 at 15 MeV. Finally, when the E_γ calculated from ENDF/B3 data is used in table 3.37 the result for k_n is exactly the same as that obtained with the MACK code.

The difference between the k_n obtained from this work and the k_n calculated by Ritts et al is very large for Be^9 and exceeds 100% in the energy range from 6 to 15 MeV. Therefore, we choose the energy point at 15 MeV to present the details of a direct calculation of k_n for Be^9 as our second and last example of verifying the results of the present work. Table 3.38 shows the ENDF/B3 nuclear parameters for Be^9 at 15 MeV together with the calculations of various terms of equation 3.4.20.

E_γ for Be^9 at 15 MeV is relatively small and is about .01 MeV·barn/atom (see gamma files in ENDF/B3 evaluation for Be^9). Our result overestimates k_n by about 0.25% because the neutron data for the (n,t) teaction did not include information about level excitations. The results of table 3.38 show that Ritts et al overestimated k_n for Be^9 at 15 MeV by more than 90%. The energy deposition in Be^9 at such energies is essentially that of the (n,2n) and elastic scattering reactions. No "spread" in published evaluated nuclear data for these two reactions was found to accout for the high neutron kerma factor estimated by Ritts et al. The calculation of the elastic scattering kerma factor is straight forward. Ritts et al do not discuss how the excitation energy of the residual nucleus in an (n,2n) reaction was treated and it was noted that, in general, his k_n is high for materials in which (n,2n) is important for energy deposition. The (n,2n) reaction in Be^9 is a special case in which their calculations should have given better agreement with the results of the present work as discussed below.

It is known that all nonelastic neutron producing reactions in Be^9 give rise eventually to two neutrons and two alpha particles. For example, Be^8 resulting from an (n,2n) reaction in Be^9 decays immediately to two alpha particles. Similarly, the residual nucleus, He^5, from an (n,n'α) reaction in Be^9 is unstable and decays immediately to a neutron plus an alpha particle. In addition Be^{9*} from an inelastic reaction in Be^9 always decays to the end products of a neutron and two alpha particles. Therefore, in all these reactions the mass difference between the incident neutron plus the Be^9 nucleus and the final end products of all nonelastic, neutron producing reactions in Be^9 is the same. The binding

energy of the last neutron in Be^9 is 1.660 MeV and Be^8 decays to two alpha particles with an exothermic Q of 0.095 MeV. Therefore, the effective Q-value is equal to -1.565 MeV. Similarly the Q-value for a $Be^9(n,n'\alpha)He^5$ reaction is -2.52 MeV and He^5 decays to a neutron and an alpha particle with an exothermic Q-value of 0.95 and the effective Q-value is the same as the $Be^9(n,2n)Be^8 \rightarrow 2\alpha$ reaction. The disagreement between published data for these reactions is about the emitted gamma spectra and the secondary neutron spectra. Since the gamma spectra in the ENDF/B3 evaluation for Be^9 did not include any contribution from these reactions we, in turn, ignored gamma emission in these reactions to provide consistency between the calculated neutron kerma factors and the gamma production cross sections. In such a case the energy deposition per reaction for the modes of the nonelastic, neutron-producing, reactions differs only through the different partition between secondary neutron and recoil nuclei which depends on the sequential decay. The kerma factor for all these reactions can be written as

$$k = k_1 + k_2 + k_3 + \ldots + k_n$$

$$= \sigma(E + Q_{eff}) - \sigma\left[\frac{\sigma_1}{\sigma}\bar{E}_{n_1} + \frac{\sigma_2}{\sigma}\bar{E}_{n_2} + \ldots + \frac{\sigma_N}{\sigma}\bar{E}_{n_N} \right]$$

where $\sigma = \sigma_1 + \sigma_2 + \ldots + \sigma_N$

σ_i = cross section for a particular mode i

(e.g. $Be^9(n,2n)Be^8 \rightarrow 2\alpha$ or $Be^9(n,n'\alpha)He^5 \rightarrow n' + \alpha$)

Q_{eff} = effective Q-value = -1.565 MeV

$\bar{E}_{n_i}$ = average kinetic energy of the two neutrons in mode i

N = number of modes

The ENDF/B3 evaluation combines the secondary neutron energy spectra for all modes and hence it provides the information for direct calculation of the last term in the above equation. Hence, we see no error in the ENDF/B3 data for Be nor in our procedure for calculating the neutron kerma factor from this data. A final point worth mentioning is that if the neutron kerma factor results of the present work for Be^9 is in error the reason would be the neglect of the gamma emission from the nonelastic, neutron producing, reactions. In this case, the actual neutron kerma factors for Be^9 are lower than our calculations here and this adds another difficulty in understanding the result of Ritts et al which is roughly twice that calculated here.

3.5 Sensitivity of Neutron Energy Deposition to Nuclear Data

Since the nuclear data for many materials and for several nuclear parameters suffer from relatively large uncertainties, it is of great concern to investigate the sensitivity of the nuclear heating to variations in nuclear data. The changes in energy deposition due to changes in nuclear data depends on the sensitivity of both neutron and gamma fluxes and kerma factors. The sensitivity of the kerma factor to a particular change in nuclear parameters is not necessarily the same as the sensitivity of the flux to the same change. For example, a 50% change in the (n,p) cross section for a particular material may have little effect on either the absolute magnitude or energy dependence of the neutron spectra, while the kerma factors may suffer a 30% change. The importance of a reaction for determining the neutron flux depends mainly on the magnitude of the reaction cross section; but for energy deposition, it is the product of the reaction cross section and the energy release per reaction that matters.

The goal of this section is to find out in general terms the importance of the various reactions and parameters in determining the neutron kerma factor in the energy range from zero to 15 MeV. This can serve two purposes. First, it provides a rapid assesment of the adequacy of given nuclear data for determining the neutron kerma factors and heating in a particular material. Second, a knowledge of the importance of the various nuclear parameters throughout the energy range of interest provides a basis for drawing conclusions about the degree of accuracy to which these parameters should be known. Since the changes in neutron heating depends also on the neutron spectra which are strongly dependent

on the specific nuclear systems considered, the two reference spectra for fusion systems given earlier in this chapter will be referred to often in the following discussion.

Inspection of the neutron kinematics equations given in chapter 2 shows that the input parameters for calculating the neutron kerma factors are:

1. reaction cross sections,
2. energy distribution of secondary particles,
3. angular distribution of secondary particles, and
4. reaction Q-values.

In addition, the multigroup representation requires the use of a heating rate-preserving weighting function and this was discussed in a previous section. The neutron kerma factor, k_{ni}, for reaction i at an energy E can be written as

$$k_{ni}(E) = \sigma_i(E)\ E_{Ri}$$

where σ and E_R are the cross section and energy release per reaction, respectively. Hence, the change, δk_{ni} in k_{ni} due to a change, $\delta\sigma_i$, in the cross section is directly proportional to $\delta\sigma_i$. The change in k_{ni} due to a change in the input parameters for E_R is more involved and can be derived from the kinematics equations of chapter 2. The following discussion is arbitrarily organized to allow bringing up some salient points.

A. Importance of Various Reactions

As an attempt to find out quantitatively the importance of the various reactions in determining the neutron kerma factor the percentage

contribution of each reaction type was calculated for several basic materials. Tables 3.21 through 3.30 tabulate the percentage contribution of each of the seven reaction kinematics-types to the neutron kerma factor for the most important CTR materials. Although these calculations are based on the neutron kerma factors calculated fromspecific nuclear data (ENDF/B 3) almost all of these evaluations are complete enough and the data is known well enough to allow data-independent general conclusions to be derived about the importance of the various reaction types.

Tables 3.21 through 3.30 show that the (n,charged particles) type, mostly (n,α) and (n,p),contribute, in general, about 60% or more to the neutron kerma factor, k_n, in the energy range of 10 to 15 MeV. This is no surprise since in the (n, charged particles) reactions all the kinetic energy of the emitted particles are deposited locally in contrast to all other reactions in which a significant fraction of the energy is carried away from the site of collision by the secondary neutrons and photons. Because of momentum conservation the kinetic energy of the recoil nucleus in a radiative capture reaction is small and hence the (n,γ) contribution to neutron heating is negligible when there are several other competing reactions. Except for light nuclei, the elastic scattering is important only below the inelastic threshold and above a few electron volts. Most materials have large inelastic cross sections at relatively high energy and consequently a large contribution to k_n. Although the total inelastic cross section increases with energy over most of the energy range from the inelastic threshold up to 15 MeV, the k_n of inelastic scattering increases slowly with energy because the fraction of energy carried away with secondary photons increases as the cross sections for

exciting the low-lying levels diminish. The importance of the (n,2n) reaction increases at high energy at the expense of inelastic scattering. The contribution of the (n,2n) reaction to k_n in the energy range 10 to 15 MeV depends strongly on the binding energy of the last neutron in the target nucleus. The higher the binding energy the smaller is the cross section in this energy range and the smaller also the energy available to the recoil nucleus.

Li-6, Li-7, Be-9, and B-10 are peculiar materials. As in all light nuclei, elastic scattering is an important mechanism for energy deposition in these materials. However, k_n is equally or more influenced by other reactions which have particularly large cross sections in these materials. In Li-6, k_n below 1 MeV results mostly from the (n,α) reaction and at about 4.5 MeV k_n is equally partitioned among the (n,α), elastic and (n, n')d reactions and above 7 MeV the (n,n')d contribution is greater than 50%. In Li-7, about 50% of k_n comes from the (n,n'α)t reaction with elastic scattering playing a more important role than in Li-6. In Be-9, the final products of the nonelastic, non-loss, reactions are two neutrons plus two alpha particles. The combined contribution to k_n from these modes is included in table 3.30 under the (n,2n) reaction type and is about 30 to 50% from 3 to 6 MeV and 50 to 75% at higher energies. In B-10, k_n below about 0.5 MeV is essentially from the (n,α) reaction. From 0.5 to 10 MeV about 20% of k_n comes from elastic scattering with the rest from the (n, charged particles) reactions and at higher energies local energy deposition from inelastic scattering increases from 10% at 10 MeV to 20% at 15 MeV.

The important conclusion from tables 3.21 to 3.30 and the analysis of the results for several other materials is that about 50% of the neutron heating by neutrons in the energy range 10 to 15 MeV comes generally from the (n, charged particles) reactions. In materials such as stainless steel this contribution is more than 70%. The importance of these reactions to energy deposition in some materials extends to lower energies depending on the reactions thresholds and the competition of other reactions. The (n,γ) is important only below a few tens of electron volts and the magnitude of its kerma factor depends largely on the radioactive decay $(\beta-)$ of the recoil nucleus in some materials. The importance of other types of reactions varies from one material to the other.

Since the (n,2n), (n,charged particles) and (n,n´charged particles) reactions occur generally at high energy, the importance of their contribution to k_n is weighted by the fraction of the spectrum in the high energy range. To see the effect of this, consider the two reference spectra for a CTR blanket and shield which were given in section 3.3. The first is a typical first wall spectrum and the second is C/E flux with C = 1.0 above 111 KeV and 0.25 below. The fraction, f_o, of neutron heating generated with neutrons of energies above E_o, as a function of E_o for the two spectra is plotted for several CTR materials in figures 3.20 through 3.24. f_o for any E_o varies with the position of the material in the blanket but is generally bracketed by the values given for the two spectra. It should be noted, however, that the C/E reference flux has a much larger fraction of neutrons below a few hundred

electron volts than what actually exists in all designs of fusion systems considered in this work.

Figure 3.20 shows that for the C/E spectrum the fraction of neutron heating generated in Li-6 with neutrons of energies above 1 MeV is less than 1%. Even for the first wall spectrum whose low energy component is largely depressed f_o in Li-6 is only 23% for an E_o of 1 MeV. Li-6 is an unusual material, however, as discussed above because its (n,α) cross section is large at low energy. The situation is entirely different for most of the other CTR materials. Figure 3.22 shows that for iron about 80% of the neutron heating is generated with neutrons above 5 MeV for the C/E spectrum and f_o is more than 90% for an E_o of 5 MeV in the first wall spectrum. For other materials such as Ni, Cr, Nb, and Na-23, f_o ranges from approximately 60 to 80% for an E_o of 5 MeV. As explained earlier, k_n for V is large at low energy due to the (n,γ) reaction and the fraction of neutron heating generated in vanadium with neutrons of energies above 5 MeV is only about 25% for the C/E spectrum. However, the same fraction is approximately 80% for the first wall spectrum.

In order to derive more quantitative conclusions, the percentage contribution to neutron heating by reaction type for the two reference CTR spectra is shown in tables 3.31 and 3.32 for the most important CTR materials. The general conclusion from these two tables is that reactions such as (n,α) and (n,p) while relatively unimportant for determining the neutron flux are extremely important mechanisms for neutron energy deposition. In practical systems, however, we are interested in the total nuclear heating. The ratio of neutron to gamma heating is given for several materials in typical blanket and shield configurations in

chapter 5. For our purpose here, it suffices to say that unless the neutron heating is negligible the contribution from the (n, charged particles) reactions must be included in energy deposition calculations since it represents generally about 50% of the neutron heating.

While reactions such as (n,α) and (n,p) are of prime importance for calculation of energy deposition, in most materials they have little effect on the neutron spectra. In addition, there are considerable difficulties in the measurements and accurate theoretical calculation of these cross sections. Therefore, the (n, charged particles) and (n,n′) charged particles cross sections are generally less well known than the other reaction cross sections for most materials. Because of this situation the evaluations for some materials in the widely used nuclear data libraries such as ENDF/B and UK do not include data for many of the possible (n,charged particles) and (n; n′, charged particles) reactions. A case of interest for CTR application is the ENDF/B 3 evaluation for molybdenum. This evaluation does not provide information about the (n, charged particles), (n; n′, charged particles) reactions and secondary photon production. Since molybdenum is frequently proposed for use in CTR, an attempt to assess the validity of the neutron kerma factor if calculated only for the reactions in ENDF/B 3 evaluation is made next. It should be clear, however, that any reference in this work to any particular data evaluation is not by any means meant to assess the credibility of the evaluation. Rather, our purpose here is to bring up important considerations in the calculation of energy deposition.

Table 3.33 tabulates the abundance, Q-values, and the cross sections at 15 MeV for the (n,α) and (n,p) reactions in molybdenum isotopes.

These cross sections were obtained from reference [28]. For some isotopes the (n,α) cross sections were not found and the (n,α) cross sections for such an isotope was taken to be equal to that of the neighboring isotope. The (n,α) reaction is exothermic with a relatively large Q-value and the (n,p) has relatively low thresholds in all molybdenum isotopes. In the absence of information about the excitation functions to various levels, we assume here that the residual nuclei in the (n,p) and (n,α) reactions are always left in the ground state. This can result in an overestimation of the neutron kerma factor from these reactions by roughly 20% but this is not important for this discussion. From table 3.33, the kerma factor at 15 MeV for the (n,p) and (n,α) reactions in natural molybdenum is calculated to be

$$k_{n,p} = 0.4838 \quad \text{MeV} \cdot \text{barn/atom}$$

$$k_{n,\alpha} = 0.3384 \quad \text{MeV} \cdot \text{barn/atom}$$

Thus $k_{n,p}$ plus $k_{n,\alpha}$ for Mo is 0.8222 MeV · barn/atom which is about 1.6 times the sum of the neutron kerma factors for all other reactions. The (n,p) and (n,α) relative contribution was found to be even higher at lower energies. The uncertainty of the cross sections should be taken into account, however. From table 3.33, $\sigma_{n,p}$ for natural molybdenum is 0.031 barns at 15 MeV which agrees with the value given by Impink [33]. It is worth noting that the (n,p) cross section given in reference [28] decreases with energy for all Mo isotopes while the UK and Impink data increases with energy from 6.5 to 11 MeV and then decreases. The average value from 13.5 to 15 MeV agree with the other two references but

at lower energies the UK values are more than three times larger than the values given by Alley et. al. [28]. A more detailed analysis shows that for a typical CTR spectrum, the (n,p) and (n,α) contribution to neutron heating in molybdenum is at least 50%. This is just to mention one of a few examples that shows a strong need for new measurements or theoretical calculations and evaluations of the nuclear data for reactions that have a neutron in the inlet channel and at least a charged particle in the exit channel.

The (n; n′, charged particles) reactions contribute, in general, a smaller fraction to neutron heating than the (n,charged particles) reactions because of higher thresholds and the fraction of energy carried away with the secondary neutrons. Their contribution is not negligible, however, and since little is known about their cross sections some caution should be exercised in dealing with these reactions. The case which is encountered quite often is that in which the cross sections for the (n; n′, charged particles) are combined with the inelastic scattering ($(n,n')\gamma$) reactions in the literature. Neutron kerma factors calculated from such data would then suffer from neglecting the kinetic energy of the emitted charged particles. The relative change in the energy release per reaction, E_R, from ignoring the kinetic energy of the emitted charged particles can be shown from equations 2.6 and 2.17 to be

$$\frac{\delta E_R}{E_R} = \frac{-E_\lambda + |Q|}{E - \overline{E}_{n',\ell} - |Q|}$$

where E_λ is the energy of the level excited by the (n,n′) part of the reaction and Q is the Q-value for the (n,n′ charged particles) reaction.

In nuclides where such reactions occur the recoil energy of the intermediate compound nucleus is small and $E - \overline{E}_{n',\ell}$ is only slightly greater than E_λ and hence $\delta E_R/E_R$ is typically about 0.8 to 0.9. Therefore, combining the (n; n', charged particles) with the $(n,n')\gamma$ amounts to roughly neglecting the energy deposition from such reactions. The effect on the total neutron heating depends, of course, on the neutron spectrum and their contribution to the neutron kerma factor. As an example, consider Al-27. The data for the $(n,n'\alpha)$ and $(n,n'p)$ reactions in this material are given in ENDF/B 3. The neutron heating from the $(n,n'\alpha)$ and $(n,n'p)$ in Al-27 is 1.35 times the neutron heating from the $(n,n')\gamma$ for a typical first wall spectrum but only 0.30 times as much for the shield spectrum. With the aid of results in tables 3.31 and 3.32 it can be seen that approximating the energy depositon in the $(n,n'\alpha)$ and $(n,n'p)$ in Al-27 by the energy deposition from the (n,n') part only results in neutron heating underestimated by 15% for a typical first wall spectrum and by 5% for a typical shield spectrum. Similar results were found for vanadium and tables 3.31 and 3.32 show explicitly the contribution from (n; n', charged particles) in chromium and nickel. The contribution of reactions such as $(n,n'\alpha)$ and $(n,n'p)$ depends strongly on the neutron spectrum since their thresholds are particularly high in most materials.

Most of the nuclear data from which the neutron kerma factors in the present work were calculated did not provide information about the (n,n') charged particles reactions. Little was found in the literature about the cross sections and the secondary neutron energy distribution for these reactions. More information about these reactions are

obviously needed. Incidentally, since the contribution from the (n;n', charged particles) to neutron heating is positive and is roughly 20 to 30% of the contribution of the (n, charged particles) reactions and the effect of gamma energy release from the (n, charged particles) on the neutron heating is negative and is also about -20 to -30% of (n, charged particles) contribution the neutron kerma factors calculated with the lack of both types of information are likely not to suffer from large under or overestimations. However, this is only a qualitative statement and there is a strong need for more information about the (n; n', charged particles) and (n, charged particles) for the purpose of calculating more accurate energy deposition. It is worth noting also that these reactions are also of basic importance for radiation damage studies.

Since the energy release per reaction is independent of the reaction cross section the change in the total neutron heating for a change, $\delta\sigma$, in the cross section with $\frac{\delta\sigma(E)}{\sigma(E)}$ independent of energy can be obtained directly from tables 3.31 and 3.32 for the two reference spectra.

B. Secondary Neutron Energy Distribution

The calculation of energy deposition in neutron producing reactions requires information about the energy spectra of the secondary neutrons. The quantity of interest is the average kinetic energy, $\overline{E}_{n',\ell}$, of the secondary neutrons in the laboratory system.

For elastic scattering, $\overline{E}_{n',\ell}$ is derived from the angular distribution of the secondary neutrons. For inelastic level scattering, $\overline{E}_{n',\ell}$

(see equation 2.7) is a function of the angular distribution and the energy of the excited level. The effect of changes in the angular distribution on $\overline{E}_{n,\ell}$ and neutron heating is studied in part C. For inelastic scattering into the continuum, $\overline{E}_{n',\ell}$ is usually derived from measured or theoretically calculated secondary neutron energy spectra. Equations 2.10 and 2.11 show that the kinetic energy of the recoil nucleus, $\overline{E}_r$, is approximately equal to $\overline{E}_{n',\ell}/A$ for nuclides of large mass number A. Therefore, the relative change in the neutron kerma factor for such reactions due to a change in the secondary neutron spectra is approximately equal to the absolute magnitude of the relative change in $\overline{E}_{n',\ell}$. In addition to neutron kerma factors, changes in the secondary neutron energy spectra affect the neutron flux and gamma energy production. A change in $\overline{E}_{n',\ell}$ which is taken into account in k_n, ϕ_n, and secondary gamma productions produces a change in the total neutron heating which is generally smaller than that due to a change in $\overline{E}_{n',\ell}$ taken into account only in the neutron kerma factor, flux, or gamma production. This again another example illustrating the need for self-consistent nuclear data and processing codes.

Approximately 80% of the neutron heating in a typical CTR blanket comes from Li-6 and Li-7. The (n,n'α)t reaction in Li-7 is the most important neutron producing reaction in these two isotopes. Therefore, the sensitivity of the neutron heating to the secondary neutron energy distribution from this reaction is investigated below.

Rosen and Stewart's [34] data for the secondary neutron energy distribution of Li-7 (n,n'α)t reaction was used as the basis for the ENDF/B3 representation. The original data is reproduced in table 3.34. The

data was given for all but the lowest incident energies in histogram form. The ENDF/B3 evaluation has represented this secondary energy distribution with an evaporation model (see equation 2.12 and 2.13)

$$f(E \rightarrow E') = \frac{E'}{I} \quad \text{Exp}\{E'/\theta(E)\} \quad 0 \leq E' \leq E - U$$

with U = 2.466 MeV and $\theta(E)$ given as

E	$\theta(E)$ in MeV
2.821	0.10
5.800	0.70
8.000	2.80
15.000	5.35

Table 3.35 shows that the ENDF/B3 representation consistently overestimates the average secondary neutron energy, $\overline{E}_{n',\ell}$, compared with the Rosen and Stewart data at all incident energies. The difference is large and varies from about 20 to 60 per cent. Why there are such large differences between the experimental and evaluated data is not the subject of this discussion but our concern here is the effect of such differences, uncertainties, or disagreements which exist in the literature on neutron heating. Table 3.35 shows the (n,n'α)t reaction and the total kerma factors for both ENDF/B3 and Rosen and Stewart data. Since Rosen and Stewart's data does not cover incident energies from threshold to 5 MeV, $\overline{E}_{n',\ell}$ at 2.84 MeV was taken equal to that derived from ENDF/B3 data and a linear interpolation from 2.84 to 5 MeV was assumed. It can be seen from table 3.35 that the pointwise kerma factor for the (n,n'α)t reaction changes by about 15 to 25% and the total kerma factor changes

by 5 to 12% when the Rosen and Stewart secondary neutron energy distribution is replaced by ENDF/B3 representation. The change in neutron heating in Li-7 was found to be -6.76% for the reference C/E spectrum and -8.39% for the reference first wall spectrum. This is a relatively small change compared with the large change in $\overline{E}_{n',\ell}$. It should be noted, however, that the change in $\overline{E}_{n',\ell}$ is about 25% in the effective range for neutron energy deposition in Li-7 by the (n,n'α)t reaction. The energy range of 5 to 7 MeV where the change in $\overline{E}_{n',\ell}$ is 50 to 70% contributes little to the neutron heating by the (n,n'α)t reaction. Therefore, it can be concluded that the relative change in neutron heating in Li-7 is roughly one-third of the relative change in $\overline{E}_{n',\ell}$ for the (n,n'α)t reaction. Incidentally, changes in the energy distribution of the secondary neutrons from the (n,n'α)t reaction may have a large effect on the tritium breeding ratio [35] if the fraction of neutrons emitted above this reaction threshold is overestimated. Another study by the author showed that a 90% change in the nuclear temperature for all neutron producing reactions in Li-7 results in a 26% change in the neutron heating for the reference shield spectrum (C/E) and 43% for the reference first wall spectrum. Since the energy deposition in Li-7 by the (n,2n) and (n,2n)α reactions is small this result is associated with the (n,n'α)t reaction.

C. Angular Distribution of Secondary Neutrons

Calculation of neutron kerma factors requires an accurate description of the angular distribution of secondary neutrons. Since most of

the nonelastic reactions are nearly isotropic in the center-of-mass, the anisotropy of the angular distribution of the secondary neutrons is most important only in elastic scattering.

For intermediate and heavy nuclei, the angular distribution of elastic scattering is highly anisotropic at high energy. For these materials, the energy deposition by elastic scattering is much smaller than the energy deposition by other reactions at high energies. This implies that small changes in the angular distribution of elastic scattering result in small changes in neutron heating in these materials. However, very large changes in the angular distribution can result in significant changes in neutron heating. The change, δk_e, in the elastic scattering kerma factor, k_e, due to a change, $\delta(\overline{\cos\theta})_{cm}$, in the average of the cosine of the center-of-mass scattering angle is

$$\frac{\delta k_e}{k_e} = \frac{\delta E_R}{E_R} = \frac{\delta(\overline{\cos\theta})_{cm}}{1-(\overline{\cos\theta})_{cm}}$$

Since $\overline{\cos\theta}_{cm}$ is typically 0.6 to 0.8 at high energies the relative change in k_e is about three times the relative change in $\overline{\cos\theta}_{cm}$.

Since the energy range of interest extends to high energies, the anisotropy of elastic scattering in light nuclei must also be accurately described. Li-7 is one of the lightest nuclides in the blanket and the effect of a 100% change in $\overline{\cos\theta}_{cm}$ for elastic scattering in this material is shown in table 3.36. The table shows that ignoring the elastic scattering anisotropy in the center-of-mass doubles roughly the energy deposition by elastic scattering at high energies. About a 50 to 60% increase in the total neutron kerma factor for Li-7 above 6 MeV results

from a 100% change in $\overline{\cos\theta}_{cm}$. The neutron heating in Li-7 increases by about 33% for the reference shield spectrum and 85% for the reference wall spectrum. Since approximately 35% of the neutron heating in a natural lithium blanket comes from Li-7 ignoring the center-of-mass anisotropy of elastic scattering in this material overestimates the total neutron heating by roughly 20%. Although the elastic scattering angular distribution is more forward-peaked in Li-6 than in Li-7 ignoring the center-of-mass anisotropy of Li-6 elastic scattering results in a smaller change in the blanket neutron heating because the energy deposition in Li-6 is dominated by the (n,α) contribution.

D. Contribution of Radioactive Decay

As discussed earlier, the contribution of radioactive decay to local energy deposition by charged particle emission needs to be added to the neutron neating. Very accurate calculations of decay contribution to the total heating requires accounting for 1 - time dependence, and 2 - transmutation of the radioactive residual nucleus by neutron interactions. This requires using a special purpose program such as CINDER [112]. However, if the centribution of radioactive decay is not large this contribution can be added to the kerma factors if we assume that: 1 - energy deposition is negligible from radioactive residual nuclei with half-lives greater than an arbitrary cut-off, e.g. 30 days, and 2 - transmutation of residual nuclei can be ignored, i.e. each residual nucleus decays before it undergoes another nuclear reaction.

The following table summarizes the percentage contribution of radioactive decay to neutron heating for CTR first wall and for C/E spectra for some CTR materials.

Material	% contribution of radioactive decay to neutron heating	
	First wall spectrum	C/E spectrum
Li^6	0.06	0.01
Li^7	0.39	1.96
V	6.75	132.4
Nb	0.70	0.42

From this table it is seen that local energy deposition by radioactive decay is less than 2% of the neutron heating in Li^6, Li^7 and niobium. Hence, very accurate calculation of radioactive decay energy deposition would only add a small correction to the total neutron heating in these materials for blanket spectra. The situation is different, however, for the case of vanadium. The decay of V^{52}, which is produced by the $V^{51}(n,\gamma)$ reaction, contributes a very significant fraction to local energy deposition by neutrons at low energies. While this fraction is only about 7% in first wall spectrum it is more than 100% in C/E spectrum. However, since the half-life of V^{52} is only 3.75 minutes the rate of transmutation of V^{52} by neutron interaction is quite negligible for typical CTR fluxes (10^{14} to 10^{16} $n/cm^2 \cdot sec$). Therefore, there is little error in calculating local energy deposition from radioactive decay in vanadium by assuming a cut-off half-life of a few days and ignoring the transmutations of the residual nuclei.

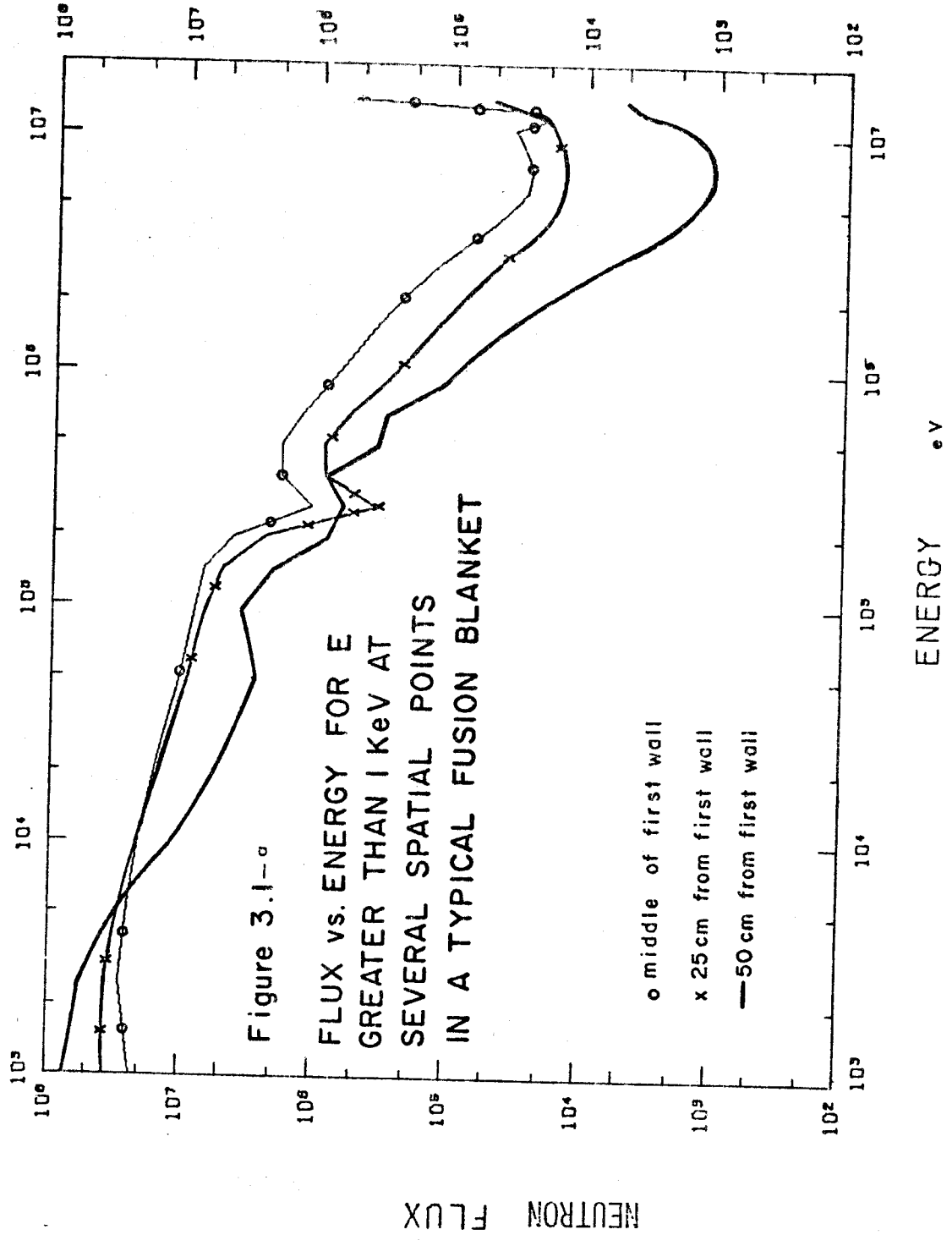
NEUTRON FLUX
ENERGY eV
FLUX vs. ENERGY FOR E GREATER THAN I KeV AT SEVERAL SPATIAL POINTS IN A TYPICAL FUSION BLANKET
o middle of first wall
x 25 cm from first wall
—50 cm from first wall

Figure 3.1-a

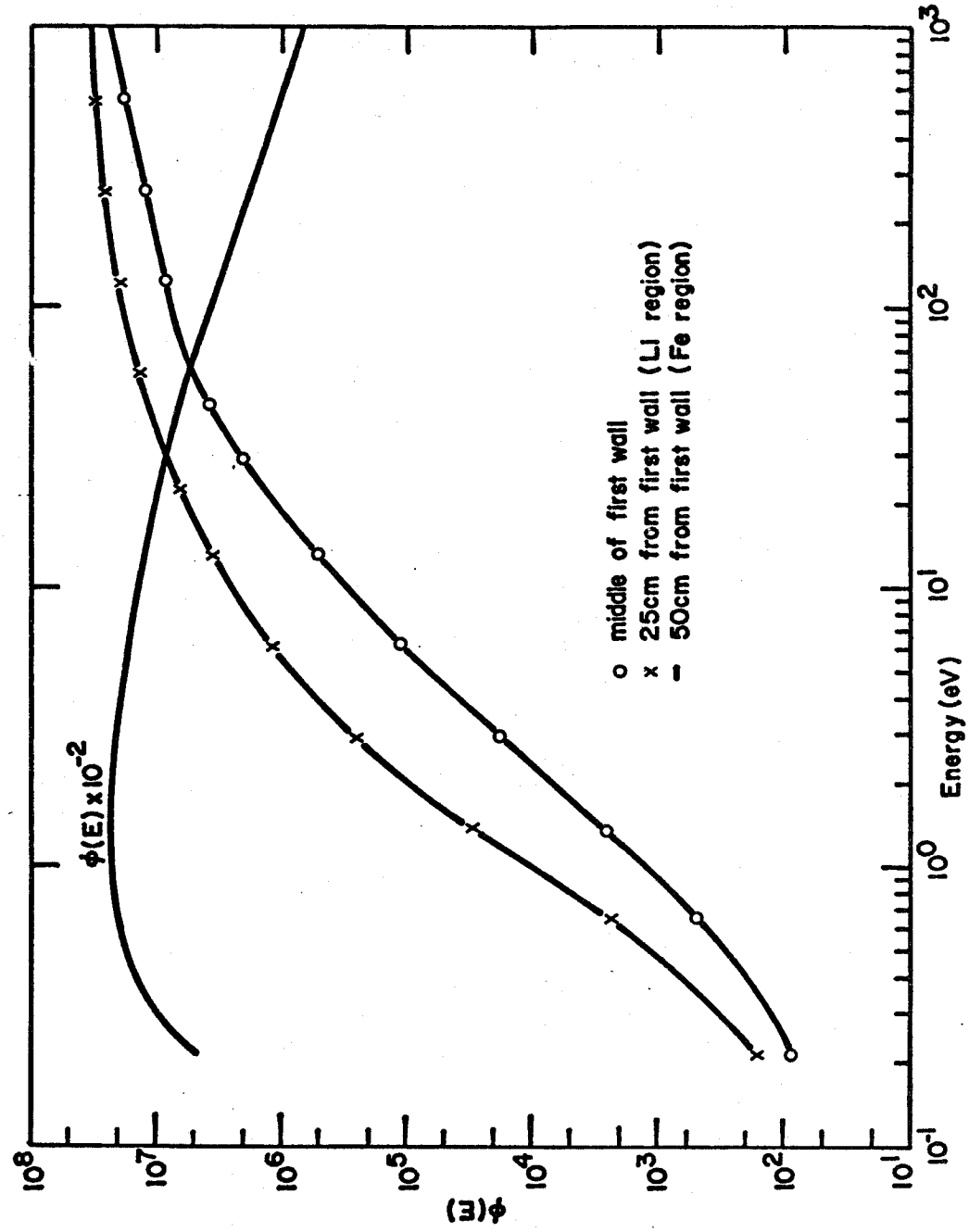

FIG. 3.1 b Flux Vs. Energy for E Less Than 1 KeV at Several Spatial Points in a Typical Fusion Blanket

Figure 3.2

LASL NEUTRON FLUX WEIGHTING SPECTRUM FOR D-T REACTORS

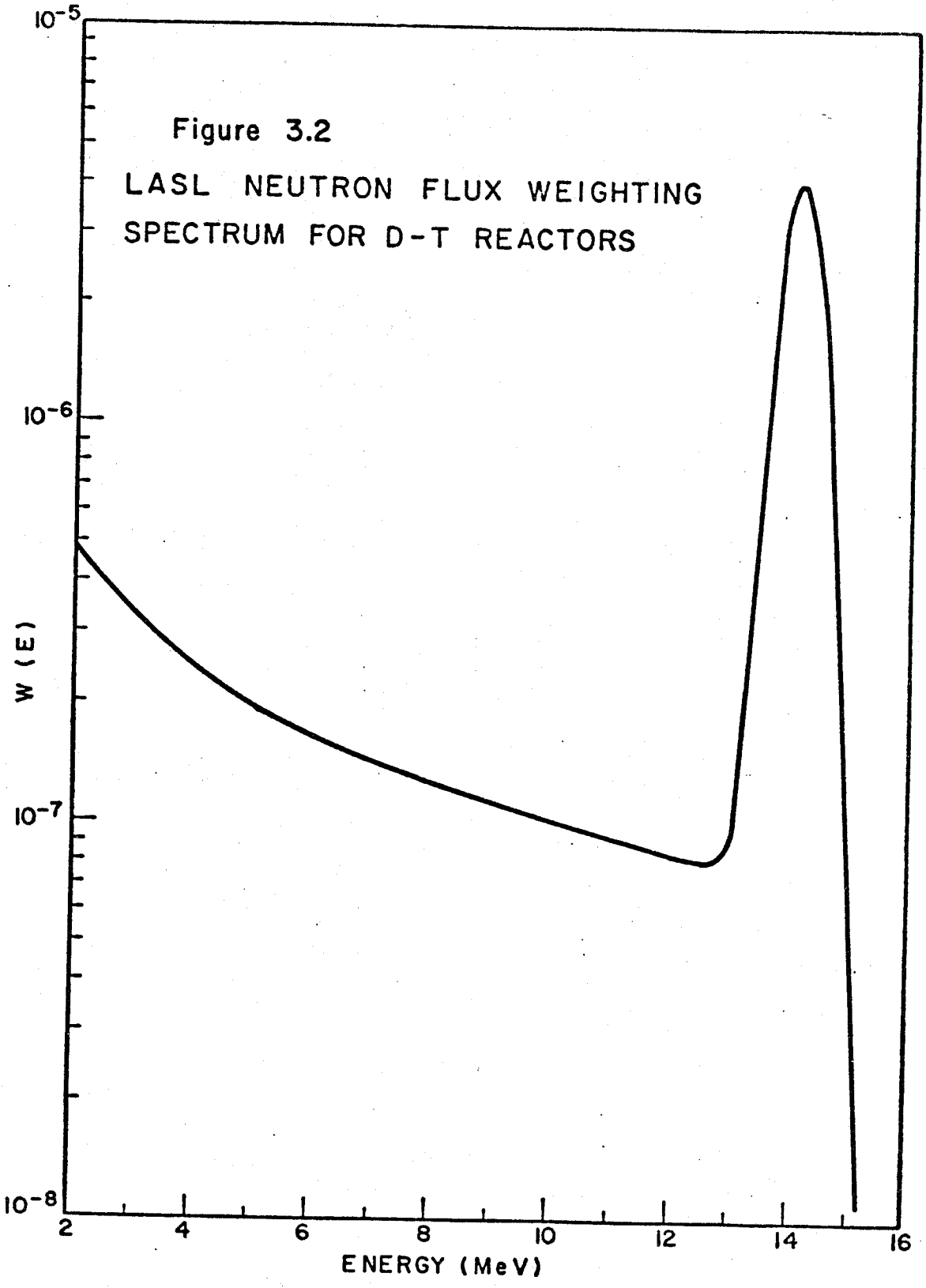

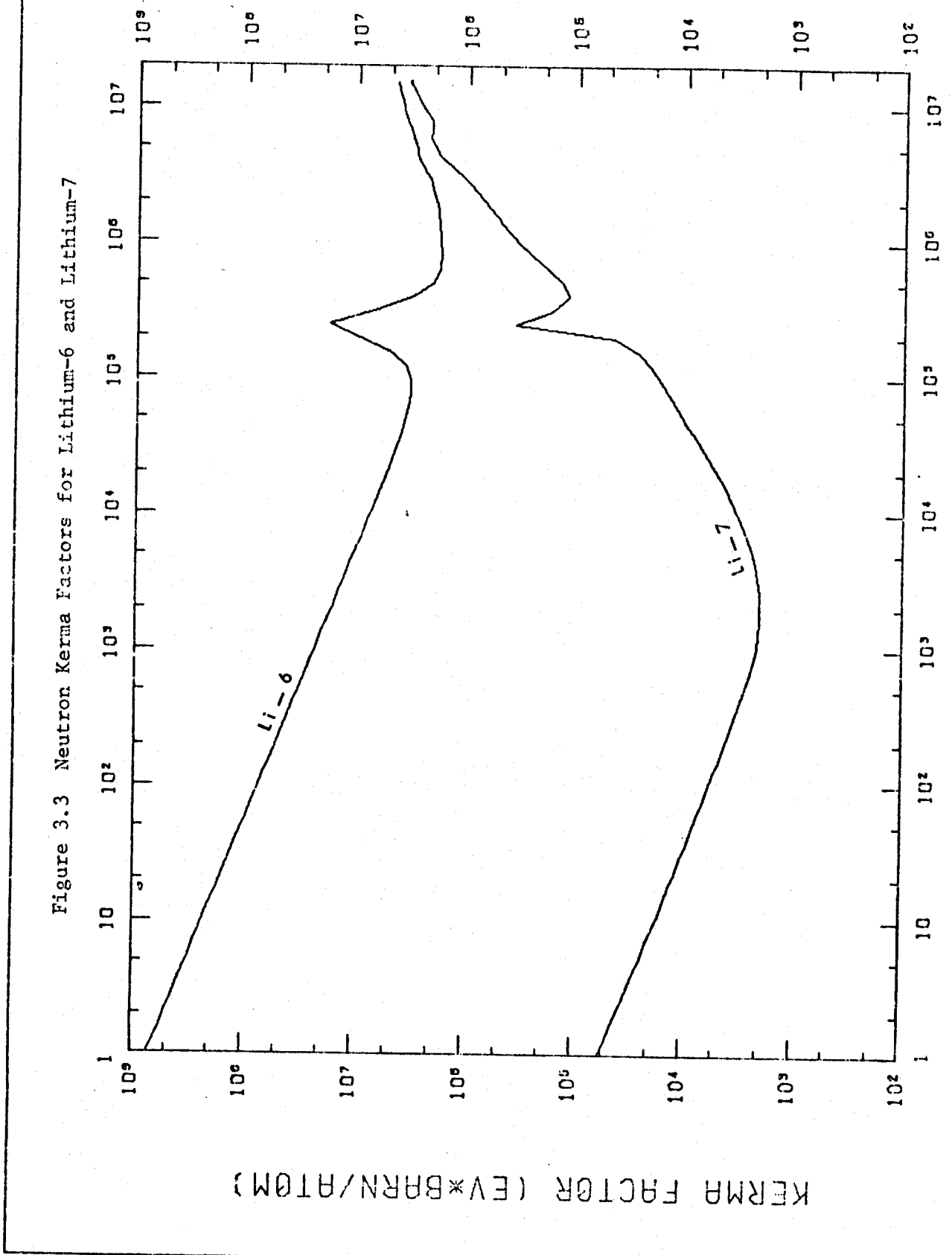

Figure 3.3 Neutron Kerma Factors for Lithium-6 and Lithium-7

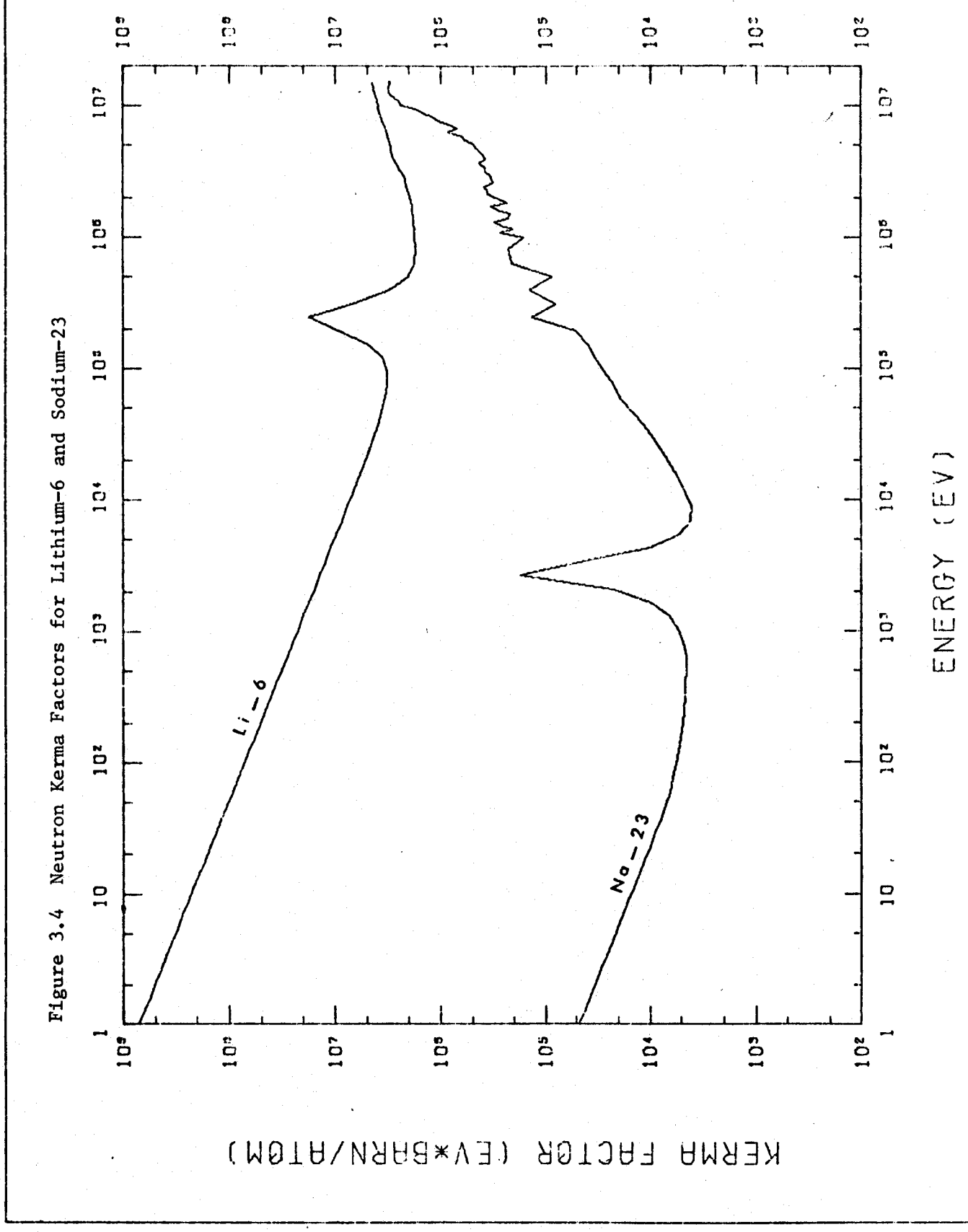

Figure 3.4 Neutron Kerma Factors for Lithium-6 and Sodium-23

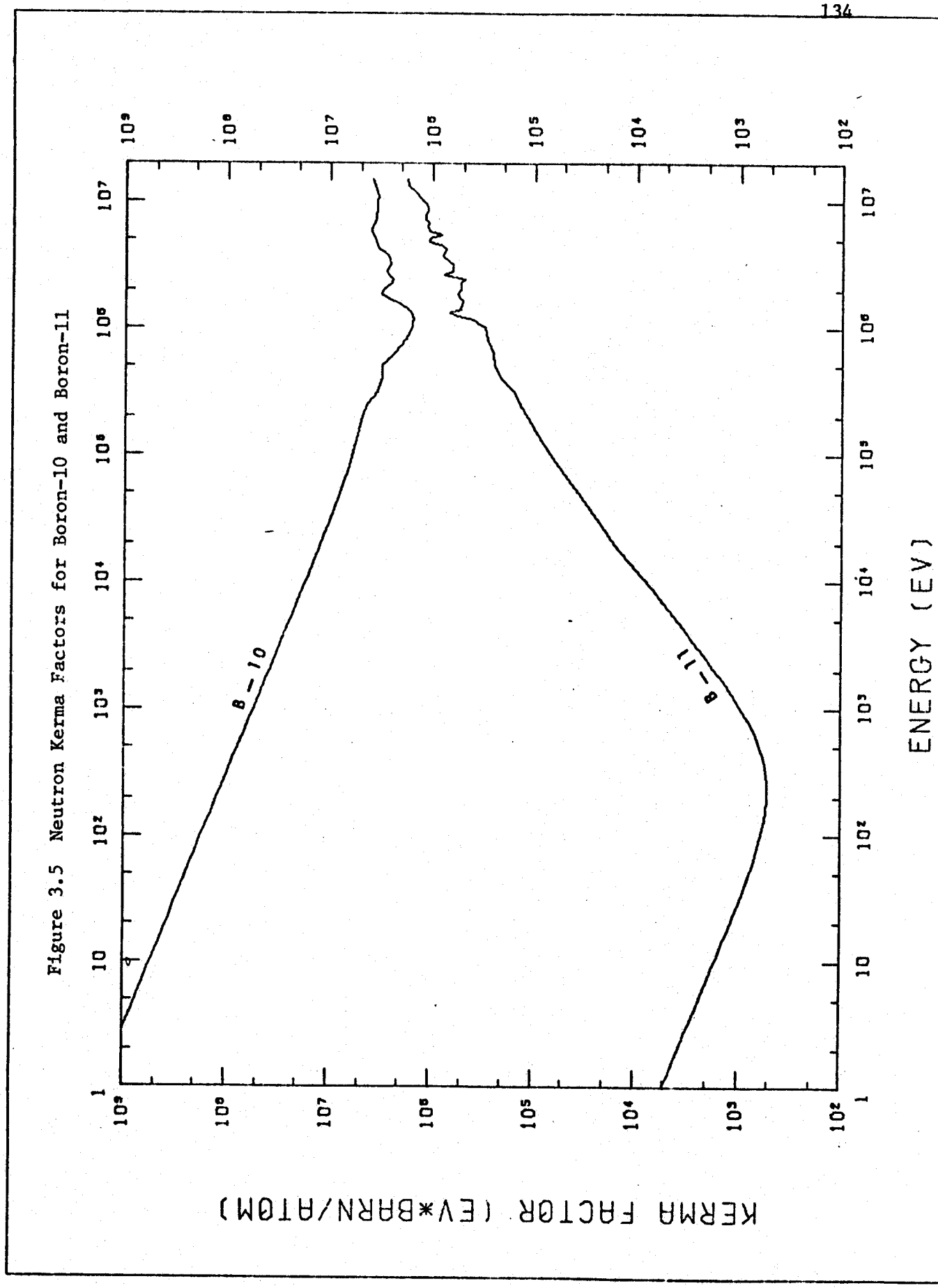

Figure 3.5 Neutron Kerma Factors for Boron-10 and Boron-11

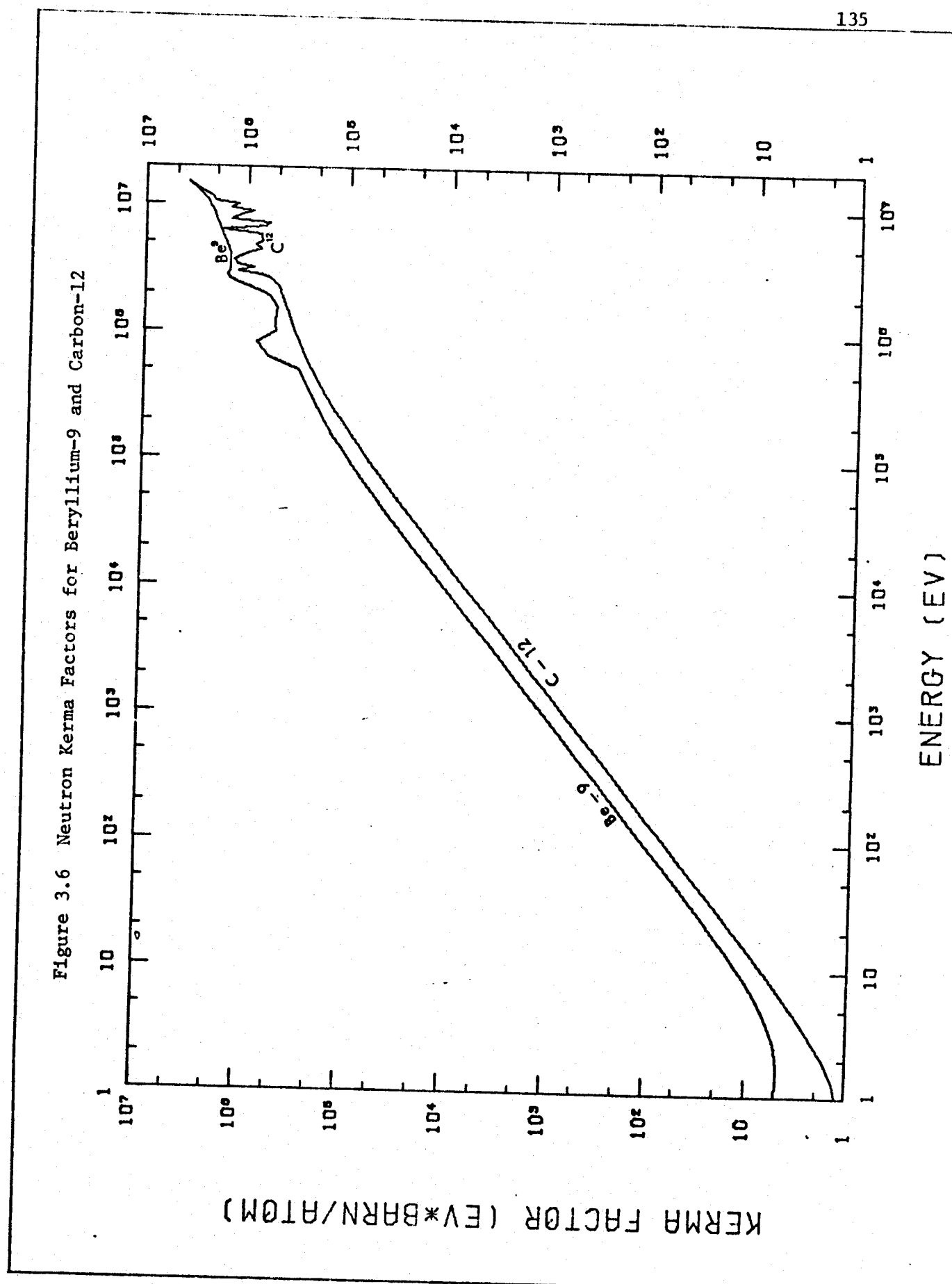

Figure 3.6 Neutron Kerma Factors for Beryllium-9 and Carbon-12

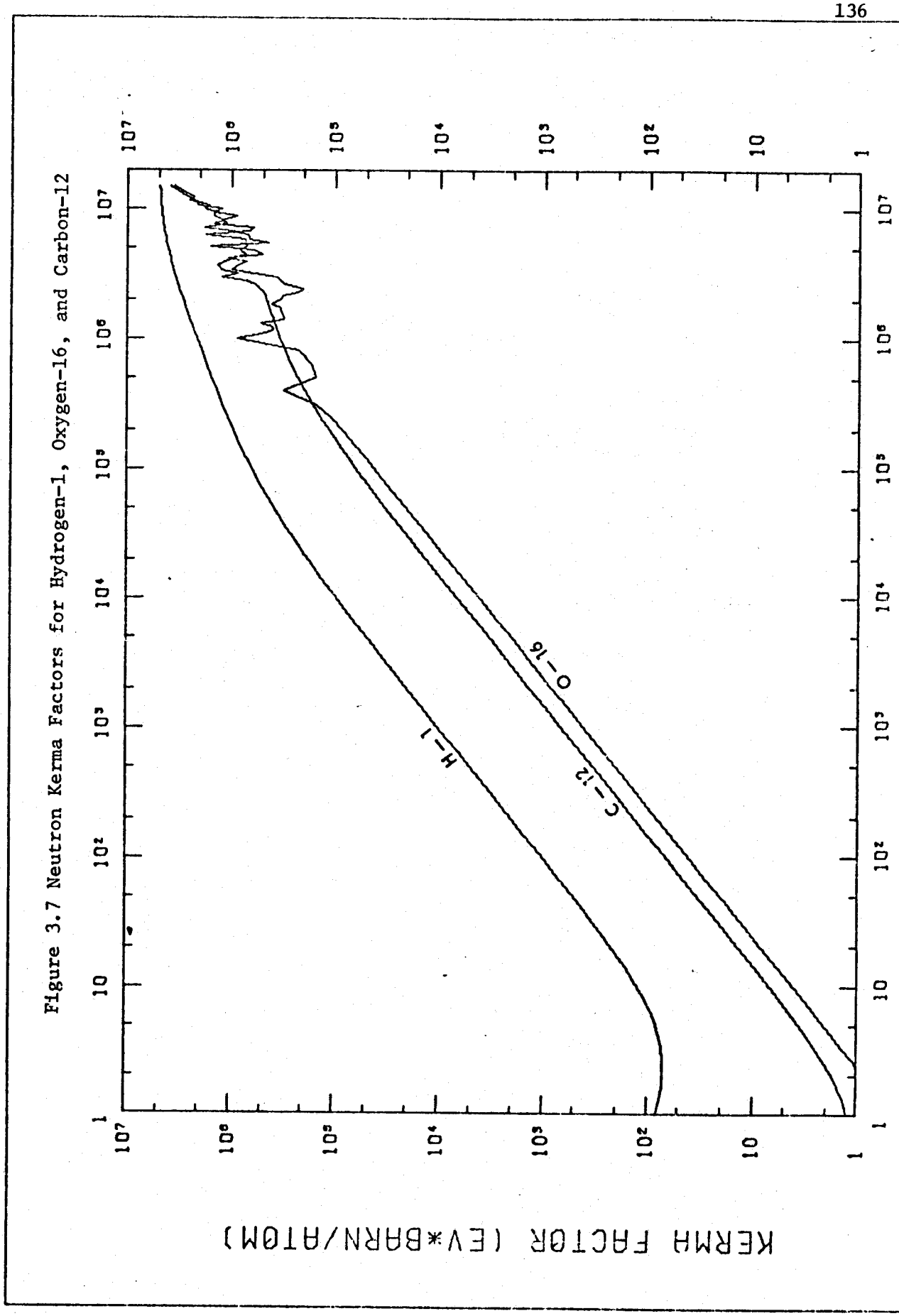

Figure 3.7 Neutron Kerma Factors for Hydrogen-1, Oxygen-16, and Carbon-12

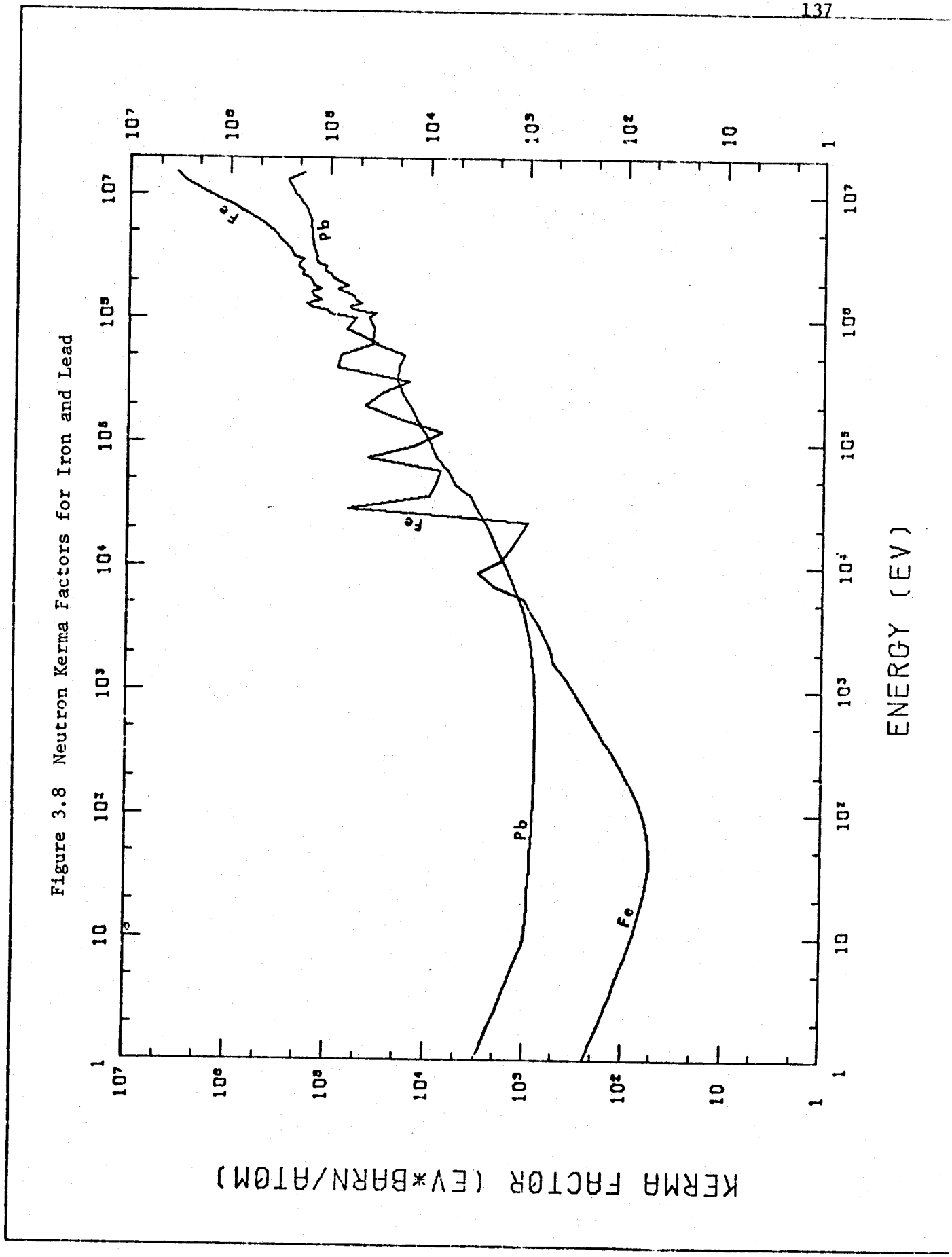

Figure 3.8 Neutron Kerma Factors for Iron and Lead

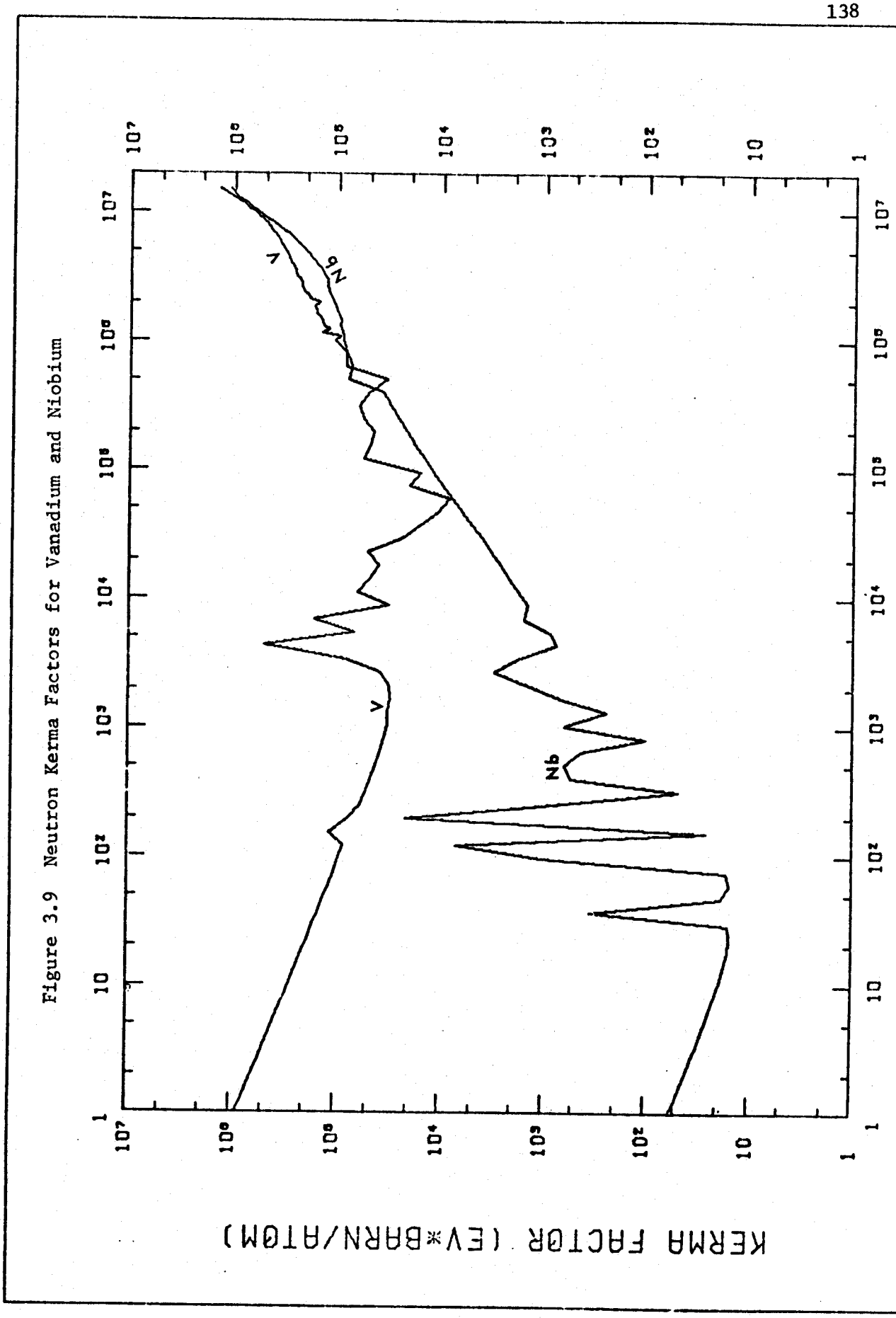

Figure 3.9 Neutron Kerma Factors for Vanadium and Niobium

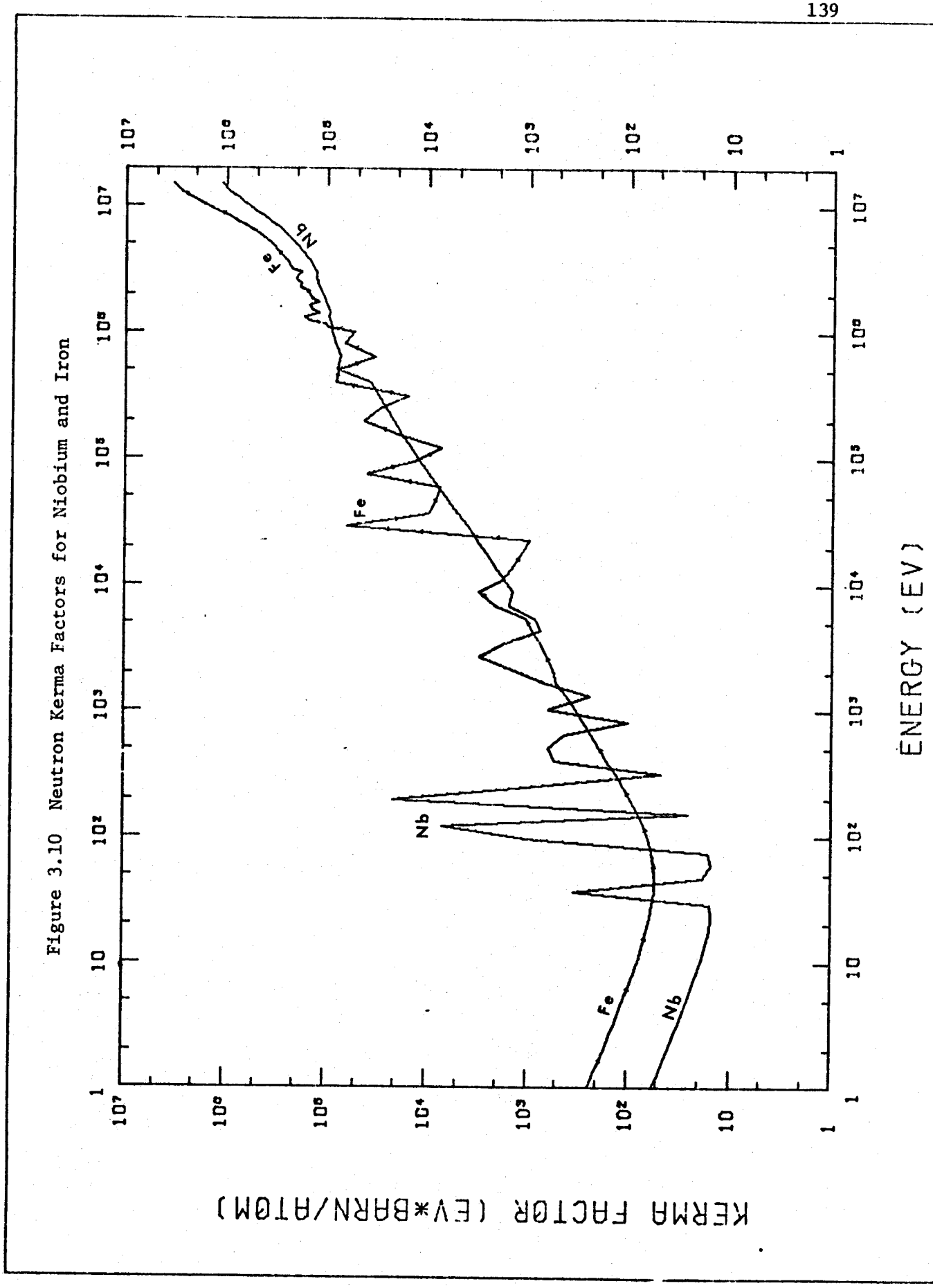

Figure 3.10 Neutron Kerma Factors for Niobium and Iron

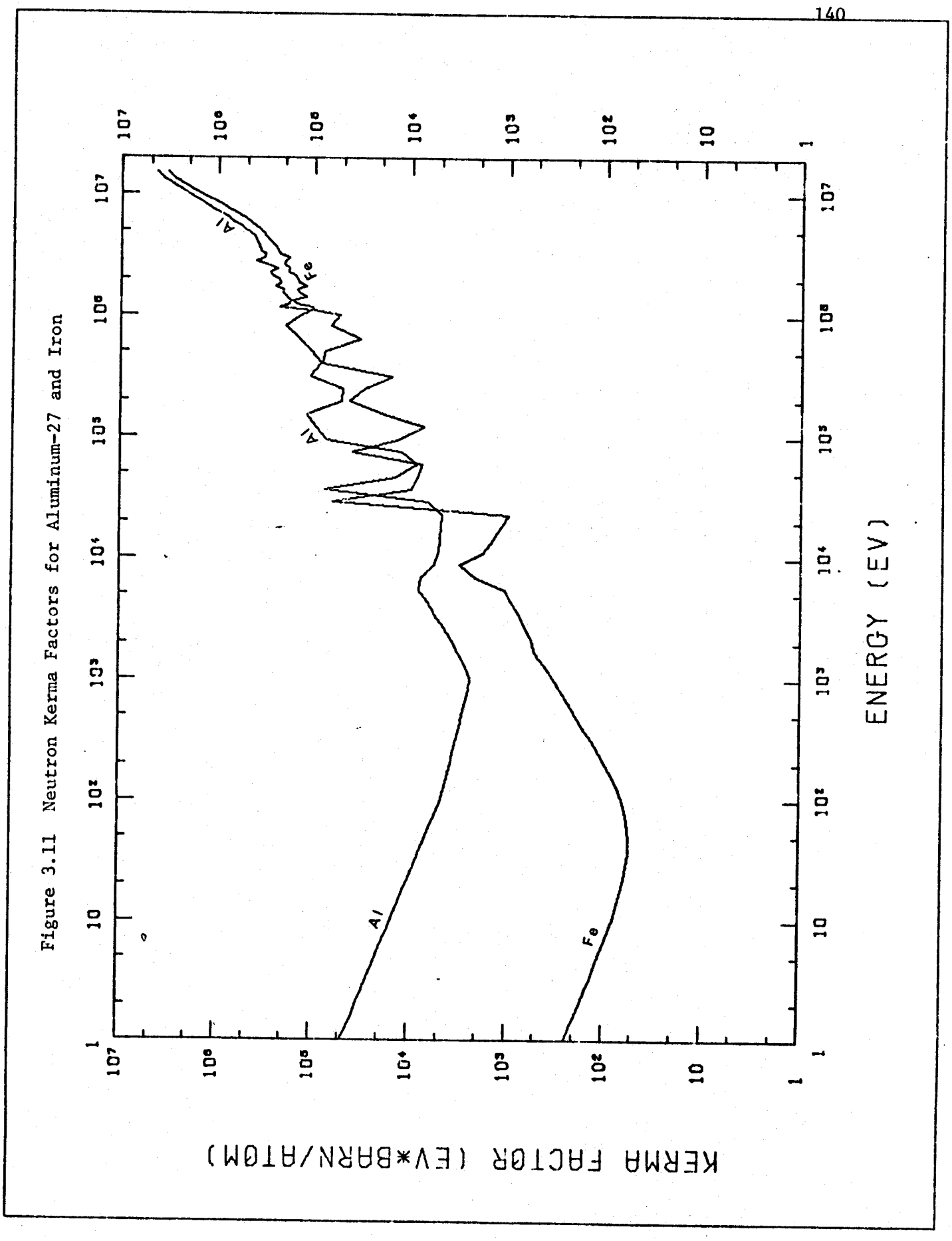

Figure 3.11 Neutron Kerma Factors for Aluminum-27 and Iron

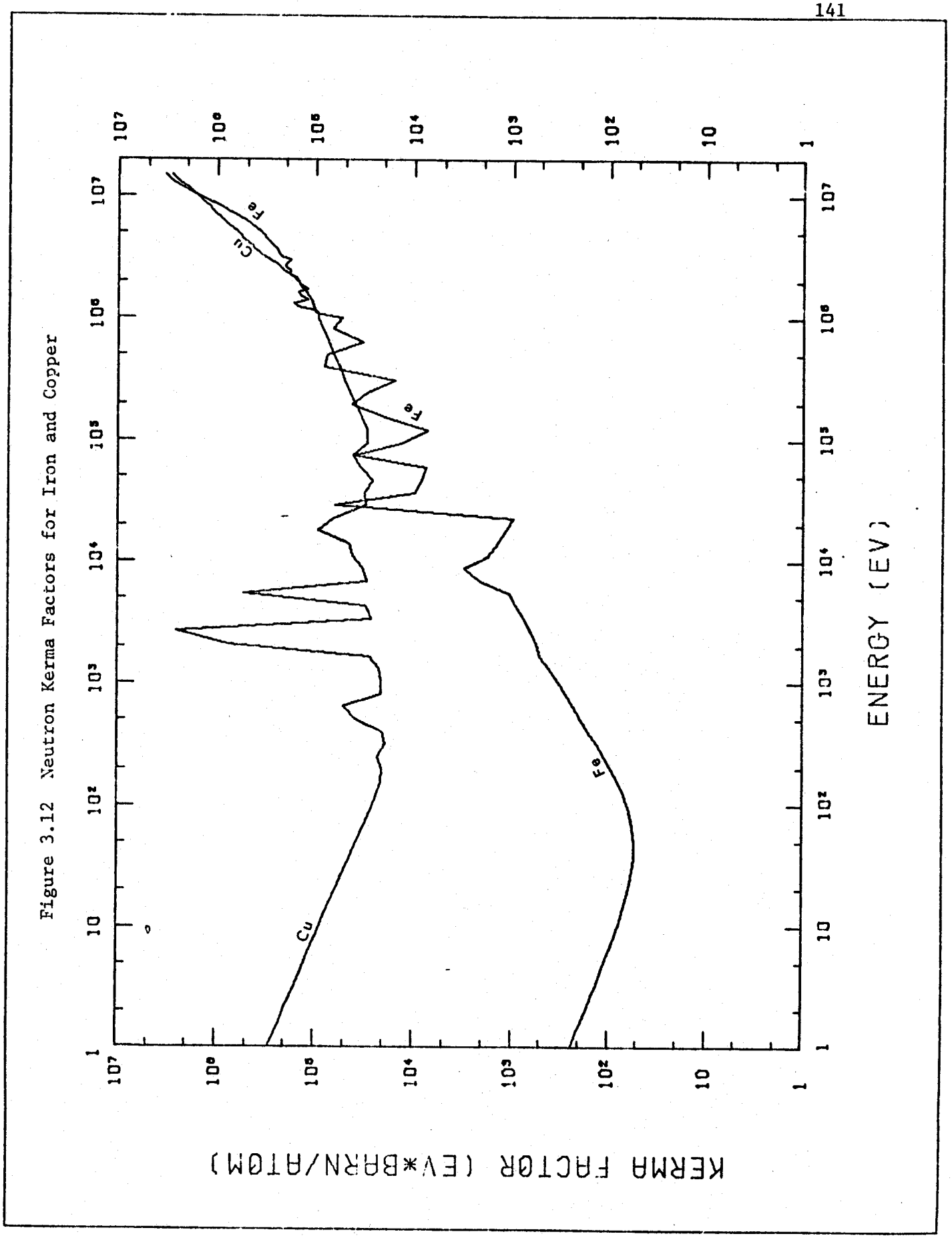

Figure 3.12 Neutron Kerma Factors for Iron and Copper

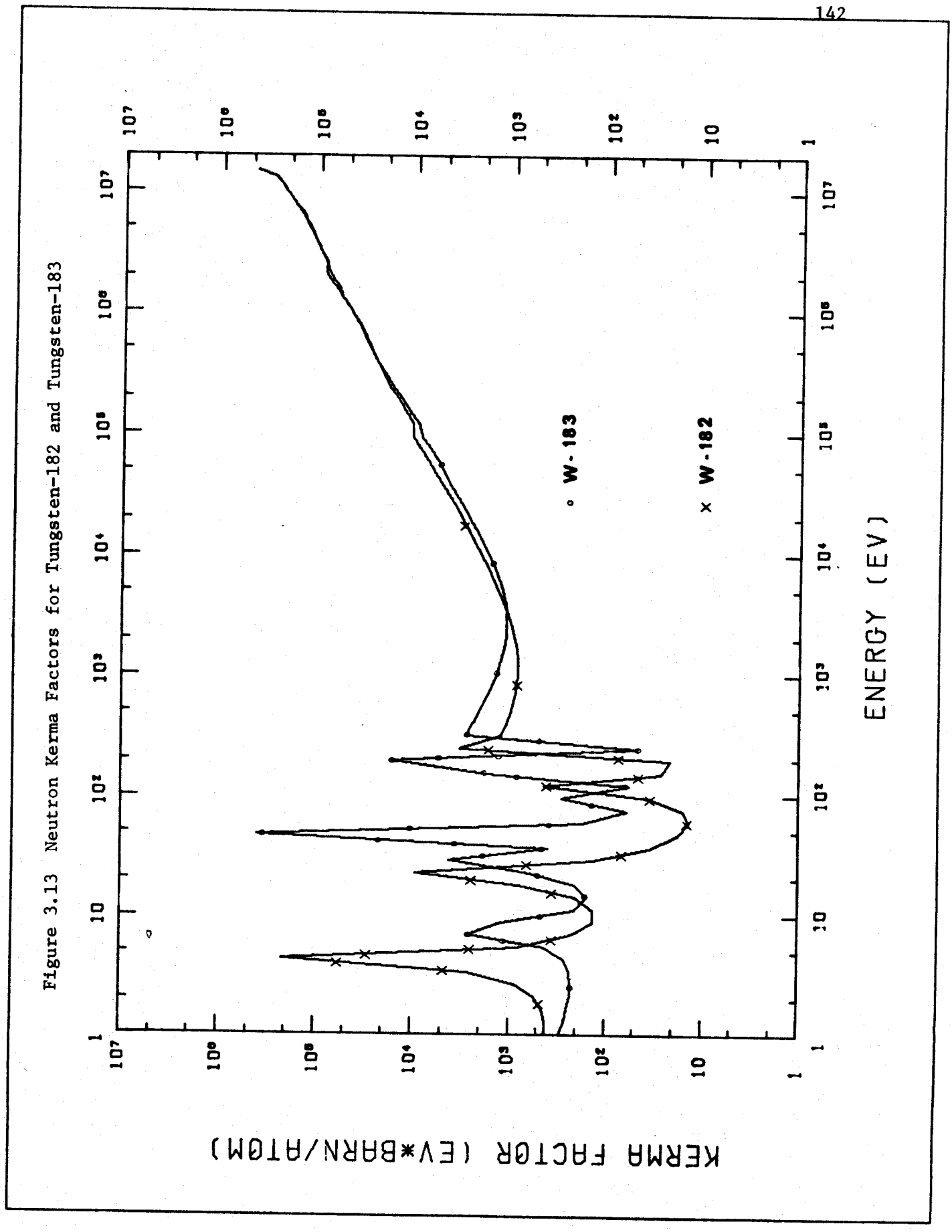

Figure 3.13 Neutron Kerma Factors for Tungsten-182 and Tungsten-183

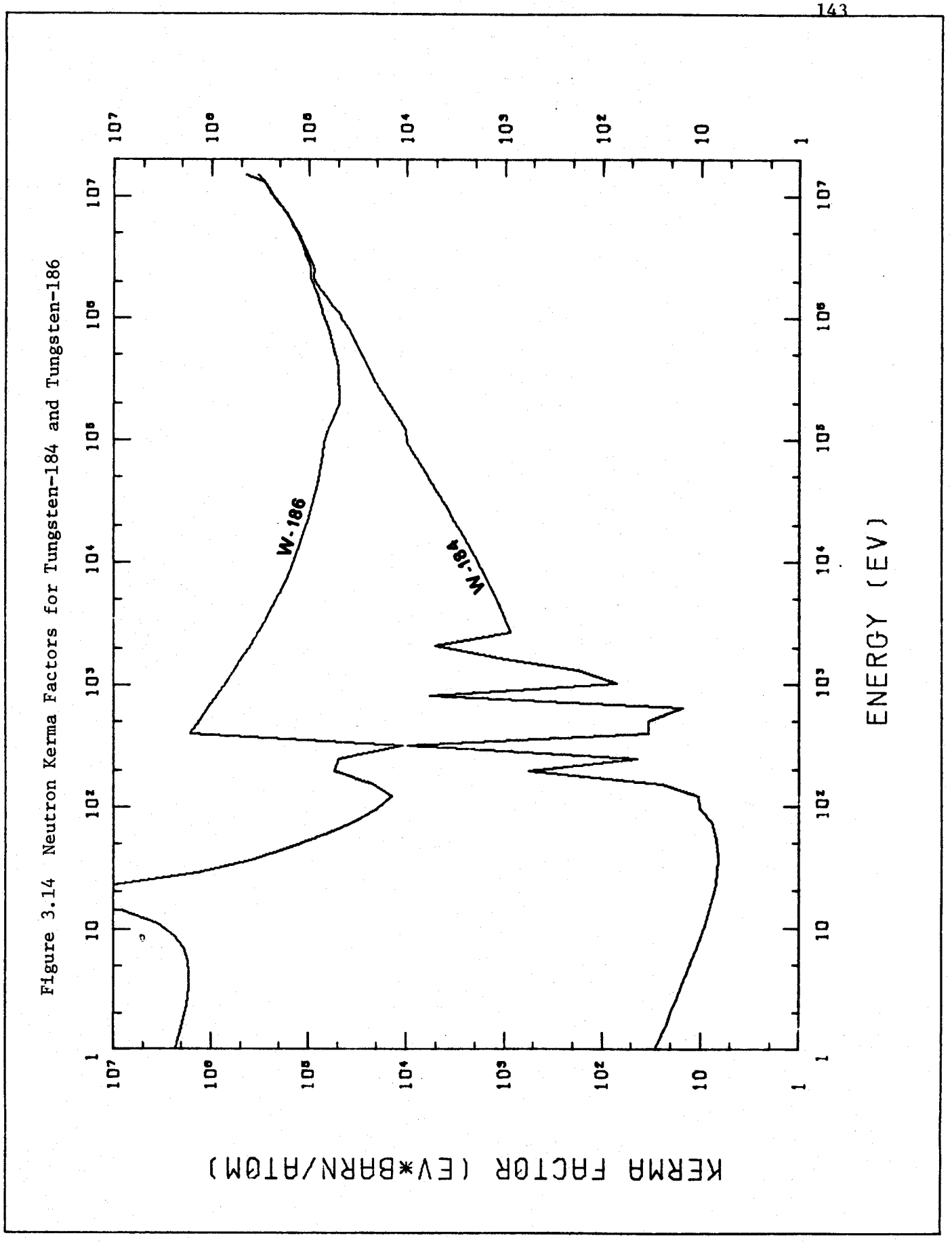

Figure 3.14 Neutron Kerma Factors for Tungsten-184 and Tungsten-186

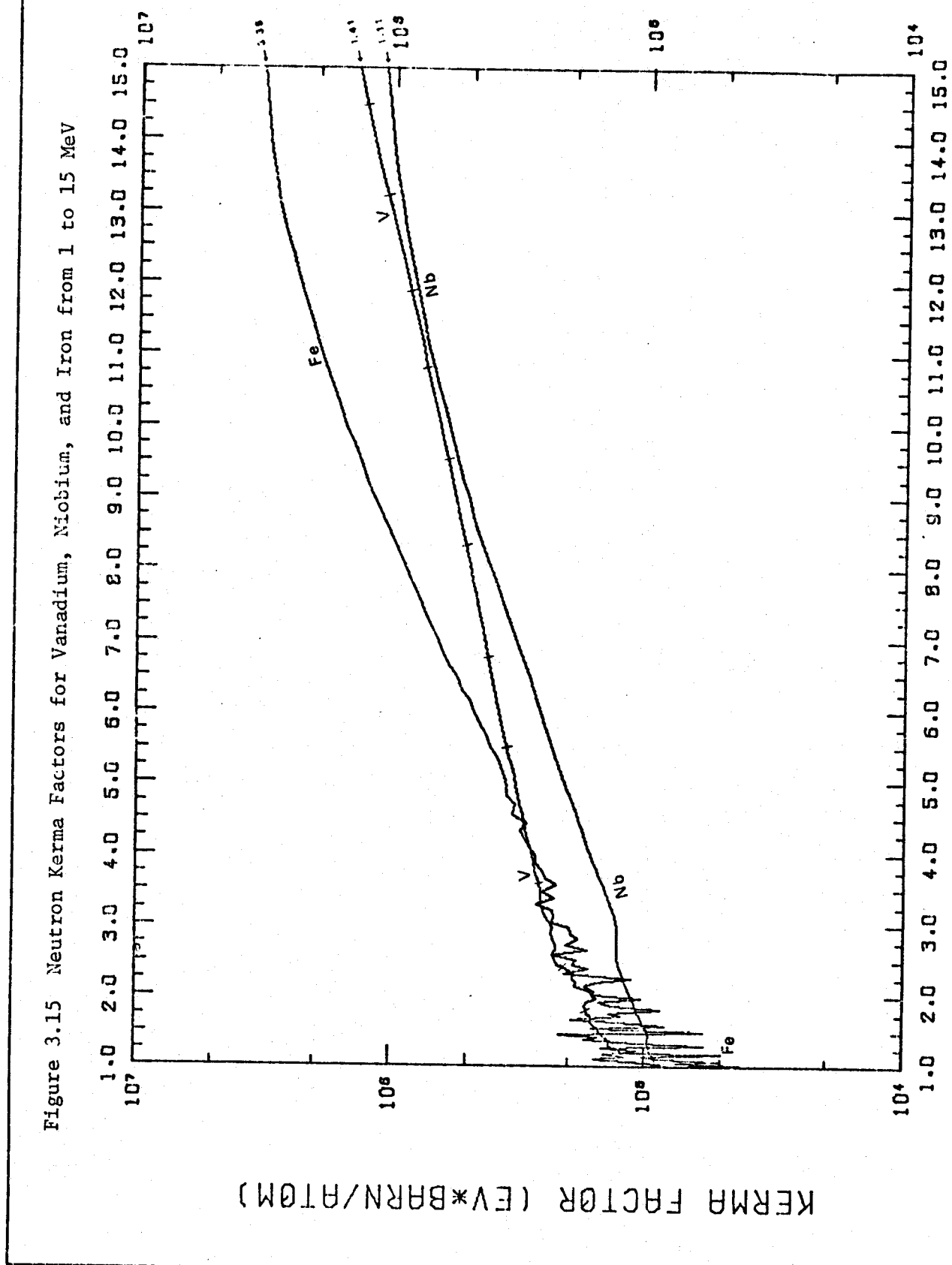

Figure 3.15 Neutron Kerma Factors for Vanadium, Niobium, and Iron from 1 to 15 MeV

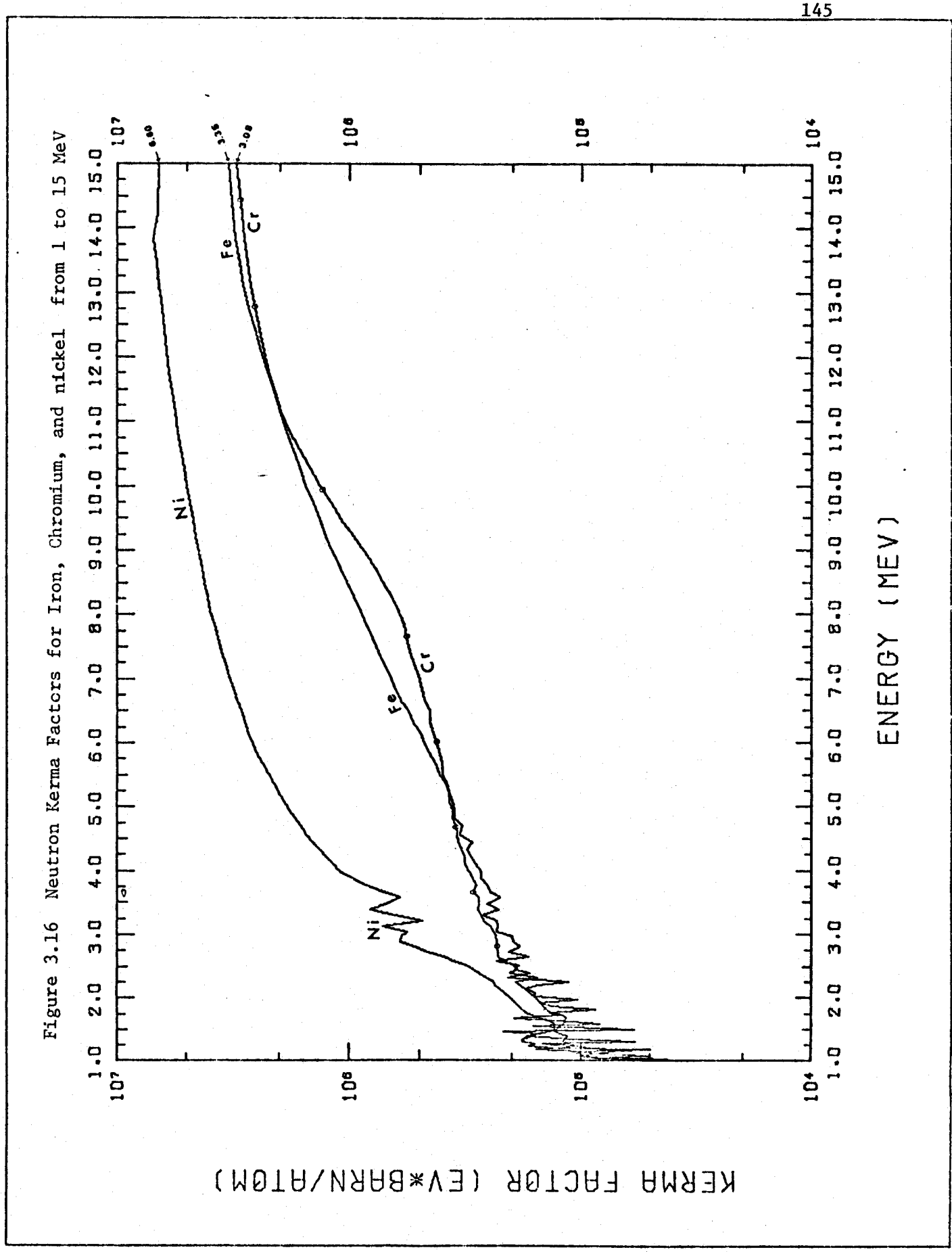

Figure 3.16 Neutron Kerma Factors for Iron, Chromium, and nickel from 1 to 15 MeV

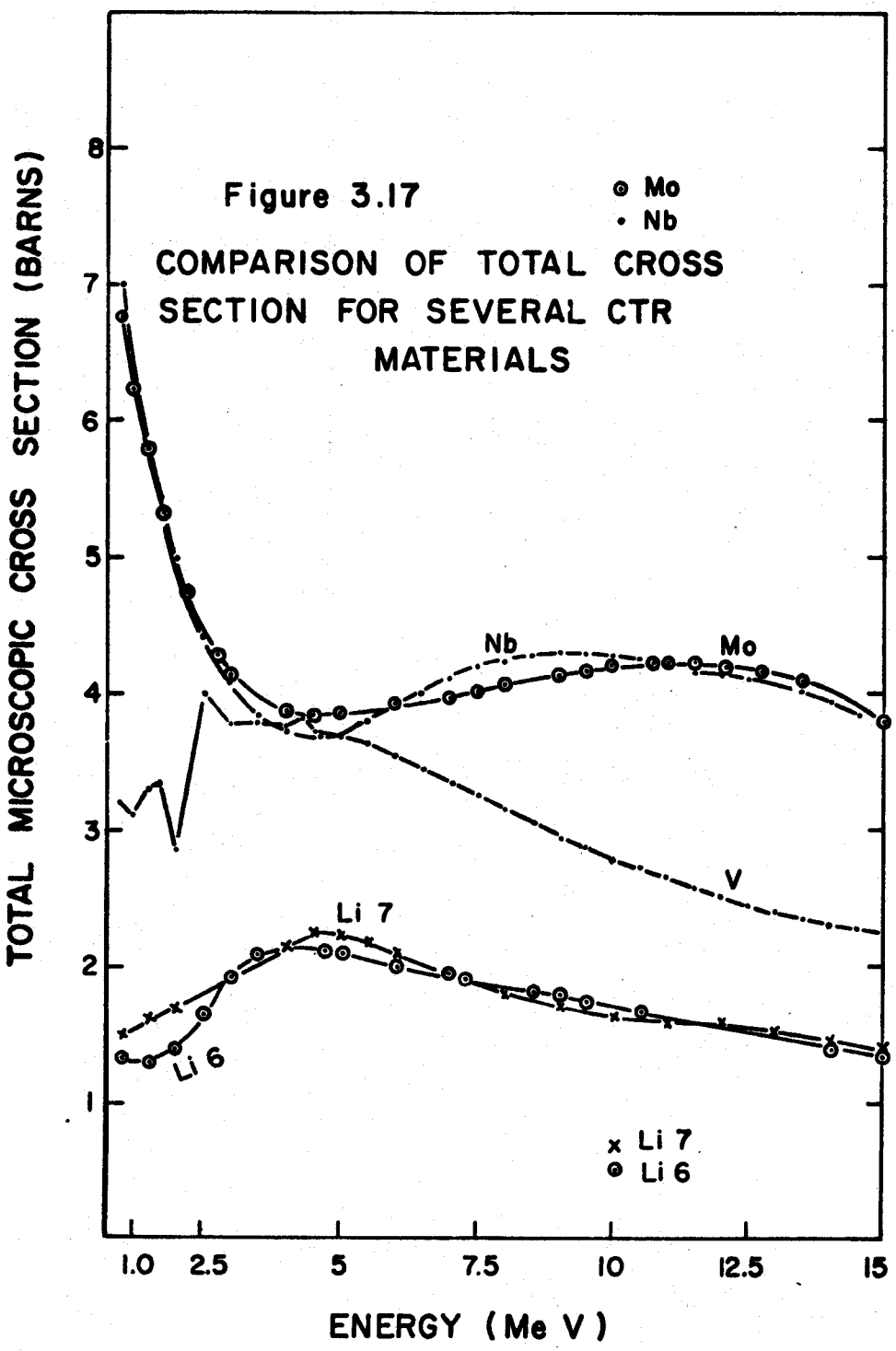
Figure 3.17
COMPARISON OF TOTAL CROSS SECTION FOR SEVERAL CTR MATERIALS
⊙ Mo
• Nb
TOTAL MICROSCOPIC CROSS SECTION (BARNS)
8
7
6
5
4
3
2
1
Nb
Mo
V
Li 7
Li 6
x Li 7
⊙ Li 6
1.0
2.5
5
7.5
10
12.5
15
ENERGY (Me V)

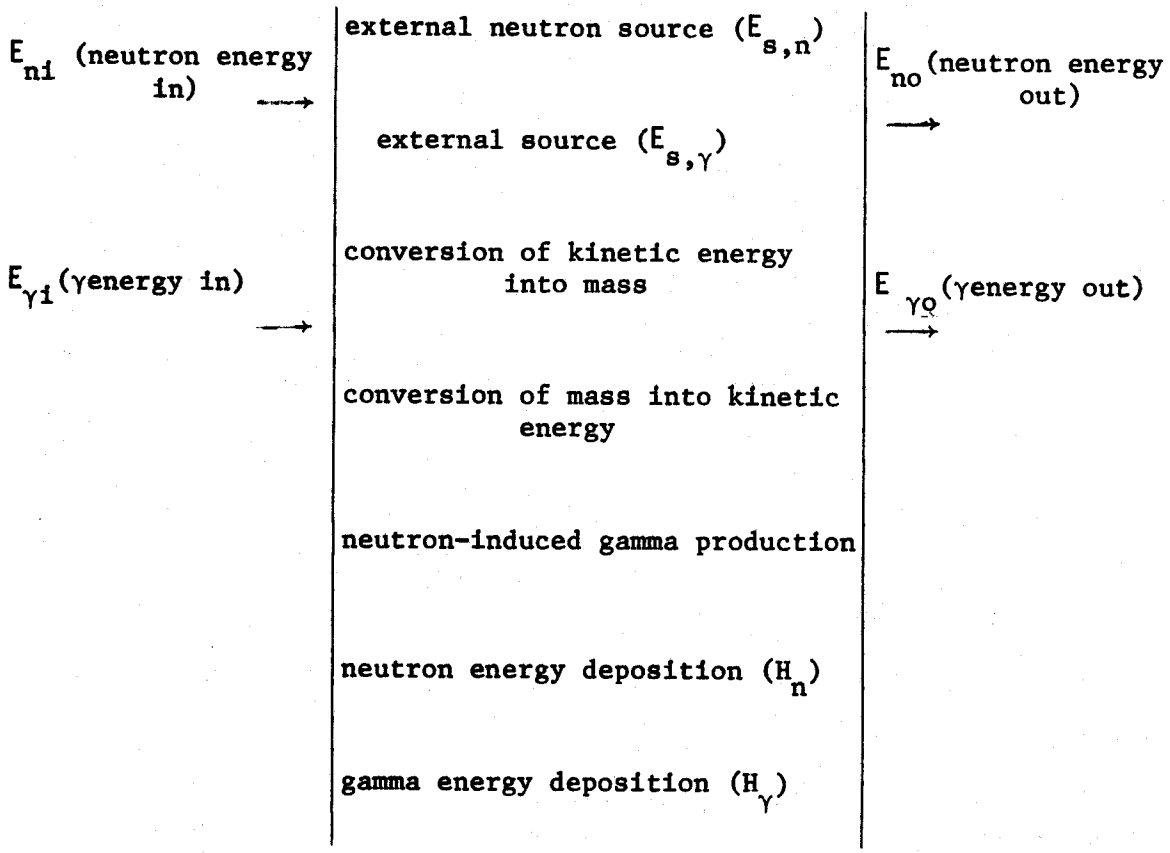

$$H_n + H_\gamma = (E_{n,i} + E_{\gamma,i}) - (E_{n,o} + E_{\gamma,o}) + E_{s,n} + E_{s,\gamma} +$$

$$\sum_j \sum_i R_{ij} Q_{ij} + \sum_j \sum_{i'} R_{i'j} E_{Di'j}$$

Figure 3.18 Energy Balance For a Segment of a Nuclear System

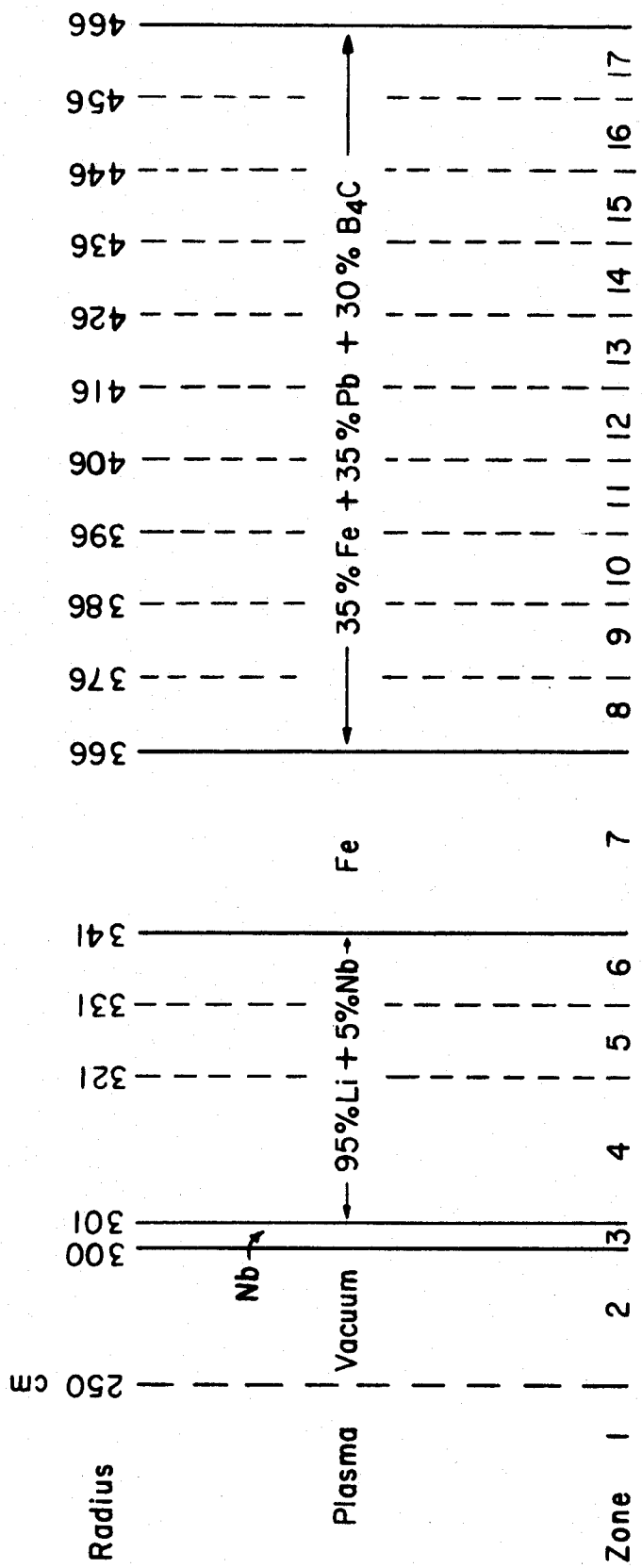

FIG. 3·19 Reference Design of a CTR Blanket & Shield

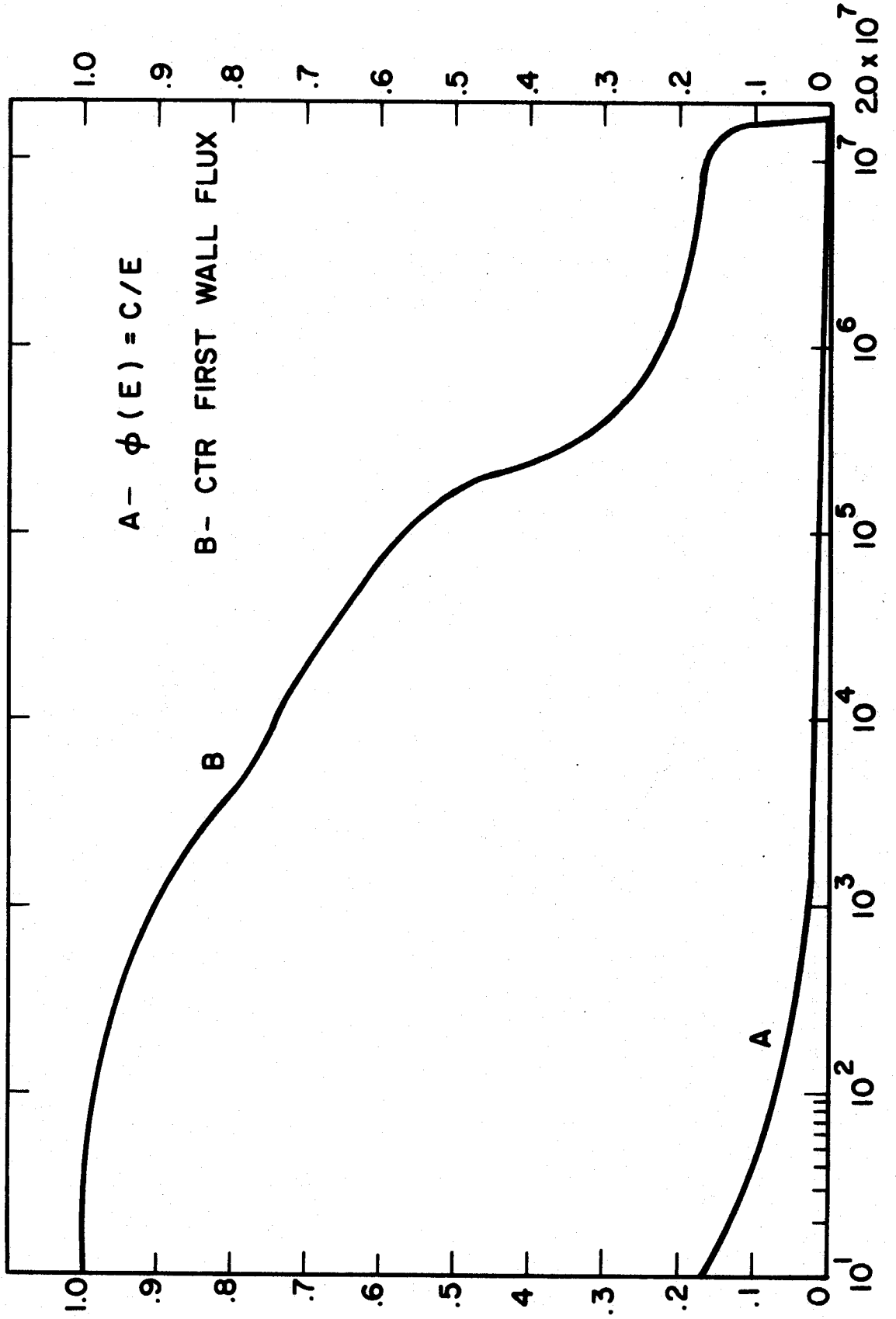

FIGURE 3.20 Fraction of Neutron Heating Generated in Li-6 With Neutrons of Energies Above E_o, as a Function of E_o for two Typical CTR Spectra

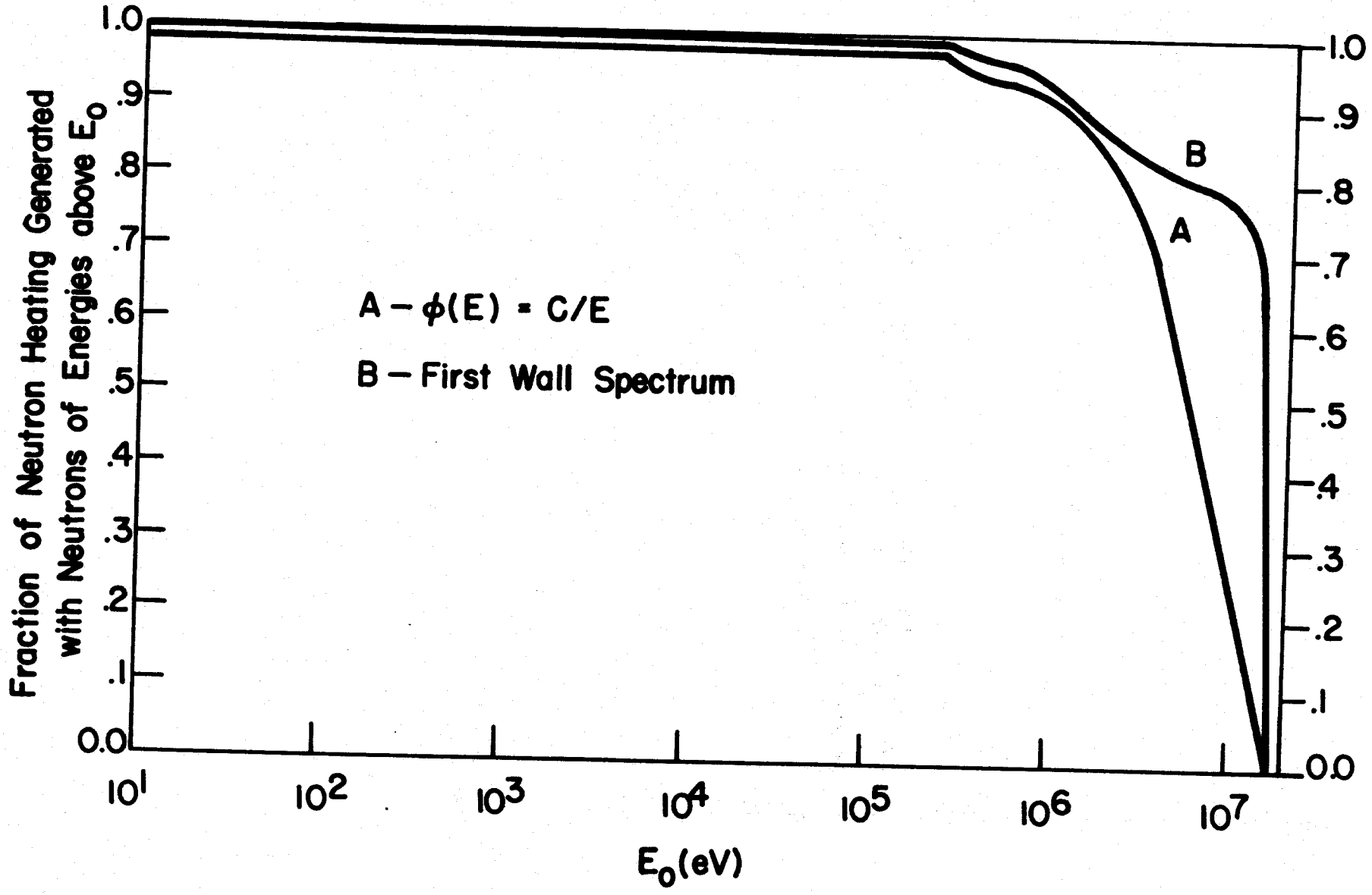

FIG. 3.21 Fraction of Neutron Heating Generated in Lithium-7 With Neutrons of Energies Above E_0, as a Function of E_0 for Typical CTR Spectra

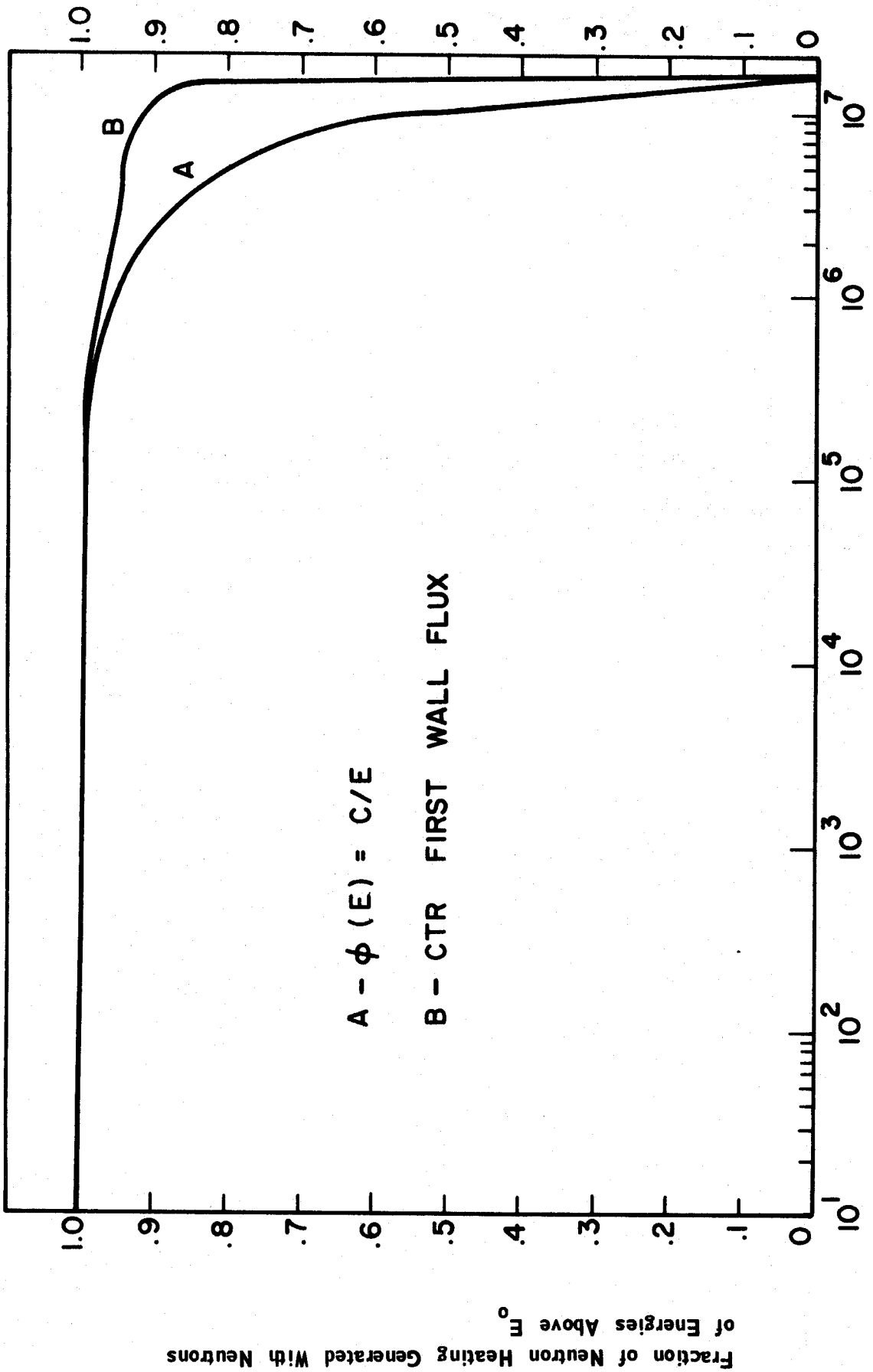

FIGURE 3.22 Fraction of Neutron Heating Generated in IRON With Neutrons of Energies Above E_o, as a Function of E_o for Typical CTR Spectra

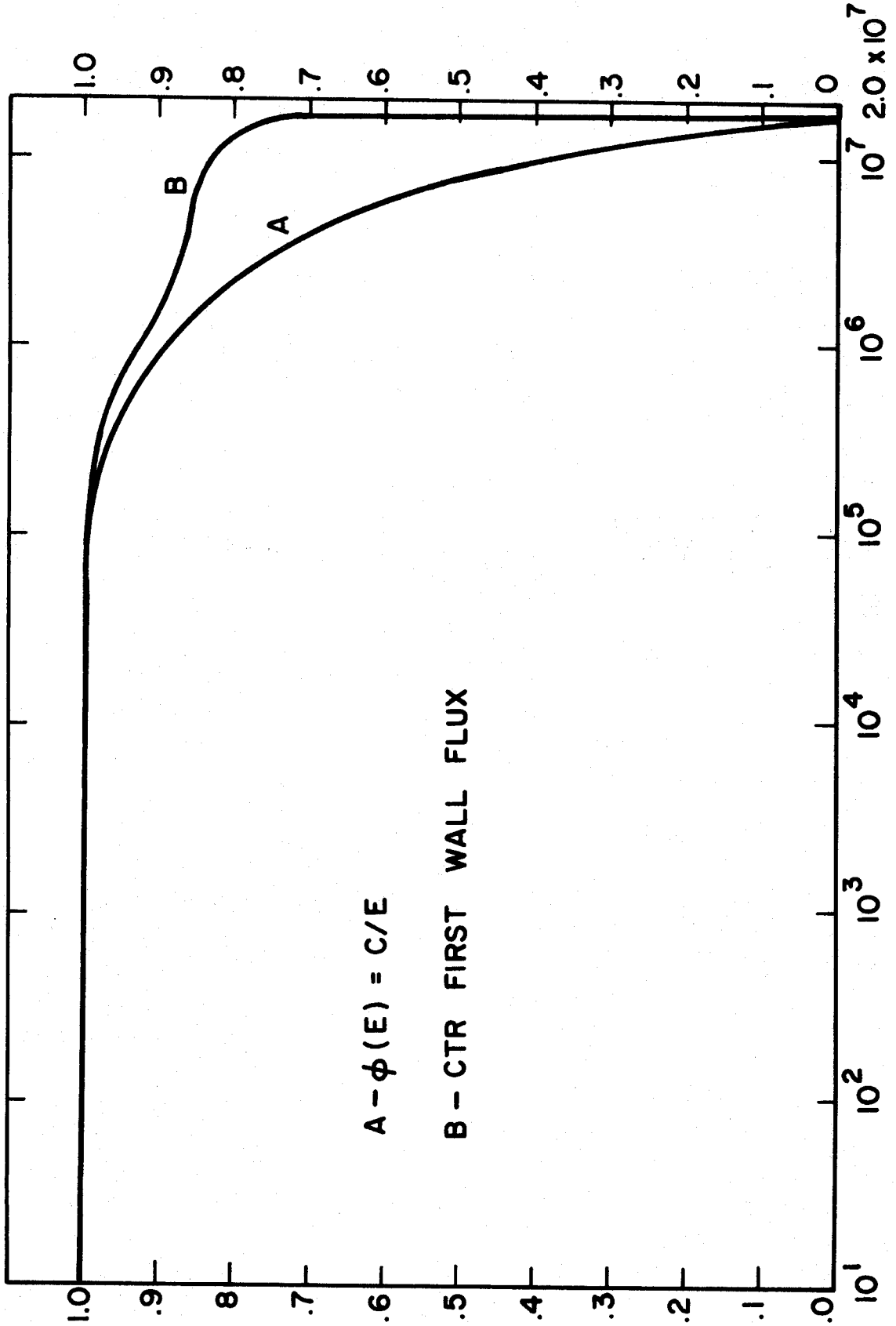

FIGURE 3.23 Fraction of Neutron Heating Generated in NIOBIUM With Neutrons of Energies Above E_o, as a Function of E_o for Typical CTR Spectra

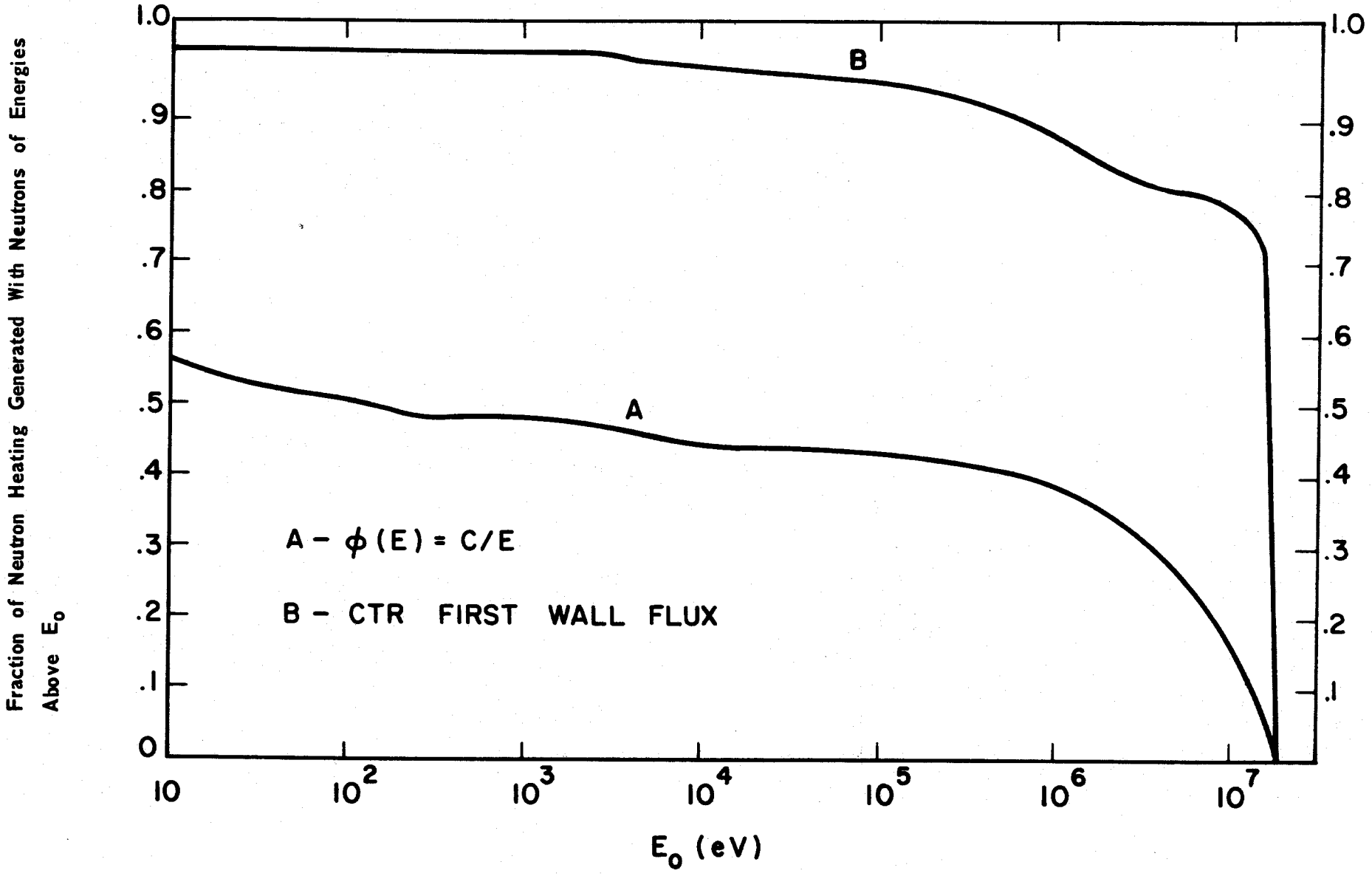

FIGURE 3.24 Fraction of Neutron Heating Generated in Vanadium With Neutrons of Energies Above E_o, as a Function of E_o for Typical CTR Spectra

TABLE 3.1

A list of materials of interest for use in CTR for which the following libraries were generated:

1. Pointwise neutron kerma factors and partial cross sections,
2. 100 neutron energy group kerma factors and partial cross sections, and
3. 43 gamma energy group kerma factors.

Material	ENDF B MAT	Material	ENDF/B MAT
He	1088	Cu-63	1085
Li-6	1115	Cu-65	1086
Li-7	1116	Cr	1121
N-14	1133	Ni	1123
O-16	1134	Fe	1180
H-1	1148	W-182	1060
Be-9	1154	W-183	1061
B-10	1155	W-184	1062
B-11	1160	W-186	1063
C-12	1165	Mo	1111
Al-27	1135	Mo	3111
Na-23	1156	Ta-181	1126
V	1017	Ta-182	1127
V	3023	Pb	1136
K	1150	Nb	1164

Table 3.2 is given on page 205.

TABLE 3.3 Average Decay Energy per Neutron Reaction for Neutron Kerma Factor Calculation

Material/ Reaction	Residual Nucleus	$T_{\frac{1}{2}}$ *	Mode of Decay	% intensity Particle Energy (endpoint for β) †	Average Decay Energy †
Lithium-6					
(n,t)	He^3	12.26 y	β-	0.0186	
(n,p)	He^6	0.80 s	β-	3.5080	1.560
Lithium-7					
(n,γ)	$Li^8(Be^8,2\alpha)$	0.85 s	β-,α	β 13.1020 α 1.4970	9.310
(n,d)	He^6	0.80 s	β-	3.5080	1.560
(n,n´p)	He^6	0.80 s	β-	3.5080	1.560
Boron-10					
(n,t)	Be^8		α	0.0475	0.095
Boron-11					
(n,γ)	B^{12}	0.02 s	β-	13.3700 (97%) 8.9400 (1.3%)	6.420
(n,p)	Be^{11}	13.60 s	β-	11.5100 (61%) 9.3700 (29%) 4.7000 (6%) 3.5200 (4%)	4.860
(n,α)	Li^8	0.84 s	β-,2α		9.310

* s = seconds, d = day, y = year, h = hour, m = month
† = (MeV)

TABLE 3.3 Average Decay Energy per Neutron Reaction for Neutron Kerma Factor Calculation (continued)

Material Reaction	Residual Nucleus	$T_{\frac{1}{2}}$ *	Mode of Decay	% intensity Particle Energy (endpoint for β) †	Average Decay Energy ÷
Beryllium					
(n,p)	Li^9	.176 s	β-	13.5000 (75%), 11.0000 (25%)	6.240
(n,d)	Li^8	.84 s	β-, α	13.1020 (β-), 1.4970 α	9.310
(n,α)	He^6_8	.80 s	β-	3.5080	1.560
(n,2n)	Be		α		These three reactions were combined and a decay energy of .095 MeV was used
(n,n´α)	He^5		α		
(n,n´)	Be^{*9}		α		
Vanadium (V-51)					
(n,γ)	V^{52}	3.75 m	β-	2.5360 (99%) 1.2040 (.9%)	1.070
(n,p)	Ti^{51}	5.80 m	β-	2.1400 (94%) 1.5300 (6%)	.934
(n,α)	Sc^{48}	1.83 d	β-	.6400 (94%) .4620 (6%)	0.210
Niobium					
(n,p)	Zr^{93}	1.50 x 10^6 y	β-	0.0300 (95%) 0.0600 (5%)	
(n,α)	Y^{90}	64.00 h	β-	2.2700	0.931

* s = seconds, d = day, y = year, h = hour, m = month
† = (MeV)

TABLE 3.3 Average Decay Energy per Neutron Reaction for Neutron Kerma Factor Calculation (continued)

Material/ Reaction	Residual Nucleus	$T_{\frac{1}{2}}$ *	Mode of Decay	% intensity Particle Energy (endpoint for β) †	Average Decay Energy †
Al-27					
(n,2n)	Al^{26}	7.4×10^5 y	β+,EC		
(n,2n)	Al^{*26} (.229 MeV level)	6.400 s	β+	2.7540(100% β+)	
(n,γ)	Al^{28}	2.310 m	β-	2.8550	1.2448
(n,p)	Mg^{27}	9.500 m	β-	1.7720 (69%), 1.5010 (31%)	0.7055
(n,α)	Na^{24}	14.960 h	β-	1.3925	0.5570
Flourine					
(n,2n)	F^{18}	109.700 m	β+,EC	.6350(97% β+)	0.2534
(n,γ)	F^{20}	11.560 s	β-	5.4100	2.4886
(n,p)	O^{19}	29.000 s	β-	4.6220 (38%) 3.2590 (62%)	1.7010
(n,α)	N^{16}	7.200 s	β-	10.4220 (26%) 4.2910 (68%) 3.3070(4.9%) 1.5520(1.1%)	2.6924

* s = seconds, d = day, y = year, h = hour, m = month
† = (MeV)

TABLE 3.3 Average Decay Energy per Neutron Reaction for Neutron Kerma Factor Calculation (continued)

Material/ Reaction	Residual Nucleus	$T_{\frac{1}{2}}$ *	Mode of Decay	% intensity Particle Energy (endpoint for β) †	Average Decay Energy †
Cr^{50}					
(n,2n)	Cr^{49}	41.90 m	β+	1.540 (53%) 1.449 (14%) 1.490 (27%)	0.60818
Cr^{52}					
(n,p)	V^{52}	3.75 m	β-	2.536 (99%) 1.204 (.9%)	1.07000
Cr-53					
(n,p)	V^{53}	2.00 m	β-	2.500	1.06540
(n,n´p)	V^{52}	3.75 m	β-	2.536 (99%) 1.204 (.9%)	1.07000
Fe^{56}					
(n,p)	Mn^{56}	2.58 h	β-	2.855 (53%) 1.044 (30%) 0.745 (16%) 0.332 (1%)	0.77700
Fe^{57}					
(n,p)	Mn^{57}	1.70 m	β-	2.550 (82%) 1.100 (18%)	0.94100

* s = seconds, d = day, y = year, h = hour, m = month
† = (MeV)

TABLE 3.3 Average Decay Energy per Neutron Reaction for Neutron Kerma Factor Calculation (continued)

Material/ Reaction	Residual Nucleus	$T_{\frac{1}{2}}$*	Mode of Decay	% intensity Particle Energy (endpoint for β) †	Average Decay Energy †
Cu-63					
(n,2n)	Cu^{62}	9.760 m	β+ (97%) EC (2.5%)	2.9200	1.2800
(n,γ)	Cu^{64}	12.800 h	β-	0.5730 (β-)	0.1930
			β+,EC	0.6560 (β+)	
(n,p)	Ni^{63}	92.000 y	β-	0.0670	
(n,α)	Co^{60}	5.260 y	β-	0.3140 (99%)	
Cu-65					
(n,2n)	Cu^{64}	12.800 h	β-	0.5730 (β-)	0.1930
			β+,EC	0.6560 (β+)	
(n,γ)	Cu^{66}	5.100 m	β-	2.6300 (91%)	1.0874
				1.5910 (9%)	
(n,p)	Ni^{65}	2.560 h	β-	2.1300 (58%)	0.6360
				1.0150 (11%),	
				0.6490 (29%),	
				0.5100(1.2%),	
				0.4100(0.8%)	
(n,α)	Co^{62}	13.900 m	β-	2.8800 (75%)	1.0090
				0.8800 (25%)	

* s = seconds, d = day, y = year, h = hour, m = month
† = (MeV)

TABLE 3.3 Average Decay Energy per Neutron Reaction for Neutron Kerma Factor Calculation (continued)

Material/ Reaction	Residual Nucleus	$T_{\frac{1}{2}}$ *	Mode of Decay	% intensity Particle Energy (endpoint for β) †	Average Decay Energy †
Na-23					
(n,γ)	Na^{24}	14.960 h	β-	1.3925	0.55700
(n,p)	Ne^{23}	37.600 s	β-	4.3800 (67%), 3.9410 (32%), 2.3000(0.9%), 1.5000(0.1%)	1.90900
(n,α)	F^{20}	11.400 s	β-	5.4100	2.48860
Oxygen-16					
(n,p)	N^{16}	7.200 s	β-	10.4220 (26%) 4.2910 (68%) 3.3070(4.9%) 1.5520(1.1%)	2.69240
Ta-181					
(n,p)	Hf^{181}	42.500 d	β-	0.4080 (93%) 0.4040 (7%)	.12329
(n,α)	Lu^{178}	30.000 m	β-	2.2500	0.90500
Ni-58					
(n,2n)	Ni^{57}	36.000 h	β+ (46%) EC (54%)	0.8500 (40%) 0.7300 (6%)	0.38380
Pb-208					
(n,γ)	Pb^{209}	3.300 h	β-	0.6350	0.20637

* s = seconds, d = day, y = year, h = hour, m = month
† = (MeV)

TABLE 3.3 Average Decay Energy per Neutron Reaction for Neutron Kerma Factor Calculation (continued)

Material/ Reaction	Residual Nucleus	$T_{\frac{1}{2}}$ *	Mode of Decay	% intensity Particle Energy (endpoint for β) †	Average Decay Energy ÷
W-183					
(n,p)	Ta^{183}	5.00 d	β-	.61693 (84%) .65790 (6%) .76050 (7%) .77830 (3%)	0.20850
W-184					
(n,γ)	W^{185}	75.00 d	β-	.42900	0.13090
(n,p)	Ta^{184}	8.70 h	β-	1.19000 (93%) 1.45000 (6%) 1.76000(.85%) 2.64000(.15%)	0.42800
(n,α)	Hf^{181}	42.50 d	β-	0.40800 (93%) 0.40400 (7%)	0.12329
W-186					
(n,2n)	W^{185}	75.00 d	β-	0.42900	0.13090
(n,γ)	W^{187}	23.90 h	β-	1.33000 (20%) 0.63000 (70%) 0.34000 (10%)	0.34138
(n,p)	Ta^{186}	10.50 m	β-	2.20000	0.88500
(n,α)	Hf^{183}	65.00 m	β-	1.60000 (100% β- to Ta^{183} which decays with 5.0 d)	0.81350

* s = seconds, d = day, y = year, h = hour, m = month

†

Table 3.4 Neutron 100 Energy Group Structure in ev

Group	Group Limits E(Top)		E(Low)		E(Mid Point)	
1	1.4918	(+7)*	1.3499	(+7)	1.4208	(+7)
2	1.3499	(+7)	1.2214	(+7)	1.2856	(+7)
3	1.2214	(+7)	1.1052	(+7)	1.1633	(+7)
4	1.1052	(+7)	1.0000	(+7)	1.0526	(+7)
5	1.0000	(+7)	9.0484	(+6)	9.5242	(+6)
6	9.0484	(+6)	8.1873	(+6)	8.6178	(+6)
7	8.1873	(+6)	7.4082	(+6)	7.7977	(+6)
8	7.4082	(+6)	6.7032	(+6)	7.0557	(+6)
9	6.7032	(+6)	6.0653	(+6)	6.3843	(+6)
10	6.0653	(+6)	5.4881	(+6)	5.7767	(+6)
11	5.4881	(+6)	4.9659	(+6)	5.2270	(+6)
12	4.9659	(+6)	4.4933	(+6)	4.7296	(+6)
13	4.4933	(+6)	4.0657	(+6)	4.2795	(+6)
14	4.0657	(+6)	3.6788	(+6)	3.8722	(+6)
15	3.6788	(+6)	3.3287	(+6)	3.5038	(+6)
16	3.3287	(+6)	3.0119	(+6)	3.1703	(+6)
17	3.0119	(+6)	2.7253	(+6)	2.8686	(+6)
18	2.7253	(+6)	2.4660	(+6)	2.5956	(+6)
19	2.4660	(+6)	2.2313	(+6)	2.3486	(+6)
20	2.2313	(+6)	2.0910	(+6)	2.1251	(+6)
21	2.0190	(+6)	1.8268	(+6)	1.9229	(+6)
22	1.8268	(+6)	1.6350	(+6)	1.7399	(+6)
23	1.6530	(+6)	1.4957	(+6)	1.5743	(+6)
24	1.4957	(+6)	1.3534	(+6)	1.4245	(+6)
25	1.3534	(+6)	1.2246	(+6)	1.2890	(+6)
26	1.2246	(+6)	1.1080	(+6)	1.1663	(+6)
27	1.1080	(+6)	1.0026	(+6)	1.0553	(+6)
28	1.0026	(+6)	9.0718	(+5)	9.5488	(+5)
29	9.0718	(+5)	8.2085	(+5)	8.6401	(+5)
30	8.2085	(+5)	7.4274	(+5)	7.8179	(+5)
31	7.4274	(+5)	6.7206	(+5)	7.0740	(+5)
32	6.7206	(+5)	6.0810	(+5)	6.4008	(+5)
33	6.0810	(+5)	5.5023	(+5)	5.7917	(+5)
34	5.5023	(+5)	4.9787	(+5)	5.2405	(+5)
35	4.9787	(+5)	4.5049	(+5)	4.7418	(+5)
36	4.5049	(+5)	4.0762	(+5)	4.2906	(+5)
37	4.0762	(+5)	3.6883	(+5)	3.8827	(+5)
38	3.6883	(+5)	3.3373	(+5)	3.5128	(+5)
39	3.3373	(+5)	3.0197	(+5)	3.1785	(+5)
40	3.0197	(+5)	2.7324	(+5)	2.8761	(+5)
41	2.7324	(+5)	2.4724	(+5)	2.6024	(+5)
42	2.4724	(+5)	2.2371	(+5)	2.3547	(+5)
43	2.2371	(+5)	2.0242	(+5)	2.1306	(+5)
44	2.0242	(+5)	1.8316	(+5)	1.9279	(+5)
45	1.8316	(+5)	1.6573	(+5)	1.7444	(+5)

Table3.4 Continued

Group	Group Limits					
	E(Top)		E(Low)		E(Mid Point)	
46	1.6573	(+5)	1.4996	(+5)	1.5784	(+5)
47	1.4996	(+5)	1.3569	(+5)	1.4282	(+5)
48	1.3569	(+5)	1.2277	(+5)	1.2923	(+5)
49	1.2277	(+5)	1.1109	(+5)	1.1693	(+5)
50	1.1109	(+5)	8.6517	(+4)	9.8803	(+4)
51	8.6517	(+4)	6.7379	(+4)	7.6948	(+4)
52	6.7379	(+4)	5.2475	(+4)	5.9927	(+4)
53	5.2475	(+4)	4.0868	(+4)	4.6671	(+4)
54	4.0868	(+4)	3.1828	(+4)	3.6348	(+4)
55	3.1828	(+4)	2.4788	(+4)	2.8308	(+4)
56	2.4788	(+4)	1.9305	(+4)	2.2046	(+4)
57	1.9305	(+4)	1.5034	(+4)	1.7169	(+4)
58	1.5034	(+4)	1.1709	(+4)	1.3372	(+4)
59	1.1709	(+4)	9.1188	(+3)	1.0414	(+4)
60	9.1188	(+3)	7.1017	(+3)	8.1103	(+3)
61	7.1017	(+3)	5.5308	(+3)	6.3163	(+3)
62	5.5308	(+3)	4.3074	(+3)	4.9191	(+3)
63	4.3074	(+3)	3.3546	(+3)	3.8310	(+3)
64	3.3546	(+3)	2.6126	(+3)	2.9836	(+3)
65	2.6126	(+3)	2.0347	(+3)	2.3236	(+3)
66	2.0347	(+3)	1.5846	(+3)	1.8096	(+3)
67	1.5846	(+3)	1.2341	(+3)	1.4094	(+3)
68	1.2341	(+3)	9.6112	(+2)	1.0976	(+3)
69	9.6112	(+2)	7.4852	(+2)	8.5482	(+2)
70	7.4852	(+2)	5.8295	(+2)	6.6573	(+2)
71	5.8295	(+2)	4.5733	(+2)	5.1847	(+2)
72	4.5733	(+2)	3.5358	(+2)	4.0379	(+2)
73	3.5358	(+2)	2.7536	(+2)	3.1447	(+2)
74	2.7536	(+2)	2.1445	(+2)	2.4491	(+2)
75	2.1445	(+2)	1.6702	(+2)	1.9074	(+2)
76	1.6702	(+2)	1.3007	(+2)	1.4855	(+2)
77	1.3007	(+2)	1.0130	(+2)	1.1569	(+2)
78	1.0130	(+2)	7.8893	(+1)	9.0097	(+1)
79	7.8893	(+1)	6.1442	(+1)	7.0168	(+1)
80	6.1442	(+1)	4.7851	(+1)	5.4647	(+1)
81	4.7851	(+1)	3.7267	(+1)	4.2559	(+1)
82	3.7267	(+1)	2.9023	(+1)	3.3145	(+1)
83	2.9023	(+1)	2.2603	(+1)	2.5813	(+1)
84	2.2603	(+1)	1.7603	(+1)	2.0103	(+1)
85	1.7603	(+1)	1.3710	(+1)	1.5657	(+1)
86	1.3710	(+1)	1.0677	(+1)	1.2193	(+1)
87	1.0667	(+1)	8.3153	(+0)	9.4962	(+0)
88	8.3153	(+0)	6.4760	(+0)	7.3956	(+0)
89	6.4760	(+0)	5.0435	(+0)	5.7597	(+0)
90	5.0435	(+0)	3.9279	(+0)	4.4857	(+0)

Table 3.4 Continued

Group	Group Limits E(Top)		E(Low)		E(Mid Point)	
91	3.9279	(+0)	3.0590	(+0)	3.4934	(+0)
92	3.0590	(+0)	2.3824	(+0)	2.7207	(+0)
93	2.3824	(+0)	1.8554	(+0)	2.1189	(+0)
94	1.8554	(+0)	1.4450	(+0)	1.6502	(+0)
95	1.4450	(+0)	1.1254	(+0)	1.2852	(+0)
96	1.1254	(+0)	8.7643	(-1)	1.0009	(+0)
97	8.7643	(-1)	6.8256	(-1)	7.7949	(-1)
98	6.8256	(-1)	5.3158	(-1)	6.0707	(-1)
99	5.3158	(-1)	4.1399	(-1)	4.7279	(-1)
100	4.1399	(-1)	2.2000	(-1)	2.1800	(-1)

*($\pm$n) represents ($10^{\pm n}$)

Table3.5 Gamma-Ray 43 Energy Group Structure in MeV

Group	Group Limits		Mid Point Energy
	E(Top)	E(Low)	
1	14.00	13.00	13.50
2	13.00	12.00	12.50
3	12.00	11.00	11.50
4	11.00	10.00	10.50
5	10.00	9.00	9.50
6	9.00	8.00	8.50
7	8.00	7.75	7.875
8	7.75	7.50	7.625
9	7.50	7.25	7.375
10	7.25	7.00	7.125
11	7.00	6.75	6.875
12	6.75	6.50	6.625
13	6.50	6.25	6.375
14	6.25	6.00	6.125
15	6.00	5.75	5.875
16	5.75	5.00	5.375
17	5.00	4.75	4.875
18	4.75	4.50	4.625
19	4.50	4.25	4.375
20	4.25	4.00	4.125
21	4.00	3.75	3.875
22	3.75	3.50	3.625
23	3.50	3.25	3.375
24	3.25	3.00	3.125
25	3.00	2.75	2.875
26	2.75	2.50	2.625
27	2.50	2.25	2.375
28	2.25	2.00	2.125
29	2.00	1.75	1.875
30	1.75	1.50	1.625
31	1.50	1.25	1.375
32	1.25	1.00	1.125
33	1.00	0.75	0.875
34	0.75	0.55	0.650
35	0.55	0.45	0.500
36	0.45	0.40	0.425
37	0.40	0.30	0.350
38	0.30	0.20	0.250
39	0.20	0.15	0.175
40	0.15	0.10	0.125
41	0.10	0.05	0.075
42	0.05	0.01	0.030
43	0.01	0.001	0.0055

TABLE 3.6 Sensitivity of Lithium-7 Group Kerma Factor* to Weighting Spectrum (for GAM-II 100 Group Structure)

Group	Midpoint Energy (eV)	W(E) = constant A	W(E) = $\frac{1}{E}$ B	LASL W(E)	% change $\frac{B-A}{A} \times 100$
1	1.350 (+7)	3.3350 (+6)	3.3330 (+6)	3.3129 (+6)	- 0.06010
2	1.221 (+7)	3.1206 (+6)	3.1192 (+6)	3.1613 (+6)	- 0.04480
3	1.105 (+7)	2.9534 (+6)	2.9519 (+6)	a	- 0.05080
4	1.000 (+7)	2.7811 (+6)	2.7795 (+6)	a	- 0.05750
5	9.048 (+6)	2.5689 (+6)	2.5672 (+6)	a	- 0.06620
6	8.187 (+6)	2.3699 (+6)	2.3684 (+6)	a	- 0.06330
7	7.408 (+6)	2.2096 (+6)	2.2085 (+6)	a	- 0.04980
8	6.703 (+6)	2.1480 (+6)	2.1479 (+6)	a	- 0.00467
12	4.493 (+6)	1.9452 (+6)	1.9443 (+6)	a	- 0.04630
20	2.019 (+6)	7.6184 (+5)	7.6116 (+5)	a	- 0.08900
35	4.505 (+5)	1.3049 (+5)	1.3042 (+5)	a	- 0.05360
40	2.732 (+5)	2.7099 (+5)	2.7261 (+5)	a	+ 0.60000
61	5.531 (+3)	2.5279 (+3)	2.5220 (+3)	a	- 0.23300
81	3.727 (+1)	8.4222 (+3)	8.4430 (+3)	a	+ 0.24700
93	1.855 (+0)	3.6935 (+4)	3.7034 (+4)	a	+ 0.26800
99	4.140 (-1)	7.8485 (+4)	7.8690 (+4)	a	+ 0.26120
100	2.180 (-1)	1.3664 (+5)	1.9468 (+5)	a	+42.50000
	η_s	4.7472 (+5)	4.7503 (+5)	4.7525 (+5)	+ 0.06530
	η_w	7.9548 (+5)	7.9498 (+5)	7.9208 (+5)	- 0.06290

* in units of electron volt . barn/atom
a = same as (B)

TABLE 3.7 Sensitivity of Vanadium Group Kerma Factor* to Weighting Spectrum (for GAM-II 100 Group Structure)

Group	Midpoint Energy (eV)	W(E) = constant A	W(E) = $\frac{1}{E}$ B	LASL W(E)	% change $\frac{B-A}{A} \times 100$
1	1.350 (+7)	1.2692 (+6)	1.2671 (+6)	1.2459 (+6)	- 0.1654
2	1.221 (+7)	1.0264 (+6)	1.0246 (+6)	1.0758 (+6)	- 0.1755
3	1.105 (+7)	8.4191 (+5)	8.4065 (+5)	8.4065 (+5)	- 0.1496
4	1.000 (+7)	7.1644 (+5)	7.1550 (+5)	7.1550 (+5)	- 0.1312
5	9.048 (+6)	6.1716 (+5)	6.1646 (+5)	6.1646 (+5)	- 0.1134
6	8.187 (+6)	5.4255 (+5)	5.4201 (+5)	5.4201 (+5)	- 0.0995
7	7.408 (+6)	4.8465 (+5)	4.8423 (+5)	4.8423 (+5)	- 0.0867
8	6.703 (+6)	4.3868 (+5)	4.3834 (+5)	4.3834 (+5)	- 0.0775
12	4.493 (+6)	3.1761 (+5)	3.1741 (+5)	3.1741 (+5)	- 0.0630
20	2.019 (+6)	1.7928 (+5)	1.7908 (+5)	1.7908 (+5)	- 0.1115
35	4.505 (+5)	5.5182 (+4)	5.5458 (+4)	5.5458 (+4)	+ 0.5000
40	2.732 (+5)	5.4378 (+4)	5.4193 (+4)	5.4193 (+4)	- 0.3402
61	5.531 (+3)	1.1487 (+5)	1.1258 (+5)	1.1258 (+5)	- 1.9935
81	3.727 (+1)	1.3368 (+5)	1.3401 (+5)	1.3401 (+5)	+ 0.2470
93	1.855 (+0)	5.9293 (+5)	5.9449 (+5)	5.9449 (+5)	+ 0.2631
99	4.140 (-1)	1.2555 (+6)	1.2588 (+6)	1.2588 (+6)	+ 0.2630
100	2.180 (-1)	2.1956 (+6)	3.1375 (+6)	3.1375 (+6)	+ 42.8994
	η_s	2.5747 (+5)	2.6699 (+5)	2.6729 (+5)	+ 3.6975
	η_w	2.9305 (+5)	2.9258 (+5)	2.8960 (+5)	- 0.1604

* in units of electron volt . barn/atom

TABLE 3.8 Sensitivity of Lithium-6 Energy Group Kerma Factor to Weighting Spectrum (for GAM-II Group Structure)

Energy Group	Midpoint Energy (eV)	W(E) = constant A	LASL W(E) B	%change $\frac{B-A}{A} \times 100$
1	1.350 (+7)	4.4111 (+6)	4.4003 (+6)	- 0.24480
2	1.221 (+7)	4.2642 (+6)	4.2925 (+6)	+ 0.66360
3	1.105 (+7)	4.1545 (+6)	4.1537 (+6)	- 0.01920
4	1.000 (+7)	4.0258 (+6)	4.0246 (+6)	- 0.02980
5	9.048 (+6)	3.8981 (+6)	3.8972 (+6)	- 0.02308
6	8.187 (+6)	3.7756 (+6)	3.7743 (+6)	- 0.03443
7	7.408 (+6)	3.6184 (+6)	3.6171 (+6)	- 0.35920
8	6.703 (+6)	3.4670 (+6)	3.4658 (+6)	- 0.03460
12	4.493 (+6)	2.9809 (+6)	2.9802 (+6)	- 0.02348
20	2.019 (+6)	2.0076 (+6)	2.0068 (+6)	- 0.03985
35	4.505 (+5)	2.1352 (+6)	2.1378 (+6)	+ 0.12170
40	2.732 (+5)	1.0099 (+7)	1.0137 (+7)	+ 0.37630
61	5.531 (+3)	9.0078 (+6)	9.0310 (+6)	+ 0.25750
81	3.727 (+1)	1.0982 (+8)	1.1011 (+8)	+ 0.26400
93	1.855 (+0)	4.9245 (+8)	4.9375 (+8)	+ 0.26400
99	4.140 (-1)	1.0429 (+9)	1.0457 (+9)	+ 0.26850
100	2.180 (-1)	1.8239 (+9)	2.6063 (+9)	+ 42.90000
	η_s	1.0878 (+8)	1.1684 (+8)	+ 7.40900
	η_w	4.9424 (+6)	4.9455 (+6)	+ 0.06272

TABLE 3.9 Lithium-6 Thermal Group Kerma Factor for Various Weighting Spectra

Energy Range	W (E)	k (thermal group kerma factor)
.022 < E <.414	constant	1.8239 (+9)
.022 < E <.414	1/E	2.6063 (+9)
.001 $\leq$ E $\leq$.200	Maxwellian (300^{O}K)	3.9140 (+9)
.200 $\leq$ E $\leq$.414	1/E	
0 $\leq$ E $\leq$ .414	Maxwellian (300^{O}K)	3.9609 (+9)
0 $\leq$ E $\leq$ .414	Maxwellian (600^{O}K)	2.8008 (+9)
0 $\leq$ E $\leq$ .414	Maxwellian (1000^{O}K)	2.1695 (+9)

TABLE 3.10 Neutron Heating per Unit Fluence for Uniform Group Flux (C/E) and CTR Blanket First Wall Flux

Material	Heating per Unit Fluence in eV. barn/atom	
	Uniform (GAM-II) Group Flux (η_s)	Blanket First Wall Flux (η_w)
H-1	1.3232 ($^{+}6$)	1.9220 ($^{+}6$)
H-2	8.9317 ($^{+}5$)	1.2875 ($^{+}6$)
He	6.8592 ($^{+}5$)	9.4207 ($^{+}5$)
Li-6	1.1684 ($^{+}8$)	4.9455 ($^{+}6$)
Li-7	4.7525 ($^{+}5$)	7.9208 ($^{+}5$)
Be-9	4.8390 ($^{+}5$)	8.8523 ($^{+}5$)
B-10	2.7463 ($^{+}8$)	7.2484 ($^{+}6$)
B-11	2.8431 ($^{+}5$)	5.0805 ($^{+}5$)
C-12	3.1895 ($^{+}5$)	7.4605 ($^{+}5$)
O-16	2.9897 ($^{+}5$)	7.3357 ($^{+}5$)
Na-23	2.7397 ($^{+}5$)	6.6978 ($^{+}5$)
Al-27	2.8324 ($^{+}5$)	8.1872 ($^{+}5$)
V	2.6729 ($^{+}5$)	2.8960 ($^{+}5$)
Cr	1.7750 ($^{+}5$)	5.7093 ($^{+}5$)
Ni	5.7031 ($^{+}5$)	1.3559 ($^{+}6$)
Fe	1.9151 ($^{+}5$)	6.2025 ($^{+}5$)
Cu-63	3.1195 ($^{+}5$)	6.6301 ($^{+}5$)
Cu-65	3.1737 ($^{+}5$)	3.5170 ($^{+}5$)
Cu(natural)	3.1362 ($^{+}5$)	5.6682 ($^{+}5$)
Nb	9.0062 ($^{+}4$)	2.2813 ($^{+}5$)
Ta-181	4.3584 ($^{+}4$)	7.6382 ($^{+}4$)
W-182	4.5902 ($^{+}4$)	8.5089 ($^{+}4$)
W-183	4.4777 ($^{+}4$)	8.5610 ($^{+}4$)
W-184	4.3192 ($^{+}4$)	8.4098 ($^{+}4$)
W-186	6.7309 ($^{+}6$)	1.5949 ($^{+}5$)
Pb	4.4141 ($^{+}4$)	7.2026 ($^{+}4$)

TABLE 3.11 Comparison of Neutron Kerma Factors* Obtained from Present Work and from Ritts et al. Data for Lithium-6

ENERGY (eV)	MACK (A)	RITTS (B)	% difference $\frac{B-A}{A} \times 100$
15.00 (+6)	7.1779 (-6)	8.1176 (-6)	+ 13.09
13.74 (+6)	6.9865 (-6)	7.5881 (-6)	+ 8.61
12.58 (+6)	6.7908 (-6)	7.1611 (-6)	+ 5.45
11.52 (+6)	6.6443 (-6)	6.8483 (-6)	+ 3.07
10.06 (+6)	6.3442 (-6)	6.3711 (-6)	+ 0.42
9.08 (+6)	6.1675 (-6)	6.1610 (-6)	- 0.10
8.10 (+6)	5.8950 (-6)	5.9246 (-6)	+ 0.50
7.19 (+6)	5.5890 (-6)	5.8186 (-6)	+ 4.10
6.05 (+6)	5.1959 (-6)	5.6248 (-6)	+ 8.25
5.16 (+6)	4.9160 (-6)	5.0907 (-6)	+ 3.55
4.08 (+6)	4.5948 (-6)	4.5653 (-6)	- 0.64
3.18 (+6)	3.8316 (-6)	3.8070 (-6)	- 0.64
2.01 (+6)	3.1263 (-6)	3.0693 (-6)	- 1.82
1.55 (+6)	2.9606 (-6)	2.9596 (-6)	- 0.03
1.07 (+6)	2.8308 (-6)	3.1239 (-6)	+ 10.35
7.88 (+5)	2.7697 (-6)	3.2987 (-6)	+ 19.09
2.57 (+5)	2.5420 (-5)	2.2755 (-5)	- 10.48
1.17 (+5)	5.5352 (-6)	6.6766 (-6)	+ 20.62
5.73 (+4)	5.3700 (-6)	7.0333 (-6)	+ 30.97
1.37 (+4)	.98464(-5)	1.1797 (-5)	+ 19.79
1.02 (+3)	3.5715 (-5)	3.6355 (-5)	+ 1.79
5.46 (+1)	1.5488 (-4)	1.5570 (-4)	+ 0.53
9.16 (+0)	3.7861 (-4)	3.8432 (-4)	+ 1.50
1.00 (+0)	1.1465 (-3)	1.1492 (-3)	+ 0.23

* in units of erg . barn/atom

TABLE 3.12 Comparison of Neutron Kerma Factors* Obtained from Present Work and from Ritts et al. Data for Lithium-7

ENERGY (eV)	MACK (A)	RITTS (B)	% difference $\frac{B-A}{A} \times 100$
15.00 (+6)	5.5610 (-6)	8.4077 (-6)	+ 51.19
13.74 (+6)	5.2127 (-6)	8.1303 (-6)	+ 55.97
12.58 (+6)	4.9426 (-6)	7.7682 (-6)	+ 57.17
11.52 (+6)	4.7118 (-6)	7.4047 (-6)	+ 57.15
10.06 (+6)	4.3100 (-6)	6.6240 (-6)	+ 53.69
9.08 (+6)	3.9599 (-6)	5.9849 (-6)	+ 51.14
8.10 (+6)	3.6304 (-6)	5.3451 (-6)	+ 47.23
7.19 (+6)	3.4451 (-6)	4.7421 (-6)	+ 37.64
6.05 (+6)	3.5092 (-6)	4.0888 (-6)	+ 16.51
5.16 (+6)	3.2791 (-6)	3.6657 (-6)	+ 11.79
4.08 (+6)	2.8070 (-6)	2.8084 (-6)	+ .05
3.18 (+6)	1.9212 (-6)	1.9025 (-6)	- .97
2.01 (+6)	1.1483 (-6)	1.1252 (-6)	- 2.01
1.55 (+6)	8.7685 (-7)	8.6984 (-7)	- .79
1.07 (+6)	6.0570 (-7)	5.9150 (-7)	- 2.34
7.88 (+5)	4.1466 (-7)	4.0516 (-7)	- 2.29
2.57 (+5)	9.2739 (-7)	9.3050 (-7)	+ .33
1.17 (+5)	3.1988 (-8)	2.7903 (-8)	- 12.77
5.73 (+4)	1.8157 (-8)	1.5379 (-8)	- 15.29
1.37 (+4)	6.1561 (-9)	4.7871 (-9)	- 22.24
1.02 (+3)	3.3403 (-9)	3.7655(-10)	- 88.72
5.46 (+1)	1.1955 (-8)	1.9531 (-8)	+ 63.37
9.16 (+0)	2.8068 (-8)	4.5971 (-8)	+ 63.78
1.00 (+0)	8.6508 (-8)	1.4156 (-7)	+ 63.63

* in units of erg . barn/atom

TABLE 3.13 Comparison of Neutron Kerma Factors* Obtained from Present Work and from Ritts et al. Data for Carbon

ENERGY (eV)	MACK (A)	RITTS (B)	% difference $\frac{B-A}{A} \times 100$
15.00 (+6)	6.1465 (-6)	6.5561 (-6)	+ 6.66
13.74 (+6)	5.0155 (-6)	5.0326 (-6)	+ 0.34
12.58 (+6)	4.3233 (-6)	3.9690 (-6)	- 8.19
11.52 (+6)	3.6849 (-6)	3.0202 (-6)	- 18.04
10.06 (+6)	1.9683 (-6)	1.7594 (-6)	- 10.61
9.08 (+6)	2.1572 (-6)	1.6399 (-6)	- 23.98
8.10 (+6)	2.3454 (-6)	2.1192 (-6)	- 9.64
7.19 (+6)	.9734 (-6)	1.0411 (-6)	+ 6.95
6.05 (+6)	1.2718 (-6)	1.2718 (-6)	0.00
5.16 (+6)	1.1282 (-6)	1.1038 (-6)	- 2.16
4.08 (+6)	1.6244 (-6)	1.6637 (-6)	+ 2.42
3.18 (+6)	1.3670 (-6)	1.2754 (-6)	- 6.70
2.01 (+6)	7.5542 (-7)	7.6059 (-7)	+ 0.68
1.55 (+6)	6.6223 (-7)	6.6836 (-7)	+ 0.92
1.07 (+6)	5.6210 (-7)	5.7267 (-7)	+ 1.88
7.88 (+5)	4.8137 (-7)	4.9239 (-7)	+ 2.28
2.57 (+5)	2.2506 (-7)	2.2980 (-7)	+ 2.10
1.17 (+5)	1.1477 (-7)	1.1659 (-7)	+ 1.58
5.73 (+4)	5.9139 (-8)	5.9989 (-8)	+ 1.44
1.37 (+4)	1.4709 (-8)	1.4919 (-8)	+ 1.42
1.02 (+3)	1.1085 (-9)	1.1289 (-9)	+ 1.84
5.46 (+1)	5.9389(-11)	6.0507(-11)	+ 1.88
9.16 (+0)	1.0222(-11)	1.0098(-11)	- 1.21
1.00 (+0)	1.9662(-12)	1.1039(-12)	- 43.85

* in units of erg . barn/atom

TABLE 3.14 Comparison of Neutron Kerma Factors* Obtained from Present Work and from Ritts et al. Data for Sodium

ENERGY (eV)	MACK (A)	RITTS (B)	% difference $\frac{B-A}{A} \times 100$
15.00 (+6)	4.8781 (-6)	1.3787 (-6)	- 72.00
13.74 (+6)	4.9535 (-6)	1.3001 (-6)	- 74.00
12.58 (+6)	4.9771 (-6)	1.1905 (-6)	- 76.00
11.52 (+6)	4.5227 (-6)	1.1133 (-6)	- 75.00
10.06 (+6)	3.8837 (-6)	9.9110 (-7)	- 74.00
9.08 (+6)	2.4656 (-6)	8.6723 (-7)	- 65.00
8.10 (+6)	2.0279 (-6)	8.2005 (-7)	- 59.00
7.19 (+6)	1.3328 (-6)	7.6774 (-7)	- 42.00
6.05 (+6)	1.0607 (-6)	7.7151 (-7)	- 27.00
5.16 (+6)	8.3001 (-7)	7.7395 (-7)	- 6.75
4.08 (+6)	7.2651 (-7)	6.6941 (-7)	- 7.86
3.18 (+6)	6.1180 (-7)	5.6253 (-7)	- 8.05
2.01 (+6)	4.7496 (-7)	5.4073 (-7)	+ 13.84
1.55 (+6)	3.1112 (-7)	3.7786 (-7)	+ 21.45
1.07 (+6)	4.529 (-7)	4.9608 (-7)	+ 9.53
7.88 (+5)	4.3213 (-7)	5.0191 (-7)	+ 16.15
2.57 (+5)	1.1632 (-7)	1.0345 (-7)	- 11.06
1.17 (+5)	5.3342 (-8)	4.9424 (-8)	- 7.34
5.73 (+4)	3.3171 (-8)	4.4720 (-8)	+ 34.81
1.37 (+4)	8.1779 (-9)	9.2012 (-9)	+ 12.50
1.02 (+3)	8.5143 (-9)	4.2942 (-9)	- 49.56
5.46 (+1)	10.5491 (-9)	7.5355 (-9)	- 28.56
9.16 (+0)	2.5090 (-8)	1.8581 (-8)	- 25.90
1.00 (+0)	7.5943 (-8)	5.6718 (-8)	- 25.31

* in units of erg . barn/atom

TABLE 3.15 Comparison of Neutron Kerma Factors* Obtained from Present Work and from Ritts et al. Data for Niobium

ENERGY (eV)	MACK (A)	RITTS (B)	% difference $\frac{B-A}{A} \times 100$
15.00 (+6)	1.7772 (-6)	1.7531 (-6)	- 1.35
13.74 (+6)	1.6317 (-6)	1.6219 (-6)	- .60
12.58 (+6)	1.4356 (-6)	1.4315 (-6)	- .30
11.52 (+6)	1.2498 (-6)	1.2469 (-6)	- .24
10.06 (+6)	9.8998 (-7)	9.8203 (-7)	- .80
9.08 (+6)	8.3228 (-7)	8.2467 (-7)	- .91
8.10 (+6)	6.7931 (-7)	6.6569 (-7)	- 2.00
7.19 (+6)	5.4666 (-7)	5.3838 (-7)	- 1.51
6.05 (+6)	4.2712 (-7)	4.6278 (-7)	+ 8.34
5.16 (+6)	3.5191 (-7)	3.7405 (-7)	+ 6.29
4.08 (+6)	2.7143 (-7)	2.8913 (-7)	+ 6.52
3.18 (+6)	2.1575 (-7)	2.3167 (-7)	+ 7.37
2.01 (+6)	1.8243 (-7)	1.9505 (-7)	+ 6.91
1.55 (+6)	1.5944 (-7)	1.6412 (-7)	+ 2.93
1.07 (+6)	1.4511 (-7)	1.4413 (-7)	- 0.67
7.88 (+5)	1.3251 (-7)	1.3125 (-7)	- .95
2.57 (+5)	4.3537 (-8)	6.0453 (-8)	+ 38.86
1.17 (+5)	2.3153 (-8)	3.0315 (-8)	+ 30.93
5.73 (+4)	1.2249 (-8)	1.5008 (-8)	+ 22.52
1.37 (+4)	3.3501 (-9)	3.0714 (-9)	- 8.32
1.02 (+3)	10.0080(-10)	2.8076(-12)	- 99.72
5.46 (+1)	2.4066(-11)	1.1725(-11)	- 51.27
9.16 (+0)	3.1067(-11)	2.8655(-11)	- 7.76
1.00 (+0)	8.8335(-11)	8.6642(-11)	- 1.91

* in units of erg . barn/atom

TABLE 3.16 Comparison of Neutron Kerma Factors* Obtained from Present Work and from Ritts et al. Data for Iron

ENERGY (eV)	MACK (A)	RITTS (B)	% difference $\frac{B-A}{A} \times 100$
15.00 (+6)	5.3687 (-6)	4.3778 (-6)	- 18.45
13.74 (+6)	4.9265 (-6)	3.7608 (-6)	- 23.66
12.58 (+6)	4.2257 (-6)	2.8277 (-6)	- 33.08
11.52 (+6)	3.4529 (-6)	2.1430 (-6)	- 37.94
10.06 (+6)	2.5111 (-6)	1.3942 (-6)	- 44.47
9.08 (+6)	1.9716 (-6)	1.1217 (-6)	- 43.11
8.10 (+6)	14.5796 (-7)	8.7463 (-7)	- 39.99
7.19 (+6)	11.2692 (-7)	6.8986 (-7)	- 38.78
6.05 (+6)	7.8779 (-7)	6.1223 (-7)	- 22.28
5.16 (+6)	6.0528 (-7)	4.3938 (-7)	- 27.41
4.08 (+6)	4.5956 (-7)	4.8268 (-7)	+ 5.03
3.18 (+6)	3.6801 (-7)	2.0940 (-7)	- 43.09
2.01 (+6)	2.5213 (-7)	1.7642 (-7)	- 30.02
1.55 (+6)	2.0984 (-7)	1.7399 (-7)	- 17.08
1.07 (+6)	10.6412 (-8)	9.3105 (-8)	- 12.50
7.88 (+5)	2.7814 (-7)	1.2859 (-7)	- 53.77
2.57 (+5)	3.6043 (-8)	3.3166 (-8)	- 7.98
1.17 (+5)	1.2461 (-8)	2.2335 (-8)	+ 79.24
5.73 (+4)	1.4445 (-8)	1.3377 (-8)	- 7.39
1.37 (+4)	2.3094 (-9)	3.3023 (-9)	+ 42.99
1.02 (+3)	5.3061(-10)	5.2481(-10)	- 1.09
5.46 (+1)	8.6046(-11)	8.9645(-11)	+ 4.18
9.16 (+0)	1.3083(-10)	1.1687(-10)	- 10.68
1.00 (+0)	3.7890(-10)	3.4598(-10)	- 8.68

* in units of erg . barn/atom

TABLE 3.17 Comparison of Neutron Kerma Factors* Obtained from Present Work and from Ritts et al. Data for Beryllium

ENERGY (eV)	MACK (A)	RITTS (B)	% difference $\frac{B-A}{A} \times 100$
15.00 (+6)	6.2053 (-6)	1.1918 (-5)	+ 92.06
13.74 (+6)	.54154(-5)	1.1609 (-5)	+114.30
12.58 (+6)	.48806(-5)	1.0955 (-5)	+124.40
11.52 (+6)	.4334 (-5)	1.0369 (-5)	+139.30
10.06 (+6)	3.8381 (-6)	9.2613 (-6)	+141.30
9.08 (+6)	3.5878 (-6)	8.5437 (-6)	+138.10
8.10 (+6)	3.3678 (-6)	7.8777 (-6)	+133.90
7.19 (+6)	3.1346 (-6)	6.9825 (-6)	+122.70
6.05 (+6)	2.9031 (-6)	5.9107 (-6)	+103.50
5.16 (+6)	2.6148 (-6)	5.0177 (-6)	+ 91.89
4.08 (+6)	2.3722 (-6)	3.8639 (-6)	+ 62.88
3.18 (+6)	2.3402 (-6)	3.2239 (-6)	+ 37.76
2.01 (+6)	1.1102 (-6)	1.0273 (-6)	- 7.46
1.55 (+6)	8.1354 (-7)	7.6024 (-7)	- 6.55
1.07 (+6)	8.2838 (-7)	8.6286 (-7)	+ 4.16
7.88 (+5)	7.4371 (-7)	7.5710 (-7)	+ 1.80
2.57 (+5)	3.1838 (-7)	3.2117 (-7)	+ .87
1.17 (+5)	1.7944 (-7)	1.7622 (-7)	- 1.79
5.73 (+4)	9.5500 (-8)	9.2990 (-8)	- 2.62
1.37 (+4)	2.3833 (-8)	2.3022 (-8)	- 3.40
1.02 (+3)	1.7825 (-9)	1.7159 (-9)	- 3.73
5.46 (+1)	9.6003(-11)	9.2855(-11)	- 3.27
9.16 (+0)	1.7957(-11)	1.7778(-11)	- .99
1.00 (+0)	7.8243(-12)	9.0808(-12)	+ 16.05

* in units of erg . barn/atom

TABLE 3.18 Energy Balance for Various Zones for Reference Design of Figure 3.19

TABLE 3.18-a -- Zone 3 (1 cm niobium wall)

Reaction	Reaction Rate (R)	Q(MeV)	R . Q	R . E_{decay}
(n,2n)	1.09927 (-1)	- 8.8040	- 0.9677970	
(n,γ)	6.33710 (-2)	+ 7.2139	+ 0.4571520	
(n,p)	3.19864 (-3)	+ 7.1870	+ 0.0229870	
(n,α)	9.44732 (-4)	+ 4.9450	+ 0.0046715	0.000879

$$\sum_i R_i(Q_i + E_D) = -0.482106$$

$$E_{ni} = +14.2080, \quad E_{no} = 11.5073$$

$$H_n = 0.127594$$

$S_{E\gamma} = 2.4409$ (Calculated from gamma production cross section for niobium given in reference 7)

$$A = E_{ni} - E_{no} + \sum_i R_i(Q_i + E_{Di}) = 2.218594$$

$$B = H_n + S_{E\gamma} = 2.568494$$

$$C = \frac{B-A}{A} = 15.77\%$$

Note: A point of interest here is that the neutron heating is small compared with the gamma source and it does not contribute to this error. In other words, if the neutron heating is ignored entirely, the energy of the gamma source is larger than it should be, i.e.

$$C_1 = \frac{S_{E\gamma} - A}{A} = 10.02\%$$

Hence, no conclusion from this example can be reached about the validity of the neutron kerma factors for niobium calculated in the present work. A definite conclusion can be reached, however, about the large inconsistency of niobium gamma production data reported in reference 7 with ENDF/B 3 evaluation for niobium (MAT 1164).

TABLE 3.18-b -- Zone 4 (20 cm -- 95% Lithium + 5% Niobium)

Material Reaction	Reaction Rate (R)	Q(MeV)	Q . R	R . E_{decay}
Niobium				
(n,2n)	4.78296 (-2)	- 8.8040	- 0.421092	
(n,γ)	6.70969 (-2)	+ 7.2139	+ 0.484030	
(n,p)	1.54249 (-3)	+ 7.1870	+ 0.011086	
(n,α)	4.33163 (-4)	+ 4.9450	+ 0.002142	0.000403
Lithium-6				
(n,2n)α	3.83138 (-3)	- 3.6960	- 0.014161	
(n,n´)dα	4.37622 (-2)	- 1.4710	- 0.064374	
(n,γ)	1.42425 (-5)	+ 7.2520	+ 0.000103	
(n,p)	9.28011 (-4)	- 2.7330	- 0.002536	0.001448
(n,α)	3.89742 (-1)	+ 4.7860	+ 1.865305	
Lithium-7				
(n,2n)	1.61853 (-2)	- 7.2520	- 0.1173760	
(n,2n)α	2.13455 (-2)	- 8.7230	- 0.1861970	
(n,n´)t	3.56618 (-1)	- 2.4660	- 0.8794200	
(n,γ)	2.00696 (-4)	+ 2.0320	+ 0.0004080	0.001868
(n,d)	6.70502 (-3)	- 7.7600	- 0.0520309	0.010460

$$\sum_i R_i Q_i(\text{Nb}) = + 0.074024 \qquad \sum_i R_i Q_i(\text{Li-6}) = 1.784337$$

$$\sum_i R_i Q_i(\text{Li-7}) = - 1.234616$$

$$\sum_j \sum_i R_{ij}(Q_{ij} + E_{Dij}) = 0.637925$$

$$E_{ni} = 11.5073, \qquad E_{no} = 4.26319$$

$$H_n(\text{Li-6}) = 2.29275, \qquad H_n(\text{Li-7}) = 3.89139$$

$$H_n(\text{Nb}) = 0.0651292$$

$$H_n = 6.249269 \qquad S_{E\gamma} = 1.8655$$

$$A = E_{ni} - E_{no} + \sum_j \sum_i R_{ij}(Q_{ij} + E_{Dij}) = 7.882035$$

$$B = H_n + S_{E\gamma} = 8.114769$$

$$C = \frac{B-A}{A} = 2.95\%$$

TABLE 3.18-c -- Zone 7 (25 cm iron)

Reaction	Reaction Rate (R)	Q(MeV)	R . Q	R . E_{decay}
(n,2n)	1.89594 (-2)	- 11.2000	- 0.212345	
(n,γ)	9.89267 (-2)	+ 7.8030	+ 0.771925	
(n,p)	1.15588 (-2)	- 2.7310	- 0.031567	0.084495
(n,α)	5.64264 (-3)	+ 0.3926	+ 0.002215	

$$\sum_i R_i(Q_i + E_D) = 0.538678$$

$$E_{ni} = 1.65568$$

$$E_{no} = 0.062016$$

$$H_n = 0.356027$$

$$S_{E\gamma} = 1.8448$$

$$A = E_{ni} - E_{no} + \sum_i R_i(Q_i + E_{Di}) = 2.132342$$

$$B = H_n + S_{E\gamma} = 2.200827$$

$$C = \frac{B-A}{A} = 3.2117\%$$

Evaluation DNA4180 Mod. 1

If this evaluation is used to generate gamma production source the energy balance is changed dramatically if the same neutron kerma factors from evaluation MAT 1180 is used as can be seen from the following calculation.

$$S_{E\gamma 1}(\text{MAT DNA4180 Mod. 1}) = 2.2729$$

$$B_1 = 2.628927$$

$$C = \frac{B_1 - A}{A} = 23.29\ \%$$

TABLE 3.18-d -- Zone 10 (35% Iron + 35% Lead + 30% Boron Carbide)

Material Reaction	Reaction Rate (R)	Q(MeV)	R . Q	R . E_{decay}
Iron				
(n,2n)	9.07493 (-6)	- 11.2040	- 1.01675 (-4)	
(n,γ)	6.94002 (-5)	+ 7.8030	+ 5.41530 (-4)	
(n,p)	6.74214 (-6)	- 2.7312	- 1.84141 (-5)	4.92850 (-6)
(n,α)	2.98703 (-6)	+ 0.3926	+ 1.17271 (-6)	
Lead				
(n,2n)	3.89052 (-5)	- 6.7330	- 2.61949 (-4)	
(n,γ)	1.16599 (-5)	+ 5.4150	+ 6.31383 (-5)	1.25122 (-6)
Carbon-12				
(n,n′)3α	1.94915 (-6)	- 7.2740	- 1.41781 (-5)	
(n,γ)	7.12735 (-10)	+ 4.9479	+ 3.52590 (-9)	
(n,α)	2.01059 (-6)	- 5.6950	- 1.14503 (-5)	
Boron-10				
(n,d)	6.64907 (-7)	- 4.3628	- 2.90086 (-6)	
(n,t)	2.57827 (-6)	+ 0.2295	+ 5.91713 (-7)	
(n,α)	4.40370 (-3)	+ 2.7916	+ 1.22934 (-2)	
Boron-11				
(n,γ)	3.30680 (-7)	+ 3.3690	+ 1.11406 (-6)	2.12296 (-6)
(n,p)	3.65740 (-8)	- 10.7300	- 3.92476 (-7)	3.41601 (-8)
(n,t)	2.91594 (-7)	- 9.5610	- 2.78793 (-6)	
(n,α)	1.02848 (-6)	- 6.6320	- 6.82088 (-6)	2.15981 (-7)

(continued on the next page)

TABLE 3.18-d (continued)

Material	Neutron Heating Rate (H_n)	$R_i(Q_i + E_{decay})$
Iron	2.70405 (-4)	+ 4.27541 (-4)
Lead	3.96809 (-5)	- 1.98685 (-4)
Carbon-12	2.06944 (-4)	- 0.25625 (-4)
Boron-10	1.27730 (-2)	+ 1.22935 (-2)
Boron-11	6.57865 (-4)	- 6.51412 (-6)
SUM	1.394789(-2)	+ 1.24902 (-2)

$$E_{ni} = 4.33595 \times 10^{-3}, \quad E_{no} = 1.17334 \times 10^{-3}$$

$$S_{E\gamma} = 1.8163 \times 10^{-3}$$

$$A = E_{ni} - E_{no} + \sum_j \sum_i R_{ij}(Q_{ij} + E_{Dij}) = 0.0156528$$

$$B = H_n + S_{E\gamma} = 0.015764$$

$$C = \frac{B-A}{A} = 0.7\%$$

Note: The neutron heating rate in this zone is about eight times the gamma source. Therefore, the energy balance for this zone represents a very good test of the validity of the neutron kerma factors calculated in the present work.

Table 3.19 Neutron 46 Energy Group Structure in eV

Group	Group Limits		
	E(Top)	E(Low)	E(Mid-Point)
1	1.4918 (+7)	1.3499 (+7)	1.4208 (+7)
2	1.3499 (+7)	1.2214 (+7)	1.2856 (+7)
3	1.2214 (+7)	1.1052 (+7)	1.1633 (+7)
4	1.1052 (+7)	1.0000 (+7)	1.0526 (+7)
5	1.0000 (+7)	9.0484 (+6)	9.5242 (+6)
6	9.0484 (+6)	8.1873 (+6)	8.6178 (+6)
7	8.1873 (+6)	7.4082 (+6)	7.7977 (+6)
8	7.4082 (+6)	6.7032 (+6)	7.0557 (+6)
9	6.7032 (+6)	6.0653 (+6)	6.3843 (+6)
10	6.0653 (+6)	5.4881 (+6)	5.7767 (+6)
11	5.4881 (+6)	4.9659 (+6)	5.2270 (+6)
12	4.9659 (+6)	4.4933 (+6)	4.7296 (+6)
13	4.4933 (+6)	4.0657 (+6)	4.2795 (+6)
14	4.0657 (+6)	3.6788 (+6)	3.8722 (+6)
15	3.6788 (+6)	3.3287 (+6)	3.5038 (+6)
16	3.3287 (+6)	3.0119 (+6)	3.1703 (+6)
17	3.0119 (+6)	2.7253 (+6)	2.8686 (+6)
18	2.7253 (+6)	2.4660 (+6)	2.5956 (+6)
19	2.4660 (+6)	1.8268 (+6)	2.1464 (+6)
20	1.8268 (+6)	1.3534 (+6)	1.5901 (+6)
21	1.3534 (+6)	1.0026 (+6)	1.1780 (+6)
22	1.0026 (+6)	7.4274 (+5)	8.726 (+5)
23	7.4274 (+5)	5.5023 (+5)	6.4648 (+5)
24	5.5023 (+5)	4.0762 (+5)	4.7892 (+5)
25	4.0762 (+5)	3.0197 (+5)	3.5480 (+5)
26	3.0197 (+5)	2.2371 (+5)	2.6284 (+5)
27	2.2371 (+5)	1.6573 (+5)	1.9472 (+5)
28	1.6573 (+5)	1.2277 (+5)	1.4425 (+5)
29	1.2277 (+5)	6.7379 (+4)	9.508 (+4)
30	6.7379 (+4)	3.1828 (+4)	4.9604 (+4)

Table 3.19(cont.)

Group	Group Limits E(Top)	E(Low)	E(Mid-Point)
31	3.1828 (+4)	1.5034 (+4)	2.3431 (+4)
32	1.5034 (+4)	7.1017 (+3)	1.1068 (+4)
33	7.1017 (+3)	3.3546 (+3)	5.2281 (+3)
34	3.3546 (+3)	1.5846 (+3)	2.4696 (+3)
35	1.5846 (+3)	7.4852 (+2)	1.1666 (+3)
36	7.4852 (+2)	3.5358 (+2)	5.5105 (+2)
37	3.5358 (+2)	1.6702 (+2)	2.6030 (+2)
38	1.6702 (+2)	7.8893 (+1)	1.2296 (+2)
39	7.8893 (+1)	3.7267 (+1)	5.8080 (+1)
40	3.7267 (+1)	1.7603 (+1)	2.7435 (+1)
41	1.7603 (+1)	8.3153 (+0)	1.2959 (+1)
42	8.3153 (+0)	3.9279 (+0)	6.1216 (+0)
43	3.9279 (+0)	1.8554 (+0)	2.8917 (+0)
44	1.8554 (+0)	8.7643 (-1)	1.3659 (+0)
45	8.7643 (-1)	4.1399 (-1)	6.4521 (-1)
46	4.1399 (-1)	2.2000 (-2)	2.1800 (-1)

Table 3.20 Detailed Comparison of Niobium Kerma Factors obtained in the Present Work with that by Ritts et al

Present Work		Ritts et al Work	
E (eV)	k_n (E) eV·barn/atom	E (eV)	k_n (E) eV·barn/atom
8.8772 (+2)	98.87	8.7800 (+2)	2.84
9.0912 (+2)	22.49(+1)	9.1490 (+2)	1.85
9.5348 (+2)	59.47(+1)	9.5169 (+2)	1.81
9.7646 (+2)	16.01(+1)	9.8847 (+2)	1.78
1.0000 (+3)	425.20(+1)		
1.0241 (+3)	62.47(+1)	1.0252 (+3)	1.75
1.0488 (+3)	18.71(+1)	1.0620 (+3)	1.72
1.0741 (+3)	17.33(+1)	1.0988 (+3)	1.70
1.100 (+3)	37.69(+1)	1.1356 (+3)	0.71

Note:

At 1 KeV the following parameters are given as can be calculated from ENDF/B (the values are the same in version II and version III)

Elastic scattering:

at 300°K $\sigma_{resonance}$ = 36.489 barn, $\sigma_{background}$ = 0.0

$\cos \theta_{c.m.}$ = 0.0

E_r = 21.250 eV $k_{elastic}$ = 775.4 eV·barn/atom

Radiative capture

at 300°K, $\sigma_{resonance}$ = 11.082 barn, $\sigma_{background}$ = .1013 barn

Q = 7.2139 MeV, E_r = 310.86 eV, k = 3476.6 eV·barn/atom

TABLE 3.21 % Contribution of Neutron Reaction Types to Total Kerma Factor for Sodium-23

Energy (MeV)	Elastic Scatt.	Inelastic Scatt.	(n,2n)	(n,γ)	(n,charged Particles)
15.000	8.7170	15.490	1.050	0.0090	74.720
14.000	8.3100	15.400	0.382	0.0080	75.890
13.000	7.5500	15.030	0.042	0.0070	77.370
12.000	6.8500	15.240	0.000	0.0065	77.890
11.000	7.0900	17.420	0.000	0.0070	75.460
10.000	6.6100	17.990	0.000	0.0070	75.380
9.000	10.4400	30.810	0.000	0.0106	58.730
8.000	14.4000	35.4600	0.000	0.0124	50.120
7.000	19.2800	48.950	0.000	0.0176	31.750
6.000	31.3200	53.310	0.000	0.0200	15.340
5.000	36.6000	61.200	0.000	0.0270	2.160
4.000	48.2300	51.690	0.000	0.0260	0.050
3.000	59.5300	40.420	0.000	0.0400	0.000
2.000	77.6900	22.260	0.000	0.0360	0.000
1.000	84.5800	15.330	0.000	0.0850	0.000
0.500	99.4900	0.300	0.000	0.2000	0.000
0.100	99.5900	0.000	0.000	0.4060	0.000
0.010	95.4400	0.000	0.000	4.5600	0.000
0.001	5.7110	0.000	0.000	94.2800	0.000
1(ev)	$\sim$0.0005	0.000	0.000	99.9900	0.000

TABLE 3.22 % Contribution of Neutron Reaction Types to Total Kerma Factor for Aluminum-27

Energy (MeV)	Elastic Scatt.	Inelastic Scatt.*	(n,2n)	(n,γ)	(n, charged Particles)†
15.000	5.6500	32.07	1.560	0.023	60.680
14.000	5.9100	27.82	0.308	0.022	65.930
13.000	6.1500	25.65	0.000	0.021	68.180
12.000	6.7100	22.37	0.000	0.022	70.890
11.000	7.8200	16.14	0.000	0.023	76.000
10.000	8.7700	17.50	0.000	0.023	73.690
9.000	10.6700	19.85	0.000	0.023	69.440
8.000	15.9300	23.45	0.000	0.023	60.580
7.000	23.2700	29.02	0.000	0.022	47.690
6.000	32.8100	34.45	0.000	0.019	32.720
5.000	46.1200	36.47	0.000	0.012	17.380
4.000	56.9800	37.79	0.000	0.023	5.190
3.000	74.0600	24.88	0.000	0.042	1.010
2.000	89.9300	9.96	0.000	0.059	0.045
1.000	98.0900	1.75	0.000	0.150	0.000
0.500	99.4700	0.00	0.000	0.530	0.000
0.100	91.7100	0.00	0.000	8.280	0.000
0.001	4.5080	0.00	0.000	95.490	0.000
1(ev)	0.0002	0.00	0.000	99.990	0.000

* combines (n,n′)γ, (n,n′)α and (n,n′)P

† (n,P), (n,d), (n,t), and (n,α)

TABLE 3.23 % Contribution of Neutron Reaction Types to Total Kerma Factors for Chromium

Energy (MeV)	Elastic Scatt.	Inelastic Scatt.	(n,2n)	(n,γ)	(n,n′) Charged Particles*	n charged Particles†
15.000	2.830	9.030	3.19	0.024	8.76	76.15
14.000	3.060	9.360	2.67	0.025	6.04	78.82
13.000	4.360	9.900	1.08	0.026	4.15	80.46
12.000	6.190	10.830	0.00	0.028	3.08	79.86
11.000	8.690	12.280	0.00	0.031	1.74	77.25
10.000	13.230	16.140	0.00	0.041	0.00	70.58
9.000	24.040	23.310	0.00	0.058	0.00	52.58
8.000	37.050	31.390	0.00	0.077	0.00	31.48
7.000	48.880	35.110	0.00	0.085	0.00	15.92
6.000	56.590	37.250	0.00	0.087	0.00	6.07
5.000	59.970	38.970	0.00	0.088	0.00	0.96
4.000	63.490	36.150	0.00	0.083	0.00	0.26
3.000	66.320	33.580	0.00	0.085	0.00	0.00
2.000	77.250	22.660	0.00	0.087	0.00	0.00
1.000	99.540	.375	0.00	0.083	0.00	0.00
0.500	99.930	0.000	0.00	0.070	0.00	0.00
0.100	99.940	0.000	0.00	0.057	0.00	0.00
0.010	99.060	0.000	0.00	0.930	0.00	0.00
0.001	93.150	0.000	0.00	6.850	0.00	0.00
1(ev)	0.052	0.000	0.00	99.95	0.00	0.00

* (n,n′)P reaction
† (n,P) plus (n,α) reactions

TABLE 3.24 % Contribution of Neutron Reaction Types to Total Kerma Factor for Iron

Energy (MeV)	Elastic Scatt.	Inelastic Scatt.	(n,2n)	(n,γ)	(n, charged Particles)
15.000	4.210	5.44	5.300	0.0016	85.04
14.000	4.050	7.03	3.570	0.0017	85.34
13.000	3.930	8.96	2.260	0.0018	84.84
12.000	4.240	12.30	0.549	0.0020	82.90
11.000	4.780	15.07	0.000	0.0025	80.15
10.000	5.890	18.19	0.000	0.0030	75.90
9.000	7.350	22.71	0.000	0.0040	69.93
8.000	9.850	30.01	0.000	0.0050	60.13
7.000	14.040	35.49	0.000	0.0070	50.44
6.000	22.330	40.08	0.000	0.0090	37.57
5.000	29.730	47.83	0.000	0.0130	22.41
4.000	41.060	46.77	0.000	0.0160	12.14
3.000	61.600	35.95	0.000	0.0200	2.43
2.000	73.280	26.68	0.000	0.0300	0.00
1.000	91.210	8.73	0.000	0.0500	0.00
0.500	99.930	0.00	0.000	0.0670	0.00
0.100	99.860	0.00	0.000	0.1300	0.00
0.010	99.890	0.00	0.000	0.1100	0.00
0.001	97.370	0.00	0.000	2.6200	0.00
1(ev)	0.180	0.00	0.000	99.8200	0.00

* (n,α) plus (n,p) reactions

TABLE 3.25 % Contribution of Neutron Reaction Types to Total Kerma Factor for Nickel

Energy (MeV)	Elastic Scatt.	Inelastic Scatt.	(n,2n)	(n,γ)	(n,n´) Charged Particles*	n, charged Particles†
15.000	1.41	2.77	0.32	0.0080	28.36	67.12
14.000	1.43	2.44	0.15	0.0080	18.22	77.74
13.000	1.64	2.71	0.04	0.0090	11.52	84.08
12.000	1.88	2.99	0.00	0.0098	6.16	88.95
11.000	2.13	3.32	0.00	0.0100	3.34	91.18
10.000	2.57	3.67	0.00	0.0110	1.27	92.46
9.000	2.78	4.08	0.00	0.0130	0.35	92.76
8.000	3.27	4.39	0.00	0.0140	0.00	92.32
7.000	3.78	4.87	0.00	0.0150	0.00	91.32
6.000	4.38	5.50	0.00	0.0170	0.00	90.08
5.000	5.41	7.02	0.00	0.0210	0.00	87.54
4.000	9.91	10.02	0.00	0.0300	0.00	80.03
3.000	22.82	12.14	0.00	0.0470	0.00	64.98
2.000	62.74	10.97	0.00	0.1000	0.00	26.17
1.000	99.84	0.00	0.00	0.1600	0.00	0.00
0.500	99.87	0.00	0.00	0.1200	0.00	0.00
0.100	99.75	0.00	0.00	0.2400	0.00	0.00
0.010	99.11	0.00	0.00	0.8900	0.00	0.00
0.001	97.00	0.00	0.00	2.9900	0.00	0.00
1(ev)	0.13	0.00	0.00	99.8700	0.00	0.00

* (n,n´)P reaction
† (n,p) plus (n,α) reactions

TABLE 3.26 % Contribution of Neutron Reaction Types to Total Kerma Factor for Niobium

Energy (MeV)	Elastic Scatt.	Inelastic Scatt.	(n,2n)	(n,γ)	(n charged Particles)*
15.000	6.22	12.310	21.26	0.006	60.19
14.000	6.44	14.540	18.94	0.007	60.06
13.000	6.92	17.290	16.85	0.008	58.92
12.000	7.83	21.390	14.42	0.009	56.34
11.000	8.99	26.170	11.18	0.010	53.63
10.000	10.96	36.110	4.39	0.013	48.52
9.000	13.72	44.340	0.20	0.017	41.71
8.000	17.42	50.030	0.00	0.023	32.53
7.000	22.08	56.040	0.00	0.032	21.86
6.000	25.67	60.560	0.00	0.042	13.72
5.000	28.88	64.490	0.00	0.059	6.55
4.000	31.16	65.810	0.00	0.083	2.93
3.000	37.34	62.530	0.00	0.120	0.00
2.000	57.63	42.190	0.00	0.180	0.00
1.000	91.40	8.120	0.00	0.470	0.00
0.500	99.08	0.350	0.00	0.560	0.00
0.100	98.60	0.018	0.00	1.370	0.00
0.010	89.24	0.000	0.00	10.760	0.00
0.001	18.23	0.000	0.00	81.760	0.00
1.000^{-6}	0.23	0.000	0.00	99.760	0.00

* (n,α) plus (n,p)

TABLE 3.27 % Contribution of Neutron Reaction Types to Total Kerma Factor for Vanadium

Energy (MeV)	Elastic Scatt.	Inelastic Scatt.	(n,2n)	(n, γ)	(n charged Particles)
15.000	12.08	6.19	20.08	0.015	61.630
14.000	13.28	10.75	16.53	0.018	59.420
13.000	14.66	17.78	11.46	0.023	56.060
12.000	16.42	28.30	4.68	0.029	50.560
11.000	17.90	36.81	0.00	0.035	45.250
10.000	19.48	41.44	0.00	0.045	39.030
99.000	21.65	45.93	0.00	0.057	32.360
8.000	24.86	49.78	0.00	0.073	25.270
7.000	29.08	52.25	0.00	0.094	18.570
6.000	34.54	52.67	0.00	0.120	12.670
5.000	40.95	51.72	0.00	0.170	7.150
4.000	50.83	45.81	0.00	0.240	3.120
3.000	63.24	36.29	0.00	0.370	0.088
2.000	68.23	30.95	0.00	0.820	0.000
1.000	85.94	12.37	0.00	1.690	0.000
0.500	89.83	6.22	0.00	3.950	0.000
0.100	37.42	0.00	0.00	62.580	0.000
0.010	60.80	0.00	0.00	39.200	0.000
0.001	0.80	0.00	0.00	99.200	0.000
1(ev)	0.00	0.00	0.00	$\sim$100.000	0.000

TABLE 3.28 % Contribution of Neutron Reaction Types to Total Neutron Kerma Factor for Lithium-6

Energy (MeV)	Elastic Scatt.	Inelastic Scatt.	(n,γ)	(n,n´)d	(n,2n)α	(n,α) + (n,P)*
15.000	16.050	0.35	Less than 0.0005	57.68	13.30	12.60
14.000	16.780	0.33		58.38	11.29	13.20
13.000	17.060	0.31		58.62	9.59	13.81
12.000	18.470	0.29		59.14	7.44	14.66
11.000	19.350	0.27		59.48	5.45	15.45
10.000	20.270	0.24		59.41	3.54	16.53
9.000	22.250	0.22		57.83	1.90	17.79
8.000	24.340	0.22		55.07	0.74	19.64
7.000	26.290	0.19		51.18	0.09	22.24
6.000	27.850	0.18		46.27	0.00	25.69
5.000	30.560	0.16		38.77	0.00	30.49
4.000	33.480	0.00		30.28	0.00	36.24
3.000	38.710	0.00		12.55	0.00	48.74
2.000	26.760	0.00		0.46	0.00	72.77
1.000	12.720	0.00		0.00	0.00	87.27
0.500	8.570	0.00		0.00	0.00	91.42
0.100	0.680	0.00		0.00	0.00	99.32
0.010	0.027	0.00		0.00	0.00	99.97
0.001	0.001	0.00		0.00	0.00	99.99
1×10^{-6}	$\simeq$ 0.000	0.00		0.00	0.00	100.00

* (n,P) is zero below 3.2 MeV

TABLE 3.29 % Contribution of Neutron Reaction Types to Total Kerma Factors for Lithium-7

Energy (MeV)	Elastic Scatt.	Inelastic Scatt.	(n,2n)	(n,γ)	(n,2n)α	(n,d)	(n,n'α)T
15.000	29.16000	7.46	1.2500	0.0030	5.600	3.04	53.48
14.000	29.78000	7.32	1.1800	0.0030	3.620	2.37	55.71
13.000	31.04000	7.55	1.1100	0.0030	2.010	1.79	56.48
12.000	32.19000	8.18	0.9730	0.0040	0.850	1.02	56.77
11.000	32.97000	9.31	0.7970	0.0040	0.260	0.54	56.11
10.000	34.10000	10.84	0.4900	0.0040	0.023	0.17	54.37
9.000	35.55000	12.72	0.0913	0.0040	0.000	0.01	51.62
8.000	37.66000	14.63	0.0000	0.0045	0.000	0.00	47.70
7.000	41.22000	15.05	0.0000	0.0047	0.000	0.00	43.72
6.000	49.13000	15.14	0.0000	0.0046	0.000	0.00	35.72
5.000	70.25000	14.61	0.0000	0.0055	0.000	0.00	15.13
4.000	85.10000	13.66	0.0000	0.0056	0.000	0.00	1.23
3.000	88.22000	11.71	0.0000	0.0085	0.000	0.00	0.06
2.000	89.62000	10.37	0.0000	0.0130	0.000	0.00	0.00
1.000	92.94000	7.02	0.0000	0.0260	0.000	0.00	0.00
0.500	99.93000	0.00	0.0000	0.0670	0.000	0.00	0.00
0.100	98.94000	0.00	0.0000	1.0600	0.000	0.00	0.00
0.010	73.06000	0.00	0.0000	26.9300	0.000	0.00	0.00
0.001	11.02000	0.00	0.0000	88.9700	0.000	0.00	0.00
1(ev)	0.00045	0.00	0.0000	99.9900	0.000	0.00	0.00

TABLE 3.30 % Contribution of Neutron Reaction Types to Total Kerma Factor for Beryllium-9

Energy (MeV)	Elastic Scatt.	(n,2n)*	(n,γ)	(n charged Particles)
15.000	17.250	74.240	0.0039	8.50
14.000	20.070	74.050	0.0041	5.87
13.000	22.030	71.360	0.0041	6.60
12.000	24.370	68.860	0.0042	6.75
11.000	26.420	65.580	0.0044	7.98
10.000	28.370	62.690	0.0043	8.92
9.000	30.120	60.090	0.0041	9.78
8.000	30.260	57.600	0.0039	12.13
7.000	30.200	55.390	0.0037	14.39
6.000	32.900	48.050	0.0034	19.03
5.000	36.420	39.400	0.0032	24.16
4.000	43.230	28.390	0.0027	28.36
3.000	59.370	11.890	0.0021	28.73
2.000	80.190	0.024	0.0029	19.77
1.000	98.740	0.000	0.0020	1.25
0.500	99.998	0.000	0.0017	0.00
0.100	99.990	0.000	0.0012	0.00
0.010	99.990	0.000	0.0031	0.00
0.001	99.970	0.000	0.0240	0.00
1(ev)	23.500	0.000	76.4900	0.00

* Combines all modes for which there are two neutrons and two alpha particles in the exit channel

TABLE 3.31 Percentage Contribution of Reaction Types to Neutron Heating in Some CTR Materials for a Typical First Wall Spectrum

Material	Elastic Scattering	Inelastic Scattering†	(n,2n)	(n,γ)	(n;n´charged Particles)	(n,charged Particles)
Li-6	5.64	10.48		0.000	1.82	82.10
Li-7	42.20	7.78	0.089	0.040	47.32	1.77
Be-9	37.74		55.090*	0.004		7.17
Na-23	18.32	15.88	0.320	0.340		65.09
Al-27	13.95	25.74	0.350	0.250		59.70
Cr	9.84	9.88	2.260	0.030	5.53	72.46
Fe	8.84	8.21	3.270	0.010		79.65
Ni	4.33	2.82	0.140	0.010	16.92	75.74
Nb	17.57	16.35	15.520	0.090		50.46
V	24.77	12.68	12.450	3.810		46.37
Cu	12.10	11.83	4.85	30.470		40.65

* (n,2n)α plus (n,n´)α plus inelastic (final products are two neutrons and two alpha particles)

† includes the (n;n´, charged particles) contribution for some materials

TABLE 3.32 Percentage Contribution of Reaction Types to Neutron Heating in Several CTR Materials for a Typical CTR Shield Spectrum (C/E)

Material	Elastic Scattering	Inelastic Scattering†	(n,2n)	(n,γ)	(n;n´charged Particles)	(n,charged Particles)
Li-6	0.20	0.001		0.000	0.24	99.57
Li-7	57.71	10.86	0.26	1.840	28.97	0.36
Be-9	50.01		36.62*	0.003		13.36
Na-23	29.40	24.05	0.05	3.710		42.70
Al-27	28.64	21.34	0.06	3.060		46.89
Cr	31.03	17.46	0.62	0.090	2.04	48.76
Fe	19.71	19.44	0.99	0.030		59.79
Ni	7.97	4.56	0.03	0.030	4.46	82.94
Nb	30.58	33.31	5.82	0.220		30.07
V	18.69	13.41	1.33	56.14		10.45
Cu	9.16	8.34	22.95	3.99		55.56

* $(n,2n)\alpha$ plus $(n,n')\alpha$ plus inelastic

† Includes the (n;n´, charged particles) contribution for some materials

TABLE 3.33 Abundance, Q-value and the 15 MeV Cross Section for the (n,α) and (n,p) reactions in Molybdenum Isotopes

(cross sections from reference 28)

		(n,p)		(n,α)	
Isotope	Abundance	Q(MeV)	$\sigma_{n,p}$ at 15 MeV (barns)	Q(MeV)	$\sigma_{n,\alpha}$ at 15 MeV (barns)
Molybdenum-92	15.84	+ 0.4332	0.070	3.6874	0.0225
Molybdenum-94	9.04	- 1.2615	0.007	5.1330	0.0225*
Molybdenum-95	15.72	- 0.1424	0.028	6.3995	0.0160*
Molybdenum-96	16.53	- 2.3677	0.030	3.9655	0.0160
Molybdenum-97	9.46	- 1.1504	0.085	5.3748	0.0160*
Molybdenum-98	23.78	- 3.8172	0.018	3.2001	0.0160*
Molybdenum-100	9.63	- 5.3128	0.018*	2.3954	0.0160

* No data, assumed equal to the neighboring value.

Table 3.34

Rosen and Stewart [34] Secondary Neutron Energy Distribution for the Li^7 (n,n'α)t Reaction

E_o(MeV)	5.1	5.4	5.8	6.5	7.0	7.5	8.0	9.3	10.6	12.0	14.0
E_1(MeV)											
0.0	179	259	220	127	81	118	96	41	33	12	15
0.5	182	125	359	195	153	148	69	37	31	28	13
1.0	45	153	100	247	258	117	125	69	56	31	22
1.5	15	119	38	130	152	173	141	83	66	45	51
2.0		5	20	40	148	202	101	148	94	83	40
2.5			3	15	69	111	148	100	108	48	40
3.0				6	13	27	169	175	74	26	44
3.5					6	-9	90	149	73	64	24
4.0						14	79	113	78	83	19
4.5								63	57	56	34
5.0								20	59	53	33
6.0									6	85	48
7.0										25	27
8.0											31
9.0											20

Energy of incident neutron, E_o.

Energy of secondary neutron, E_1.

TABLE 3.35 Comparison of Rosen & Stewart[34] and ENDF/B III Average Secondary Neutron Energy of the Lithium-7 (n,n′)αt Reaction and Effect on Kerma Factors

	Average Secondary Neutron Energy			Lithium-7 (n,n′α)t Kerma Factor*			Lithium-7 Total Kerma Factor*		
Energy (MeV)	A	B	$\frac{A-B}{B} \times 100$	A	B	$\frac{A-B}{B} \times 100$	A	B	$\frac{A-B}{B} \times 100$
5.11	1.005	0.635	58.02	0.368	0.451	-18.40	2.035	2.118	- 3.920
5.62	1.191	0.811	46.85	0.675	0.806	-16.25	2.190	2.321	- 5.640
6.01	1.504	0.882	70.52	0.778	1.015	-23.35	2.199	2.436	- 9.730
7.03	2.354	1.512	55.69	0.927	1.281	-27.63	2.149	2.503	-14.140
8.05	3.044	2.315	31.49	1.077	1.386	-22.29	2.257	2.567	-12.076
9.03	3.543	2.748	28.93	1.264	1.597	-20.85	2.458	2.791	-11.930
10.06	4.066	3.048	33.40	1.459	1.880	-22.39	2.690	3.111	-13.530
12.00	5.041	4.285	17.64	1.707	1.994	-14.39	3.007	3.294	- 7.880
13.92	6.007	4.953	21.28	1.834	2.189	-16.22	3.285	3.604	- 9.750

A -- refers to data obtained using ENDF/B3 secondary neutron energy distribution

B -- refers to data obtained using Rosen & Stewart[34] secondary neutron energy distribution

* in units of MeV . barn/atom

TABLE 3.36 Effect of Anisotropy of Elastic Scattering on Neutron Kerma Factor for Lithium-7

Energy (MeV)	Elastic Scattering Kerma Factor			Total Kerma Factor		
	Anisotropy Included (A)	Anisotropy* Ignored (B)	% difference $\frac{B-A}{A} \times 100$	Anisotropy Included (C)	Anisotropy* Ignored (D)	% difference $\frac{D-C}{C} \times 100$
15.000	1.0122 (+6)	3.1057 (+6)	206.80	3.4713 (+6)	5.5647 (+6)	60.3
14.000	9.8342 (+5)	3.0173 (+6)	206.80	3.3016 (+6)	5.3354 (+6)	61.6
13.000	9.7673 (+5)	2.8847 (+6)	195.34	3.1358 (+6)	5.0437 (+6)	60.8
12.000	9.7132 (+5)	2.7708 (+6)	185.30	3.0174 (+6)	4.8169 (+6)	59.6
11.000	9.4591 (+5)	2.6016 (+6)	175.00	2.8652 (+6)	4.5209 (+6)	57.8
10.000	9.2003 (+5)	2.4442 (+6)	165.70	2.6904 (+6)	4.2145 (+6)	56.7
9.000	8.7611 (+5)	2.2485 (+6)	156.60	2.4584 (+6)	3.8308 (+6)	55.8
8.000	8.4998 (+5)	2.1132 (+6)	148.60	2.2571 (+6)	3.5203 (+6)	56.0
7.000	8.8583 (+5)	1.9466 (+6)	119.70	2.1489 (+6)	3.2097 (+6)	49.4
6.000	1.0894 (+6)	1.9205 (+6)	76.30	2.1991 (+6)	3.0303 (+6)	37.8
5.000	1.4101 (+6)	1.9532 (+6)	38.50	2.0073 (+6)	2.5504 (+6)	27.1
4.000	1.4599 (+6)	1.6176 (+6)	10.80	1.7131 (+6)	1.8708 (+6)	9.2
3.000	9.9446 (+5)	1.1166 (+6)	12.28	1.1257 (+6)	1.2478 (+6)	10.8
2.000	6.4237 (+5)	6.6064 (+5)	2.80	7.1680 (+5)	7.3506 (+5)	2.5
1.600	5.0763 (+5)	5.0510 (+5)	- 0.50	5.6630 (+5)	5.6377 (+5)	- 0.4
0.500	1.3565 (+5)	1.1782 (+5)	- 13.10	1.3575 (+5)	1.1792 (+5)	- 13.1
0.020	4.3930 (+3)	4.4731 (+3)	1.80	4.9644 (+3)	5.0446 (+3)	1.6
$\leq$0.009			0.00			0.0
η_s	2.7427 (+5)	4.3309 (+5)	57.9	4.7525 (+5)	6.3407 (+5)	33.4
η_w	3.3427 (+5)	7.2472 (+5)	116.8	7.9208 (+5)	1.1825 (+6)	85.1

* Refers to center-of-mass system

TABLE 3.37 Detailed Calculations of the Neutron Kerma Factor for Lithium-7 at 15 MeV from ENDF/B3 Data
(See equation 3.4.20 for notation)

Reaction Neutron Producing	m	σ_i(barns)	$\bar{E}_{n,i}$(MeV)	$m*\sigma_i\bar{E}_{ni}$	Nuclear Temperature (MeV)
Elastic	1	0.942	13.92544	13.11776	
(n,2n)γ	2	0.023	1.61200	0.07415	0.8133
(n,2n)α	2	0.043	0.87696	0.07542	0.4388
(n,n')γ	1	0.080	11.28519	0.90281	
(n,n')t	1	0.310	6.54520	1.98223	5.3500

$$\sum_i m_i \sigma_i \bar{E}_{n,i} = 16.199159$$

$$(\overline{\cos\theta})_{c.m.} = .67407 \text{ for elastic scattering}$$

Reaction*	σ_i	Q_i(MeV)	$\sigma_i Q_i$
(n,2n)γ	0.02300	- 7.2520	- 0.166796
(n,2n)α-D	0.04300	- 8.7230	- 0.375089
(n,n')α-T	0.31000	- 2.4660	- 0.764460
(n,γ)	0.00001	+ 2.0320	+ 0.000020
(n,d)	0.01200	- 7.7600	- 0.093120

$$\sum_i \sigma_i Q_i = -1.399455$$

* (Conversion of K.E. to mass and vice versa)

From Table 3.3:

E_{decay} for (n,γ) = 9.31 MeV,

E_{decay} for (n,d) = 1.56 MeV

$$\sum_i \sigma_i E_{Di} = 0.018813$$

E = 15 MeV, σ_t = 1.410

TABLE 3.37 (continued)

From Equation 3.4.20:

$$T(15\ \text{MeV}) = k_n + E_\gamma = 3.570201\ \text{MeV . barn/atom}$$

as shown in text $E_\gamma(15\ \text{MeV}) = 0.0989\ \text{MeV . barn/atom}$

$k_n(15\ \text{MeV}) = 3.4713\ \text{MeV . barn/atom}$

(Present work) MACK Result $k_n(15\ \text{MeV}) = 3.4713\ \text{MeV . barn/atom}$

(Reference 7) Ritts Result $k_n(15\ \text{MeV}) = 5.2482\ \text{MeV . barn/atom}$

NOTE: K_n from Ritts result is 47% higher than the sum of k_n and E_γ

TABLE 3.38 Detailed Calculations of Neutron Kerma Factor for Beryllium-9 at 15 MeV

(see equation 3.4.20 for notation)

E = 15 MeV, σ_t = 1.42625 barn

A = 8.9348, $(\overline{\cos\theta}_{c.m.})$ = 0.71723 (for elastic scattering)

Neutron Producing Reaction	m	σ_i(barns)	$\overline{E}_{n,i}$(MeV)	$m\,\sigma_i \overline{E}_{n,i}$
Elastic	1	0.87000	14.23206	12.381892
(n,2n)*	2	0.50818	3.88810	3.951709

$$\sum_i \sigma_i \overline{E}_{n,i} = 16.33360$$

* combines all modes for which there are two neutrons plus two alpha particles in the exit channel

Reaction†	σ_i	Q(MeV)	$\sigma_i Q_i$	$\sigma_i \cdot E_{Di}$
(n,γ)	1.00000 (-4)	+ 6.8200	+ 6.82000 (-4)	
(n,p)	4.17740 (-4)	- 12.8300	- 5.35960 (-3)	2.606698 (-3)
(n,d)	0.00000	- 14.6600	0.00000	0.000000
(n,t)	0.03800	- 10.4300	- 3.96340 (-1)	
(n,α)	9.54550 (-3)	- 0.6000	- 5.72730 (-3)	1.489098 (-2)
(n,2n)	0.50818	- 1.6600	- 0.84358	4.827710 (-2)

$$\sum_i \sigma_i Q_i = -1.250324, \quad \sum_i \sigma_i \cdot E_{Di} = 0.0657748$$

† (Conversion of K.E. to mass and vice versa)

From equation 3.4.20

$$T(15\ \text{MeV}) = k_n + E_\gamma = 3.87560\ \text{MeV . barn/atom}$$

(Present work) MACK Result k_n(15 MeV) = 3.8735 MeV . barn/atom

(Reference 7) Ritts Result k_n(15 MeV) = 7.4395 MeV . barn/atom

NOTE: Gamma production in Be-9 at 15 MeV is essentially by the (n,t) reaction only and E_γ is about 0.01 MeV . barn/atom (see text).

Table 3.2 Reaction Types

For the Purpose of Kerma Calculation, The Nuclear Reactions are Classified Into the Following Types

	REACTION TYPE	MT
(n,n)	Elastic	2
(n,n')γ	Inelastic	51-90
(n,n')γ	Inelastic Continuum	91
(n,mn')a_{c_1},a_{c_2}...	(n,mn') Charged Particles	22,23,24,28 and
	m =1 or 2	51-91 with Flag LR
(n,a_{c_1},a_{c_2},a_{c_3}...)	(n, Charged Particles)	103-109 700-799
(n,γ)	Radiative Capture	102
(n,2n)		16

A complete list of the reactions included in neutron kerma factor calculations for each material is given in Appendix D.

BIBLIOGRAPHY

1. a. Radiation Quantities and Units, compiled by Commission on Radiological Units and Measurements (ICRU), National Bureau of Standard Handbook 84 (ICRU report 10a), November 1962.

   b. D. K. Trubey, "Use of ICRU-Defined Quantities and Units in Shielding," ORNL-RSIC-16 (October 1968).

2. Protection Against Neutron Radiation up to 30 Million Electron Volts, compiled by the Subcommittee on Heavy Particles (Neutrons, Protons, and Heavier), National Bureau of Standards Handbook 63 (November 1957).

3. B. J. Henderson, Conversion of Neutron or Gamma Ray Flux to Absorbed Dose Rate, XDC 59-8-179, General Electric Company (August 1959).

4. J. A. Auxier and W. S. Snyder, The Calculation of Kerma as a Function of Neutron Energy, Oak Ridge National Laboratory, ORNL-4168 (1967).

5. R. L. Bach and R. S. Caswell, "Energy Transfer to Matter by Neutrons," Radiation Res., 35, 1 (1968).

6. J. J. Ritts, M. Solomito, and P. N. Stevens, "Calculation of Neutron Fluence-to-Kerma Factors for the Human Body," Nucl. Applic. and Tech., 7(1), 89-99 (July 1969).

7. J. J. Ritts, M. Solomito, and D. Steiner, "Kerma Factors and Secondary Gamma-Ray Sources for Some Elements of Interest in Thermonuclear Blanket Assemblies," ORNL-TM-2564 (June 1970).

8. MUG; A Program for Generating Multigroup Photon Cross Sections," J. R. Knight and F. R. Mynatt, CTC-17 (January 1970).

9. M. J. Stanley, "Klein-Nishina Photon Cross Sections (Program GAMMA)," APEX-487, General Electric Company (May 1959).

10. M. K. Drake, Editor "Data Formats and Procedures for the ENDF Neutron Cross Section Library," BNL-50279 (October 1970).

11. W. W. Engle, Jr., "A Users Manual for ANISN" K-1693, Oak Ridge Gaseous Diffusion Plant, March 1967.

12. R. D. Evans, "The Atomic Nucleus," McGraw Hill Book Co., Inc. (1955).

13. R. B. Leighton, "Principles of Modern Physics," McGraw Hill Book Company, Inc. (1959).

14. C. M. Lederer, J. M. Hollander, and I. Perlman, "Table of Isotopes," 6th edition, John Wiley and Sons, New York (1967).

15. Odelli Ozer, Editor, "Description of the ENDF/B Processing Codes and Retrieval Subroutines," BNL 50300 (Revised June 1971).

16. R. Q. Wright, N. M. Greene, J. L. Lucius, and C. W. Craven, Jr., "SUPERTOG: A Program to Generate Fine Group Constants and P_n Scattering Matrices from ENDF/B," ORNL-TM-2679 (1969).

17. K. Gregson, M. F. James, and D. S. Norton, "MLBW - A Multilevel Breit-Wigner Computer Programme," UKAEA Report AEEW-M-517, March 1965.

18. J. M. Otter, "Comment on the Calculation of the Scattering Cross Section for Multiple Resonances," Technical Note, Nucl. Sci. Eng. 28 (1967).

19. K. Gregson and M. F. James, "TEMPO - A General Doppler Broadening Programme for Neutron Cross-Sections," UKAEA Report AEEW-M-518, February 1965.

20. B. J. Toppel, A. L. Rago, and D. M. O'Shea, "MC^2: A Code to Calculate Multigroup Cross Sections, USAEC Report ANL-7318 (June 1967).

21. R. E. Schenter, J. L. Baker, and R. B. Kidman, "ETOX: A Code to Calculate Group Constants for Nuclear Reactor Calculations," USAEC Report BNWL-1002 (ENDF-127) (May 1969).

22. P. F. Zweifel and H. Hurwitz, Jr., J. Appli. Phys. 25, 1241 (1954).

23. H. Amster, J. Appl. Phys. 29, 623 (1958).

24. J. E. Lynn, "The Theory of Neutron Resonance Reactions," Claredon Press (1968).

25. G. I. Bell and S. Glasstone, "Nucleus Reactor Theory," Van Nostrand R. Comp. (1970).

26. R. N. Hwang, "Doppler Effect Calculations with Interference Corrections," Nucl. Sci. Eng. 21, 523 (1965).

27. S. K. Penny and L. W. Owen, "A Re-Evaluation of Vanadium Neutron and Gamma-Ray Production Cross Sections," ORNL-TM-4007 (November 1972).

28. W. E. Alley and R. M. Lessler, "Semiemperical Neutron-Induced Reaction Cross Sections," UCRL-50484 Rev. 1 (August 1972).

29. D. W. Muir, Los Alamos Scientific Laboratory, Private Communication (December 1972).

30. W. Kohler et al., Proceedings Texas Symposium on Technology of Controlled Fusion Experiments and the Engineering Aspects of Fusion Reactors, Austin, Texas (November 1972).

31. R. Q. Wright and R. W. Roussin, "DLG 2/100G Neutron Transport Code Cross Section Data Generated by SUPERTOG from ENDF/B3," (July 1972). This library can be obtained through the Radiation Shielding Information Center (RSIC) at Oak Ridge Nation Laboratory.

32. R. Q. Wright, ORNL (private communication).

33. A. J. Impink, Jr. "Neutron Economy in Fusion Reactor Blanket Assemblies," Technical report No. 435, M. I. T. Research Laboratory of Electronics, Cambridge, Mass. (1965).

34. L. Rosen and L. Stewart, "The Neutron-Induced Disintegration of Li^6 and Li^7 by 5 to 14 MeV incident Neutrons," LA-2643 (1961).

35. J. T. Kriese, ORNL (private communication).

36. C. W. Maynard and M. A. Abdou, "Neutron and Gamma Physics Problems in Fusion Reactors," Conference on New Developments in Reactor Physics and Shielding, CONF-720901, Book 2 (September 1972).

37. M. N. Rosenbluth, R. D. Hazeltine and F. L. Hinton, "Plasma Transport in Toroidal Confinement Systems," Phy. Fluids 15, 116 (1972).

38. S. Blow, V. Crocker, and B. Wade, "Neutronics Calculations for Blanket Assemblies of a Fusion Reactor. Paper 5.5 in reference 60 below.

39. J. D. Lee, "Tritium Breeding and Energy Generation in Liquid Lithium Blankets," Paper 5.3 in reference 60 below.

40. D. Steiner, "The Nuclear Performance of Fusion Reactor Blankets, Nuclear App. and Tech. 9, 83(1970).

41. D. K. Trubey, and Betty F. Maskewitz, "A Review of the Discrete Ordinates S_n Method for Radiation Transport Calculations," ORNL-RSIC-19 (1968).

42. "Proceedings of The International Working Sessions on Fusion Reactor Technology," Oak Ridge National Laboratory, CONF-710624 (June 28-July 2, 1971).

43. R. Q. Wright et al., "UKAEA to ENDF/B Translation ....," ORNL-TM-2880; also ENDF-134.

44. J. Blatt and V. Weisskopf, "Theoretical Nuclear Physics," J. Wiley and Sons, Inc., New York (1940).

45. B. Nicolaenko, "Energy-Dependent Baltzman Equation in the Fast Domain," J. Math. Physics, 11, 174 (1970).

46. J. J. Ritts -- TVA (private communication -- May 1973).

47. L. Spitzer, Jr., D. J. Grove, W. E. Johnson, L. Tonks, and W. G. Westendorp, NYO 5047 (1954).

48. E. P. Johnson, NYO 7900 (1957).

49. P. R. Bell and others, ORNL 2457 (1958).

50. N. C. Christofilos, N. W. Cook, W. B. Myers, C. E. Taylor, and W. Wells TID 7558, Suppl. 1 (1960).

51. D. J. Rose and M. Clark, Jr., Plasma and Controlled Fusion, 2nd revised printing, M.I.T. Press, Cambridge, Mass. (1965) Chapter 13.

52. A. J. Impink, Jr., Neutron Economy in Fusion Reactor Blanket Assemblies, Technical report No. 434, M.I.T. Research Laboratory of Electronics, Cambridge, Mass. (1965).

53. W. G. Homeyer, Thermal and Chemical Aspects of the Thermonuclear Blanket Problem, Technical report No. 435, M.I.T. Laboratory of Electronics, Cambridge, Mass. (1965).

54. L. N. Lontai, Study of a Thermonuclear Reactor Blanket with Fissile Nuclides, Technical Report No. 436, M.I.T. Laboratory of Electronics, Cambridge, Mass. (1965).

55. P. S. Spangler, Fusion Reactor Blanket Experiment, Technical Report 437, M.I.T. Research Laboratory of Electronics, Cambridge, Mass. (1965).

56. L. M. Petrie, Jr., Gamma-Ray Spectra In Fusion Blanket Mock-Ups, Technical Report 438, M.I.T. Research Laboratory of Electronics, Cambridge, Mass. (1965).

57. D. J. Rose, "On the Feasibility of Power by Nuclear Fusion," ORNL-TM-2204, Oak Ridge National Laboratory (1968).

58. D. Steiner, "Neutronic Calculations and Cost Estimates For Fusion Reactor Blanket Assemblies," ORNL-TM-2360 (1968).

59. A. Fraas, Parameters for a Series of Reference Designs of Thermonuclear Reactors, Appendix III, reference (11).

60. Proceedings of B. N. E. S. Nuclear Fusion Reactor Conference Culham (1969).

61. Blow, S., Crocker, V. S. and Wade, B. O., Neutronics calculations for Blanket Assemblies of a fusion reactor, Proceedings of B. N. E. S. Nuclear Fusion Reactor Conference, Culham (1969) Paper 5.5.

62. D. Steiner, Neutronic Behavior of Two Fusion Reactor Blanket Designs, Proceedings of B. N. E. S. Nuclear Fusion Reactor Conference, Culham (1969) 483.

63. J. D. Lee, Tritium Breeding and Energy Generation in Liquid Lithium Blankets, Proceedings of B. N. E. S. Nuclear Fusion Conference, Culham (1969) Paper 5.3.

64. R. W. Werner, Module Approach to Blanket Design-A Vacuum Wall Free Blanket Using Heat Pipes, Proceedings of B. N. E. S. Conference, Culham (1969) Paper 6.2.

65. G. R. Hopkins and G. Melese-d' Hospital, Direct Helium Cooling Cycle for a Fusion Reactor, Proceedings of B. N. E. S. Nuclear Fusion Reactor Conference, Culham (1969) Paper 6.1.

66. R. W. Werner, B. Meyers, P. B. Mohr, J. D. Lee, and N. C. Christofilos, Preliminary Design Consideration for an Astron Power Reactor System, Proceedings of B. N. E. S. Nuclear Fusion Reactor Conference, Culham (1969) Paper 5.2.

67. E. F. Johnson, Overall Tritium Balances in Fusion Reactors, Proceedings of B. N. E. S. Nuclear Fusion Reactor Conference, Culham (1069) Paper 5.1.

68. A. P. Fraas, Conceptual Design of a Fusion Power Plant to Meet the Total Energy Requirements of an Urban Complex, Proceedings of B. N. E. S. Nuclear Fusion Reactor Conference, Culham (1969) 1.

69. D. Steiner, The Nuclear Performance of Fusion Reactor Blankets, Nuclear App. and Tech. 9, 83 (1970).

70. A. P. Fraas and H. Postma, Preliminary Appraisal of the Hazards Problems of a D-T Fusion Reactor Power Plant, ORNL-TM-2822 (Revised) (1970).

71. A. P. Fraas, Conceptual Design of the Blanket and Shield Region of a Full-Scale Fusion Reactor, ORNL-TM-3096 (1970).

72. D. Steiner, "The Neutron-Induced Activity and Decay Power of the Niobium Structure of a D-T Fusion Reactor Blanket, ORNL-TM-3094 (1970).

73. Proceedings of IAEA Fourth Conference on Plasma Physics and Controlled Nuclear Fusion Research, Madison, Wisconsin (June 1971).

74. Reference 42 above.

75. H. Borgwaldt, W. H. Kohler, and K. E. Schroeter, Neutronic Thermal Design Aspects of Thermonuclear Fusion Reactor Blankets, Reference (27), Paper CN-28/K-12 (Revised).

76. D. Steiner, Emergency Cooling and Radioactive Waste-Disposal Requirements for Fusion Reactors, Reference (27), Paper CN-28/K-11.

77. Th. Bohn, and S. Forster, Blanket Cooling Concepts and Heat Conversion Cycles for Controlled Thermonuclear Reactors Reference (27), Paper CN-28/K-13.

78. A. P. Fraas, A Diffusion Process For Removing Tritium From The Blanket of A Thermonuclear Reactor, ORNL-TM-2358 (1968).

79. M. A. Abdou and C. W. Maynard, "Computational Techniques for Fusion Reactor Neutronics and Photonics," University of Wisconsin Fusion Design Memo 3 (1971).

80. M. A. Abdou, A Revised Manual For ANISN-1108 University of Wisconsin Report PLP-429.

81. W. E. Ford III, ORNL (private communication).

82. D. J. Dudziak, R. E. Seamon, and D. V. Susca "LAPHANO: A P$_0$ Multigroup Photon-Production Matrix and Source Code for ENDF," LA-4750-MS (ENDF-156) (January 1972).

83. W. E. Ford III, "POPOP4: A Code for Converting Gamma-Ray Spectra to Secondary Gamma-Ray Production Cross Sections," USAEC report CTC-12 (May 1969).

84. W. E. Ford III, "POPOP4 Library of Neutron-Induced Secondary Gamma-Ray Yield and Cross Section Data," USAEC Report CTC-42.

85. J. D. Jenkins, "RICE: A Program To Calculate Primary Recoil Atom Spectra from ENDF/B Data," ORNL-TM-2706 (February 1970).

86. W. F. Sheely, "Correlation of Radiation Damage to Steel with Neutron Spectrum," Nucl. Sci. Eng., 29, 165 (1967).

87. R. E. Dahl and H. H. Yoskikawa, "Neutron Exposure Correlation for Radiation Damage Studies," Nucl. Sci. Eng., 21, 312 (1965).

88. D. G. Doran, "Neutron Displacement Cross Sections for Stainless Steel and Tantalum Based on a Linhard Model," Nucl. Sci. Eng. 49, 130 (1972).

89. S. Blow, "The Effect of the Neutron Energy Spectrum on Neutron Displacement Damage in Niobium," J. Phys. D: Appl. Phys., 1971, Vol. 4.

90. D. G. Martin, "Radiation Damage Effects in the Containment Vessel of a Thermonuclear Reactor," United Kingdom Atomic Energy Authority Report CLM-R 103 (March 1970).

91. Doran, Kulcinski, and Abdou, "Gaseous Products and Transmutation Effects in CTR Materials," University of Wisconsin Fusion Design Memo (February 1973).

92. D. K. Sze and W. E. Stewart, "Lithium Cooling for a Low-β Tokamak Reactor," Proc. Texas Symp. Technology of Controlled Thermonuclear Fusion Experiments and the Engineering Aspects of Fusion Reactors (November 1972).

93. M. A. Hoffman, and G. A. Carlson, "Calculation Techniques for Estimating the Pressure Losses For Conducting Fluid Flows in Magnetic Fields," Lawrence Radiation Laboratory, TID-4500, UC-20.

94. S. J. Leverette, "An Investigation of The Temperature Distribution in the Lithium Blanket of a Fusion Reactor," ORNL-TM-3701 (1973).

95. M. A. Abdou et al., "Preliminary Conceptual Design of a Tokamak Reactor," Proc. Texas Symp. Technology of Controlled Thermonuclear Fusion Experiments and the Engineering Aspects of Fusion Reactors (November 1972).

96. M. V. Davis, "Selected Properties of Materials with Application to CTR Design," ANL/CTR-72-01 (Revised December 1972).

97. W. F. Vogelsang, University of Wisconsin Fusion Design Group, (private communication).

98. D. J. Dudziak, "A Technical Note on D-T Fusion Reactor After-heat," Nuclear Technology 10, 391 (March 1971).

99. A. P. Fraas, "Conceptual Design of the Blanket and Shield Region of a Full Scale Toroidal Fusion Reactor," to be published (1973).

100. "An Assessment of Fusion Power," Wash-1239.

101. W. F. Vogelsang, "Breeding Ratio, Inventory, and Doubling Time in a D-T Reactor," Trans. Am. Nucl. Soc., 14, 33 (1972).

102. J. R. Weir, J. O. Stiegler, and E. E. Bloom, "Irradiation Behavior of Cladding and Structural Materials," USAEC Report ORNL-TM-2258 (September 1968).

103. "Proceedings of The Conference on Continuum Aspects of Graphite Design," Catlinburg, Tennessee, CONF-701105 (November 1970).

104. R. W. Boom and Phillip A. Sanger (private communication), University of Wisconsin Fusion Design Group.

105. W. C. Young and R. W. Boom, "Materials and Cost Analysis of Constant-Tension Magnet Windings For Tokamak Reactors," 4th International Conference, Brookhaven (September 1972).

106. M. S. Lubell et al., "Economics of Large Superconducting Toroidal Magnets For Fusion Reactors," ORNL-TM-3927 (1972) and I. E. E. E. Conf. Record, I. E. E. E. Cat. No. 72 CHO 682-5 TABSC.

107. R. Harrington and R. Giberson, "Chemical and Physical Changes in Gamma-Irradiated Plastics," Mod. Plastics (1958).

108. Proceedings of the 1968 Summer Study on Superconducting Devices and Accelerators, Brookhaven National Laboratory (June 10 - July 19, 1968).

109. H. Brechna, "Effect of Nuclear Radiation on Organic Materials; Specifically Magnet Insulations in High-Energy Accelerators," SLAC-40; also UC-28 (March 1965).

110. T. W. Evans, "The Effects of Irradiation on Boron Carbide," BNWL-679 (February 1968).

111. W. M. Mueller, et al "Metal Hydrides," Academic Press (1968).

112. T. R. England, "An Investigation of Fission Product Behavior and Decay Heating in Nuclear Reactors," Ph.D. Thesis, Univ. of Wisconsin (August 1969).

113. H. K. Forsen and D. G. McAlees, "Neutron Wall Current and Energy Considerations for Alternate Fusion Fuel Cycles," UW - FDM - 9 (February 1972).